Contributions to the techno-economic assessment of technological innovations in electrical engineering

Loïc Quéval

Habilitation à diriger des recherches

université PARIS-SACLAY

Contributions to the techno-economic assessment of technological innovations in electrical engineering

Habilitation à diriger des recherches de l'Université Paris-Saclay

présentée et soutenue à Paris-Saclay, le 15/12/2022, par

Loïc QUEVAL

Composition du jury

Xavier ROBOAM Directeur de Recherche, CNRS, Laplace, Toulouse	Rapporteur
Sandrine SELOSSE Chargée de Recherche HDR, Mines ParisTech, CMA, Sophia Antipolis	Rapportrice
Frédéric WURTZ Directeur de Recherche, CNRS, G2Elab, Grenoble	Rapporteur
Xavier GUILLAUD Professeur, Ecole Centrale de Lille, L2EP, Lille	Examinateur
Marija JANKOVIC Professeuse, CentraleSupélec, LGI, Paris-Saclay	Examinatrice
Jean LEVEQUE Professeur, Université de Lorraine, GREEN, Nancy	Examinateur

université PARIS-SACLAY

Title: Contributions to the techno-economic assessment of technological innovations in electrical engineering.

Keywords: techno-economic analysis, wind energy conversion system, underground cable transmission system, HVDC converter station, photovoltaic water pumping system

Abstract: This thesis is written in view of obtaining an accreditation to supervise research (HDR - Habilitation à Diriger des Recherches). It summarizes the author's contributions, as a postdoctoral researcher (2013-2015) and as an assistant professor (2015-2022), to the techno-economic assessment of technological innovations in electrical engineering.

The energy transition to a low-carbon society is both a major challenge for innovation and a great opportunity for the economy. Technology choices must be well thought out because they have long-term impacts. This is due to the evolution of the technical and environmental performance of each element of a system over its lifetime and to the huge levels of investment involved. Therefore, in addition to demonstrating the technical feasibility of an innovation, it is also necessary to evaluate its economic competitiveness throughout its life cycle.

In this context, first we discuss a framework for the techno-economic assessment of a technological innovation. Then we focus on 4 early-stage technologies being developed at GeePs, CentraleSupélec, University Paris-Saclay: fully superconducting generator for wind energy conversion systems, superconducting cables for HVAC underground cable transmission systems, cryo-modular multilevel converter for HVDC converter stations, and SAUREA's motor-pump for photovoltaic water pumping systems.

For each innovation, we highlight some of the theoretical and experimental contributions of our team in recent years, and we open the discussion with an abbreviated techno-economic evaluation. Finally, we propose some perspectives both in terms of methods and applications.

Titre : Contributions à l'évaluation technico-économique des innovations technologiques en génie électrique

Mots clés : analyse technico-économique, système de conversion de l'énergie éolienne, système de transmission par câble souterrain, station de conversion CCHT, système de pompage d'eau photovoltaïque

Résumé : Cette thèse est rédigée en vue de l'obtention d'une habilitation à diriger des recherches (HDR). Elle résume les contributions de l'auteur, en tant que chercheur postdoctoral (2013-2015) et en tant qu'assistant professeur (2015-2022), à l'évaluation technico-économique des innovations technologiques en génie électrique.

La transition énergétique vers une société bas carbone est à la fois un défi majeur pour l'innovation et une grande opportunité pour l'économie. Les choix technologiques doivent être mûrement réfléchis car ils ont des impacts à long terme. Cela est dû à l'évolution des performances techniques et environnementales de chaque élément d'un système au cours de sa durée de vie et aux énormes niveaux d'investissement impliqués. C'est pourquoi, en plus de démontrer la faisabilité technique d'une innovation, il est également nécessaire d'évaluer sa compétitivité économique en considérant son cycle de vie.

Dans ce contexte, nous discutons d'abord d'un cadre pour l'évaluation technico-économique d'une innovation technologique. Ensuite, nous nous concentrons sur 4 technologies en phase de développement au GeePs, CentraleSupélec, Université Paris-Saclay : générateur entièrement supraconducteur pour les systèmes de conversion de l'énergie éolienne, câbles supraconducteurs pour les systèmes de transmission par câble souterrains HVAC, cryo-convertisseur modulaire multiniveaux pour les stations de conversion HVDC, et motopompe SAUREA pour les systèmes de pompage d'eau photovoltaïque.

Pour chaque innovation, nous soulignons quelques contributions théoriques et expérimentales de notre équipe au cours des dernières années, et nous ouvrons la discussion en proposant une courte évaluation technico-économique. Enfin, nous présentons quelques perspectives tant au niveau méthodologique qu'applicatif.

Contents

Foreword

This thesis aims to review my research activities from 2013 to 2022, as a postdoctoral researcher and as an assistant professor. It is written in view of obtaining the French "Habilitation à Diriger des Recherches" (HDR - authorization to supervise research). It is submitted to the doctoral school EOBE (Electrical, Optical, Bio-Physics and Engineering) of the Université Paris-Saclay, France.

It is organized under the common thread that seems to animate all my work: the techno-economic assessment of innovative systems. My interest in this topic came gradually. My doctoral thesis focused on the modeling and simulation of grid-connected superconducting wind turbine generators, under the supervision of Prof. H. OHSAKI at the University of Tokyo, Japan. It led me to the theoretical analysis of innovative systems, and deeply influenced my activities since I am still working on the applications of superconductors. At the same time, it pushed me towards experimental work, as I gradually understood that *a model is worth what it is worth* and that it must be systematically confronted with measured data. This realization led me to pursue two postdocs with a strong experimental component. The first one was on the thermal characterization of synchronous machines for electric vehicle applications, under the supervision of Prof. R. GOTTKEHASKAMP at the University of Applied Sciences in Düsseldorf, Germany. The second postdoc project was on the study of a "solar motor" for photovoltaic water pumping, under the supervision of Dr. L. VIDO and Prof. B. MULTON at the University of Cergy-Pontoise, France. These projects made me realize the importance of optimizing systems in different usage scenarios (e.g. driving cycle for electric vehicles, or irradiance variations for water pumping). At the end of 2015, I joined CentraleSupélec in Université Paris-Saclay as an assistant professor. Since then, I have been teaching at CentraleSupélec while being affiliated with the electric grid group of the GeePs laboratory. I mainly study components for distribution and transmission grids, both theoretically and experimentally. For electric grid applications, due to the lifetime of the assets and the significant levels of investment involved, a thorough evaluation must be performed prior to installing a component. This led me to look into techno-economic assessment methods with a focus on early-stage technologies.

This manuscript is organized in two parts.

- **Part I**: The first part summarizes my research activities over the last 10 years. After a short introduction on vocabulary and methods for the techno-economic assessment of technological innovations, I propose a focus on 4 innovative systems I have been working on: fully superconducting generator for wind energy conversion systems, superconducting cables for HVAC underground cable transmission systems, cryo-MMC for HVDC converter stations, and SAUREA's motor-pump for photovoltaic water pumping systems. I will present each innovation in detail, while highlighting some of our team's contributions and opening the discussion with an abbreviated techno-economic evaluation. Finally, by way of perspective, I will address a few unresolved issues that I find particularly intriguing and worthy of further study.
- **Part II**: The second part summarizes my scientific production more quantitatively, more specifically, my research projects, teachings, collaborations and experiences in supervising students and young researchers.

In the following texts, the references with letters in orange (e.g. [M3]) point to the work of young researchers I supervised; the list can be found in Chapter 8. The references with letters in green (e.g. [p7]) refer to the list of publications given in Chapter 9. The references without any letter in blue (e.g. [149]) refer to the Bibliography at the end of the document.

The completion of this manuscript required significant time alongside other activities. I extend my sincere gratitude to my colleagues for their unwavering support throughout this endeavor. In particular, I am deeply grateful to C. MARCHAND for his encouragement and guidance in successfully completing this HDR. Special thanks are also due to F. TRILLAUD and S. MEUNIER for their meticulous proof-reading of the manuscript. I also want to sincerely thank Kristen for her infallible patience, encouraging me to go to the end of my projects.

Short CV

Loïc Quéval

Assistant professor, PhD
CentraleSupélec, University of Paris-Saclay
GeePs laboratory

Plateau de Moulon, 3 rue Joliot Curie
91192 Gif-sur-Yvette cedex, France
+ 33 (0)1 69 85 15 35
loic.queval@geeps.centralesupelec.fr

Education

2010-2013	PhD degree, field of advanced energy Univ. of Tokyo, Japan
2009	Specialization in automatism Federal Univ. of Santa Catarina, Florianópolis, Brésil
2006-2009	Electronics Engineering degree ENSEEIHT, Toulouse, France
2004-2006	Preparatory classes for entrance exams into national engineering schools. Lycée Louis le Grand, Paris, France Lycée Chaptal, Paris, France

Experience

2015-now	GeePs CNRS laboratory CentraleSupélec, France
2014-2015	SATIE CNRS laboratory Univ. of Cergy-Pontoise, France
2013-2014	Lab for Electrical Machines Univ. Applied Sciences Düsseldorf, Germany
2010-2013	Ohsaki laboratory, Univ. of Tokyo, Japan
2009	GRUCAD laboratory Florianópolis, Brazil
2008	blueEnergy Bluefields, Nicaragua

■ RESEARCH ACTIVITES

Current projects:
a) Techno-economic assessment of superconducting wind turbine generator.
b) Experimental work on superconducting components for the electric grid of the future (cables, ScFCL, etc.).
c) Experimental work on modular multilevel converters for HVDC grids.
d) Multidisciplinary analysis of a photovoltaic water pumping system installed in Burkina Faso.

Summary

41	Journal articles
1	In peer-review
57	Intl. conferences
32	Natl. conferences
857	Number of citations (G. Scholar)
15	h-index (G. Scholar)
6	PhD thesis co-supervision
7	Master thesis supervision

Awards

2020	EPE Young Author Best Paper Award, EPE'20 ECCE Europe
2019	Award of the best paper in renewable energies, EVER2019
2016	Superconductor Science and Technology Highlights of 2016.
2014	University of Cergy-Pontoise postdoc fellowship

■ TEACHING ACTIVITIES

Lectures: ~180 h/year at CentraleSupélec, ~40 h/year extra
Project advisor (bachelor, master, engineering curriculum): ~170 h/year (~30 students/year)

Part I

Synthesis report

Chapter 1

Introduction

The EU has ambitious climate and energy goals in response to the urgency of climate change [1]. By 2030 greenhouse gas emissions should be cut by 40% (from 1900 levels). The share for renewable energy should increase to at least 32%. And energy efficiency should improve by 32.5% [2].

The energy transition to decarbonized societies appears both as a major challenge for innovation and as a great opportunity for economy. Climatic policies, even if guided by political and economic considerations, cannot escape technological implementation. Technological choices should be well reasoned. Short-term choices undoubtedly have long-term impacts due to the effectiveness and lifespan of each technology, and to the enormous investment levels involved.

This is why, in addition to demonstrating the technical feasibility of an innovation, one need to assess its economic competitiveness as well, considering its life cycle. *A technological innovation has little chance of being adopted if it is not competitive over its life cycle.*

1.1 How to assess a technological innovation?

The evaluation of a technological innovation implies carrying out a techno-economic assessment. Despite several theoretical discussions in the literature, there is no standard method yet for conducting a techno-economic assessment [12]. We adopt here the general framework described in the "Techno-Economic Assessment & Life Cycle Assessment Guidelines for CO2 Utilization (Version 2.0)" published by the Global CO2 Initiative [13]. It is inspired by the method and vocabulary used for life cycle assessment (LCA), a standardized methodology for evaluating the environmental impacts associated with all stages of the life cycle of a product, process or service (ISO 14040 and ISO 140144, [M12]).

1.1.1 Definitions

Before we go any further, let's define some terms.

System element Smallest unit for which data are inventoried. It can be hardware, software, data, humans, organisms, processes, procedures, facilities, materials, or any combination of these. [15]

Product system "[...] Collection of materially and energetically connected [system elements/]unit processes, which perform one or more defined functions." [10]

Functional unit "Quantified description of the function of a product [system] that serves as the reference basis for all calculations [...]." [11]

System boundary "Set of criteria specifying which [system elements/]unit processes are part of a product system. (ISO 2006)" [10]

Time horizon Study period, usually expressed in years, over which the product system is analyzed. It is sometimes called life cycle.

1.1.2 Techno-economic assessment framework

The method is split into 5 phases, which are illustrated in Figure 1.1 and briefly summarized below.

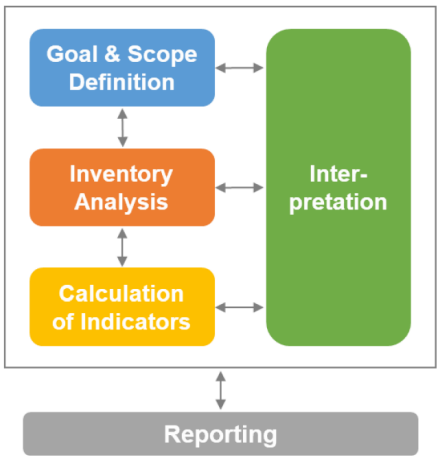

Figure 1.1: Techno-economic assessment framework [13]

Phase 1: Goal and scope definition

The "goal definition" consists of determining various aspects, such as (i) the intended application of the study, (ii) the purpose of the study and (iii) the target audience. In addition, it should also include the time horizon, the location, and the scenarios to be analyzed.

The "scope definition" consists of describing the assumptions and the methodology implemented to perform the study, such as (i) the function of the product system, (ii) the functional unit and (iii) the system boundary. In addition, it should also identify the performance indicators that will be used for the assessment.

Phase 2: Inventory analysis

The "inventory analysis" aims at (i) identifying the system elements and (ii) collecting and quantifying the technological parameters (e.g. efficiency) and the economic parameters (e.g. capital expenses and operating expenses) of each system element of the product system.

Phase 3: Calculation of indicators

The "calculation of indicators" should cover two aspects: (i) the modeling and (ii) the characterization.

The modeling consist in selecting the technical and economic models. The level of detail (e.g., black box or detailed process) can vary between system elements according to the goal and scope of the study, and to data availability. Usually the larger the system, the coarser the models in order to keep the data collection time and computing time reasonable...

During characterization, the performance indicators are calculated for the overall product system as well as for each system element individually.

Phase 4: Interpretation

The "interpretation" is split into 4 steps: (i) describe uncertainty and sensitivity of the results, (ii) provide conclusions, presenting the whole spectrum of criteria relevant for decision making, (iii) discuss limitations and (iv) state recommendations, if any. Scenario analysis using the scenarios identified in the goal phase should also be performed as part of the interpretation.

Phase 5: Reporting

"Reporting" can take numerous forms, depending on the audience and the objectives of the commissioner. It is critical to provide transparency, accuracy, and consistency. Ideally, it should offer enough data to enable reproducibility of one's results by others.

1.1.3 Techno-economic comparison

In order to get a real appreciation of the "potential" of a technological innovation, it is necessary to compare it to different competing technologies providing the same service. This is consistent with stan-

dard practice: techno-economic assessments usually compare the "benchmark product system" that is currently used to perform the specified function to the "proposed product system" being considered as an alternative. Comparison is necessary because the value of an indicator is only useful if it can be compared to the one of a known technology. From our point of view, the comparison of a technological innovation to an existing technology raises 3 additional difficulties.

Optimization problem

Ultimately, the comparison aims to select, out of several alternatives that provides the required service, the technology that has the best performance. The performance of a system depends on its elements, its environment and its usage. Usually there are several variables that can be played with (sizing and settings, usage scenario). We argue here that, to be fair, *one should only compare two systems that have been optimized on the same set of specifications and for the same scenario.*

This notion is already present in the literature. In [13], it is stated that "the most common or best-in-class benchmark products should be selected for comparison". This is to ensure that the proposed product system does not seem more economically viable than it actually would be upon deployment. This suggests that the benchmark product system has already been optimized for the target application.

Prospective performances

Following the same logic, to evaluate the potential of a technological innovation, it is not very meaningful to consider its current technical and economic performance. Indeed, unlike the mature benchmark product system, it has not yet been optimized to reduce production costs and improve outputs.

We argue here that, to be fair, *the techno-economic assessment of a technological innovation should rely on projections of the value of its technological and economic parameters when it will reach market maturity.*

Performance indicator

The performance of a system is quantified by performance indicators. They can be technical (e.g. primary energy demand, GHG emissions), economic (e.g. product margin, payback time) or techno-economic (e.g. TRL) [13].

Since the functional unit quantifies the function of a product system, it allows us to compare two systems - even very different ones - that perform the same function. The number of functional units quantifies the technical performance of a product system, while the cost of the functional unit quantifies its economic performance. We argue here that *the life cycle techno-economic performance of any technology can be quantified using the "levelized cost per (functional) unit".* This indicator is defined and discussed in the following sections.

1.2 Estimation of the cost per unit

1.2.1 Definitions

Before proceeding to the discussion, we provide definitions to commonly used concepts related to economic analysis [7, 3].

System lifetime Duration, usually expressed in years, over which the system "remains integer and usable for its primary function for which it was conceived and produced" [4].

Cash flow Real or virtual movement of money.

Present value of a cash flow Value at the present time of a future cash flow, discounted to account for the time value of money. The present value $PV(F)$ of a cash flow F is calculated by,

$$PV(F) \triangleq \frac{F}{(1+r)^t} \tag{1.1}$$

where r is the discount rate and t is the duration, usually expressed in years, between the present time and the date of the future cash flow. The cash flow within a 12 months period are not discounted.

Cost A cost (positive value) is a negative cash flow.

Revenue A revenue (positive value) is a positive cash flow.

Fixed costs Costs that are not affected by the level of activity, e.g. rents, insurance, property taxes, administrative salaries, and the interest on borrowed capital.

Variable costs Costs that are affected by the level of activity, e.g. fuel costs, materials costs, labor costs, distribution costs, and storage costs.

Capital expenses Fixed and variable costs due to capital, e.g. equipment, system design, engineering, installation and decommissioning [6].

Operating expenses Fixed and variable costs due to operation, e.g. maintenance, reparation, salary of the operator, site access, guarantees and fuel [198, 6].

Operating revenues Revenue generated by activities from a company's primary business [8]

Non-operating revenues Revenue generated by activities outside of a company's primary business, e.g. interest income, gains from the sale of assets and lawsuit proceeds [8].

Salvage value Present value of the one-time non-operating revenue consisting of the assets, equipment, buildings, or business sold at the time horizon.

1.2.2 Life-cycle cost

The estimation of the "cost" of a system is done on its life-cycle. It is therefore called here life-cycle cost (also called whole-life cost). The life-cycle cost LCC of a system is calculated here as the sum of the present value of all the costs over the time horizon,

$$LCC \triangleq \sum_{t=0}^{H} \frac{C_t}{(1+r)^t} \tag{1.2}$$

where C_t are the costs in year t, r is the discount rate, and H is the time horizon. Since all the costs have positive value, the LCC is positive as well. Note that $t = 0$ represents the present time and therefore C_0 is the initial investment.

1.2.3 Life-cycle revenue

The estimation of the "revenue" of a system is done on its life-cycle. It is therefore called here life-cycle revenue. The life-cycle revenue LCR of a system is calculated here as the sum of the present value of all the revenues over the time horizon,

$$LCR \triangleq \sum_{t=0}^{H} \frac{R_t}{(1+r)^t} \tag{1.3}$$

where R_t are the revenues in year t, r is the discount rate, and H is the time horizon. Since all the revenues have positive value, the LCR is positive as well. Note that $t = H$ represents the time horizon and therefore $R_H/(1+r)^H$ is the salvage value.

1.2.4 Net present value

The net present value NPV of a system is calculated here as the sum of the present value of the net cash flows over the time horizon,

$$NPV \triangleq \sum_{t=0}^{H} \frac{R_t - C_t}{(1+r)^t} \tag{1.4}$$

Following (1.2) and (1.3),

$$NPV = LCR - LCC \tag{1.5}$$

A project with a positive NPV is said to be "profitable". When comparing several alternatives, one normally want to choose the alternative with the highest NPV.

The NPV gives perspective on the profitability of a project. But it does not allow one to easily compare two technologies, especially if they have different scale or time horizon.

1.2.5 Levelized cost per unit

NPV method

In the following, we assume that:
(i) the time horizon H is equal to the system lifetime T.
(ii) the costs include only the capital and operating expenses.
(iii) the revenues include only the operating revenues and the salvage value.

From (1.2) and (1.3),

$$LCC \overset{\text{hyp}}{=} \sum_{t=0}^{T} \frac{CAPEX_t + OPEX_t}{(1+r)^t} \tag{1.6}$$

$$LCR \overset{\text{hyp}}{=} \sum_{t=1}^{T} \frac{r_t \cdot Q_t}{(1+r)^t} + SV \tag{1.7}$$

where $CAPEX_t$ is the capital expenses in year t, $OPEX_t$ is the operating expenses in year t, r is the discount rate, r_t is the (operating) revenue per (functional) unit in year t, Q_t is the number of (functional) unit in year t, T is the system lifetime and SV is the salvage value.

The levelized cost per (functional) unit $LCpu$ is defined here as the average revenue per (functional) unit for which the net present value of the system is zero [7],

$$r_t = LCpu \Rightarrow NPV = 0 \tag{1.8}$$

The $LCpu$ represents thus the average revenue per (functional) unit over the system lifetime required to break even. Insert (1.6) and (1.7) into (1.5),

$$0 = \sum_{t=1}^{T} \frac{LCpu \cdot Q_t}{(1+r)^t} + SV - \sum_{t=0}^{T} \frac{CAPEX_t + OPEX_t}{(1+r)^t} \tag{1.9}$$

And isolate $LCpu$,

$$\boxed{LCpu = \frac{\sum_{t=0}^{T} \frac{CAPEX_t + OPEX_t}{(1+r)^t} - SV}{\sum_{t=1}^{T} \frac{Q_t}{(1+r)^t}}} \tag{1.10}$$

The $LCpu$ can be used to assess the profitability of a technology. If the market price is higher than the $LCpu$, then the margin per unit is positive (market price - $LCpu$ is greater than zero) and the project can be profitable. When comparing several alternatives, one normally want to choose the alternative with the lowest $LCpu$.

The $LCpu$ allows one to compare competing technologies providing the same service, even if they have different scale or time horizon.

Annuity method

In addition to (i)-(ii), we assume that:
(iv) the capital expenses occur only at $t = 0$.
(v) the operating expenses are zero at $t = 0$, and are constant $\forall t > 0$.
(vi) the operating revenues are constant $\forall t > 0$.

From (1.10),

$$LCpu = \frac{CAPEX_0 + OPEX_t \sum_{t=1}^{T} \frac{1}{(1+r)^t} - SV}{Q_t \sum_{t=1}^{T} \frac{1}{(1+r)^t}} \tag{1.11}$$

Define the annuity factor ANF,

$$ANF \triangleq \sum_{t=1}^{T} \frac{1}{(1+r)^t} \tag{1.12}$$

It is a finite geometric series and the summation term can be simplified,

$$ANF = \left[\frac{1}{r} - \frac{(1+r)^{-T}}{r}\right] \tag{1.13}$$

(1.11) becomes,

$$\boxed{LCpu = \frac{CAPEX_0 + OPEX_t \cdot ANF - SV}{Q_t \cdot ANF}} \tag{1.14}$$

1.3 Levelized cost per unit in the literature

With the *levelized cost per (functional) unit*, we generalize and formalize the concept behind several well-known indicators of the literature, including: the levelized cost of electricity, the levelized cost of storage and the levelized cost of hydrogen.

1.3.1 Levelized cost of electricity $LCOE$

The Levelized Cost of Electricity $LCOE$ is a popular indicator when comparing electric power generation projects. It represents the average revenue per unit of electric energy produced over the system lifetime required to break even. And it is often expressed in euro per megawatt hour [€/MWh]. It is sometimes called "Levelized Cost of Energy", but this expression is ambiguous and requires clarification. To be more precise, it should maybe be called "Levelized Cost Of Generation of Electricity ($LCOE = LCOGE$).

Under the hypothesis of section 1.2.5, the $LCOE$ is expressed from (1.8) as,

$$LCOE = \frac{\sum_{t=0}^{T} \frac{CAPEX_t + OPEX_t}{(1+r)^t} - SV}{\sum_{t=1}^{T} \frac{EG_t}{(1+r)^t}} \tag{1.15}$$

where $CAPEX_t$ is the capital expenses in year t, $OPEX_t$ is the operating expenses in year t, r is the discount rate, EG_t is the electricity generated in year t, T is the system lifetime and SV is the salvage value. Note that neglecting the salvage value, (2.1) corresponds to the $LCOE$ definition of UK Department of Energy and Climate Change [198, 6] which is widely used in our community [138].

1.3.2 Levelized cost of storage $LCOS$

The Levelized Cost of Storage $LCOS$ represents the average revenue per unit of electric energy discharged from a storage device over the system lifetime required to break even. And it is often expressed in euro per megawatt hour [€/MWh].

Under the hypothesis of section 1.2.5, the $LCOS$ is expressed from (1.8) as,

$$LCOS = \frac{\sum_{t=0}^{T} \frac{CAPEX_t + OPEX_t}{(1+r)^t} - SV}{\sum_{t=1}^{T} \frac{ED_t}{(1+r)^t}} \tag{1.16}$$

where $CAPEX_t$ is the capital expenses in year t, $OPEX_t$ is the operating expenses in year t, r is the discount rate, ED_t is the electricity discharged from the storage device in year t, T is the system lifetime and SV is the salvage value. Note that (1.16) corresponds to the $LCOS$ definition of [16] in line with recent publications [17].

1.3.3 Levelized cost of hydrogen $LCOH$

The Levelized Cost of Hydrogen $LCOH$ represents the average revenue per unit of hydrogen generated over the system lifetime required to break even. And it is often expressed in euro per kilogram [€/kg].

Under the hypothesis of section 1.2.5, the $LCOH$ is expressed from (1.8) as,

$$LCOH = \frac{\sum_{t=0}^{T} \frac{CAPEX_t + OPEX_t}{(1+r)^t} - SV}{\sum_{t=1}^{T} \frac{HG_t}{(1+r)^t}} \tag{1.17}$$

where $CAPEX_t$ is the capital expenses in year t, $OPEX_t$ is the operating expenses in year t, r is the discount rate, HG_t is the hydrogen generated in year t, T is the system lifetime and SV is the salvage value. Note that (1.17) corresponds to the $LCOH$ definition of the Fuel Cells and Hydrogen Observatory [18].

1.3.4 Other levelized cost per unit

With fossil fuels covering more than 60% of building heat global demand in 2020, the cost-competitiveness of renewable heat technologies versus fossil fuel options is being studied intensively. In [9], the "levelized cost of heating", expressed in $\$/\mathrm{kWh_{th}}$, has been used to compare different space and water heating technologies for different countries.

1.3.5 Advantages and drawback

Here we offer a brief summary of the advantages and drawbacks of the $LCOE$, keeping in mind that the discussion applies to any other $LCpu$ indicator.

Advantages

- The $LCOE$ reflects in a single figure the key production costs of the power plant over its lifetime [19, 24, 25]. One number is readily understood. This significantly reduces complexity and allows for quick and easy comparison of different solutions. The $LCOE$ can be used to support decision-making. This is a key element in making it a useful tool for decision making.
- From an economic perspective, the $LCOE$ contains the most important factors to provide a reasonable first-order economic evaluation of a project [26].
- The approach has a wide scope of application [27, 28]. It has been used to evaluate different power generation technologies as well as individual projects [19, 20, 21, 22, 23].
- The $LCOE$ is not only dependent on the technology used, but is also influenced by the interaction between the power plant and its environment. The $LCOE$ is not the "cost" of a technology, it is the cost of a technology associated with a set of requirements.

Drawbacks

- There are several ways to estimate the $LCOE$. They are similar in foundation but with differences in the calculation stages, variables and assumptions used [6, 27, 198]. Therefore, it is important that the assumptions of each calculation are sufficiently substantiated and understandable. Care should therefore be taken when comparing different studies.
- The $LCOE$ is associated with uncertainties. These are mainly due to the fact that the calculation requires values of technical and economic parameters for the whole life of the installation, some of which have to be predicted. See discussion in section 6.1.4.
- As Joskow [20] pointed out, electricity is a time-heterogeneous good, which means that the value of electricity depends on when it is produced.
- $LCOE$ can be used to assist in decision making. However, it is impossible to make conclusive statements about the economic viability of a technology solely on the basis of an analysis with the $LCOE$ method. It is a simplified assessment of the economic performance. An actual investment decision requires a detailed consideration of how the project would be financed and how its costs would be distributed over time.
- This single figure approach to project costing has limitations. It increases the risk of misinterpretation and poor decision making due to the narrowness of the viewpoint.
- The $LCOE$ does not consider the different stakeholders who can have different interests, and thus impact the economic attractiveness. The $LCOE$ should be evaluated with other financial indicators, such as the Project Internal Rate of Return (Project IRR), the Equity Internal Rate of Return (Equity IRR), or the Debt Service Coverage Ratio (DSCR).
- When a system has a primary function but also has other functions, it is known as multifunctionality. As it is done with LCA [13], $LCOE$ estimation may require some level of cost allocation for decision-making purposes.

1.4 Summary

We discussed a framework for the techno-economic assessment of a technological innovation. It needs to be compared to competing technologies providing the same service, keeping in mind that: (i) one should only compare two systems that have been optimized on the same set of specifications and for the same scenario, (ii) the techno-economic assessment of a technological innovation should rely on projections of the value of its technological and economic parameters when it will reach market maturity, and (iii) the life cycle techno-economic performance of any technology can be quantified using the "levelized cost per (functional) unit ($LCpu$)".

The "levelized cost per (functional) unit" $LCpu$ represents the average revenue per (functional) unit required to break even. It allows for the comparison of two technologies regardless of unequal life spans, differing capital costs, size of the projects, and the differing risk associated with each project. We clarified the link between the $LCpu$ and different indicators appearing in the literature: $LCOE$, $LCOS$, $LCOH$, etc. Finally, we offered a brief review of the advantages and drawbacks of the $LCpu$.

In the remaining chapters of this thesis, we apply the concept of levelized cost per unit to assess 4 different technological innovations in electrical engineering, from the electricity generation to the consumption. In chapter 2, we examine the prospects of the fully superconducting generator for wind energy conversion systems (generation). In chapter 3, we study the potential of the superconducting cable for high voltage alternating current underground cable transmission systems (transmission). In chapter 4, we look at the cryo-modular multi-level converter for high voltage direct current converter stations (conversion). Finally, in chapter 5, we propose an analysis of SAUREA's motor-pump for photovoltaic water pumping systems (consumption). Each chapter will be to the occasion to expose our contributions during the past years to the development of each technology.

Chapter 2

Fully superconducting generator for wind energy conversion systems

2.1 Context

Driven by its commitment on GHG emissions reduction, the uncertainty of fossil fuel prices and the energy security problems, Europe increased its total wind power capacity from 12.7 GW to 215.4 GW between 2000 and 2020 [109]. Despite these impressive numbers, stronger efforts are required to achieve the EU goal of climate neutrality by 2050 [110].

Today offshore wind has a total installed capacity of only 25 GW [108], but it is expected to play a key role in the future. This is because it has many advantages (regular winds, large and deserted areas, low visual impact, etc.) and because it is already competitive (all offshore wind auction results in 2019 ranged between 40 €/MWh and 50 €/MWh [107]).

The average rated power of newly installed offshore turbines grew from 3 MW to 8.2 MW between 2010 and 2020 [108, Fig. 6]. Increasing the rated turbine power is desirable, because it simplifies the installation and maintenance [111, 112]. This is because the wind turbine itself represents only a quarter of the cost of the wind farm over its life cycle; while installation and operating and maintenance costs account for three quarters of the cost. A cost analysis shows why installers often choose direct drive synchronous generators combined with full-scale converters [124]. A system without a gearbox has better efficiency, greater reliability, as well as lower installation and maintenance costs [113]. In addition, the use of a full-power converter provides the necessary flexibility to comply with the new rules for connecting to the power grid (reactive power supply, low-voltage ride through, etc.).

However, direct drive multi-MW generators tend to be bulky and heavy [114], leading to costly nacelles, towers, and foundations. This is particularly problematic when considering to install such system on floating foundations in deep water areas [108]. Innovative technologies such as superconducting machines have been proposed to solve this challenge.

In this chapter, we describe the work that has been carried out on the techno-economic assessment of fully superconducting generators for wind energy conversion systems.

2.2 Overview of a wind energy conversion system

We consider the wind energy conversion system (WECS) shown in Fig. 2.1. It performs several energy conversions:

a) Turbine: kinetic energy of the wind → mechanical energy of the shaft
b) Generator: mechanical energy of the shaft → electrical energy at the stator level
c) Power converter: electrical energy at the stator level (variable frequency) → electrical energy at transformer primary (fixed frequency)
d) Transformer: electrical energy at the transformer primary (low voltage) → electrical energy at the transformer secondary (high voltage).

Note that we consider a direct-drive system, so there is no gearbox. An overview of the turbine and nacelle is shown in Fig. 2.2. The power converter is a back-to-back converter made of two 2-level voltage source converters (VSC) and a DC link capacitor. The foundation is a floating Tension Leg Platform (TLP) as shown in Fig. 2.3.

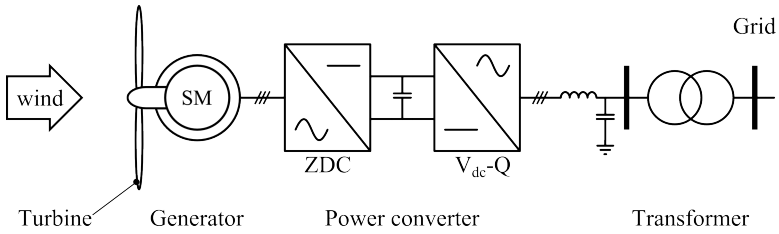

Figure 2.1: Wind energy conversion system overview.

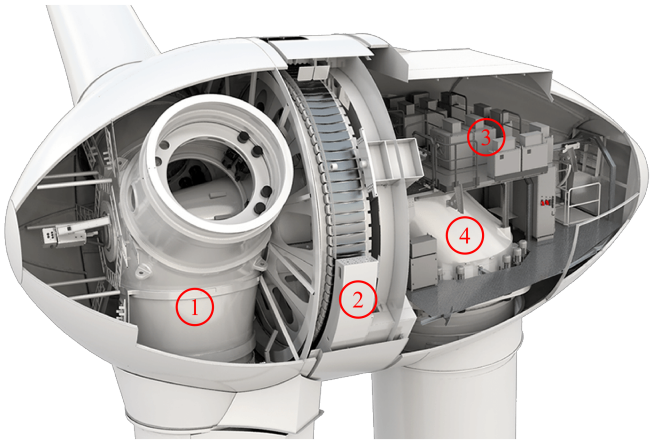

Figure 2.2: Enercon's turbine and nacelle with a direct-drive system [139]. (1) hub, (2) generator, (3) power converter, (4) bed-plate.

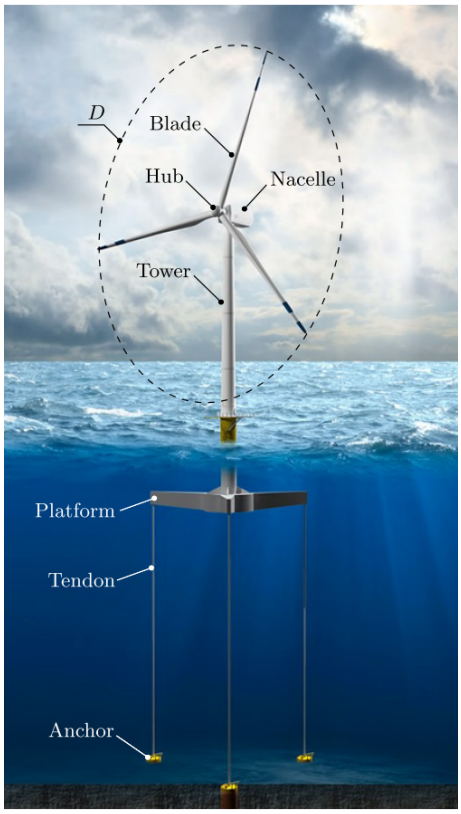

Figure 2.3: Wind turbine on a floating tension leg platform. Reproduced from [29]

This system includes 4 parts that are shown in Fig. 2.4. The turbine part includes 4 types of components: blade, hub, shaft and bearing. The nacelle part includes 6 types of components: generator,

power converter, AC filter, protections, bed plate and nacelle cover. The tower part includes 4 types of components: tower, 3-phase AC cable, transformer and grounding. The foundation part includes 3 types of components: platform, tendon and anchor.

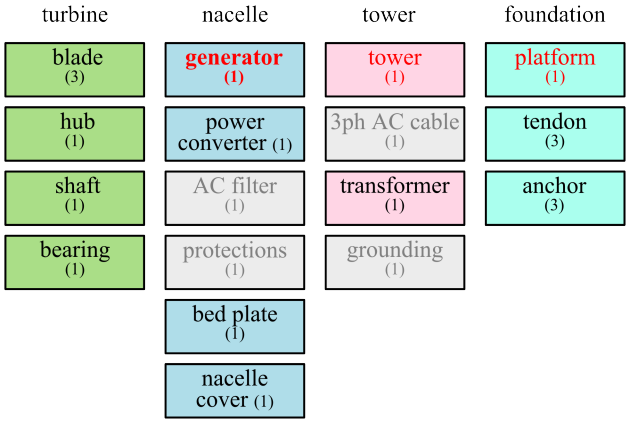

Figure 2.4: Wind energy conversion system components. The numbers in parenthesis indicate the number of such component in the system. The components in red font are directly impacted by the technology shift. The components in gray block are not considered in the following analysis.

To give an idea of the order of magnitude of the quantities involved, we consider the set of parameters of the EolSupra20 project [p11] that are summarized in Table 2.1.

Table 2.1: Wind energy conversion system parameters

Parameter	Symbol	Value	Notes
Nominal 3-ph power	P_n	20 MW	-
Nominal voltage	U_n	3.3 kV	L-L RMS
Nominal generator speed	rpm	6.3 rpm	-

2.3 A conventional technology: the permanent magnet synchronous generator

Direct drive multi-MW generators are typically permanent magnet synchronous generators (PMSG). For the sake of discussion, we consider here a PMSG topology that has surface-mounted permanent magnets and a double layer stator winding. Such design is advantageous for direct-drive wind generators in terms of weight, cost, and torque ripple [115, 116, 117, 118]. The generator electromagnetic parameterized design is shown in Fig. 2.5.

2.4 An innovative technology: the fully superconducting synchronous generator

2.4.1 Innovation

To reduce the weight of the nacelle, it has been proposed to use high-temperature superconducting synchronous generators (SCSG) [119, 120, 121]. Indeed, the high current density of the superconducting coils allow for a lighter and more compact design than what can be done with copper coils, or permanent magnets [122, 123]. But the additional cost of using a superconductor must be offset by a gain on the cost of the tower and foundations (fixed or floating) [129].

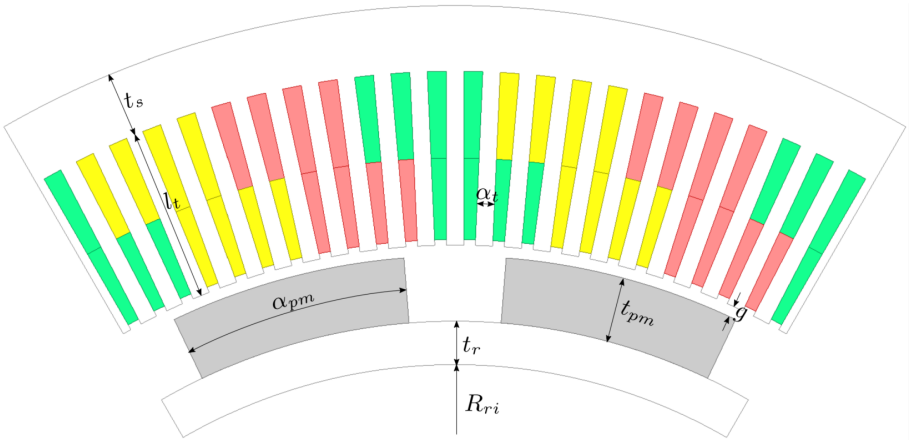

Figure 2.5: PMSG electromagnetic parameterized design.

2.4.2 Description

Numerous conceptual designs for multi-MW wind turbine SCSG have been proposed [121, 130, 131, 127, 132, 133, 134, 135]. They differ on the machine type (synchronous, asynchronous, etc.), the partial or full use of superconducting windings or bulks, the superconductor type (BSCCO, ReBCO or MgB2), etc.

For the sake of discussion, we detail here the 2018 base design of the EolSupra20 generator [p11]. This is a fully superconducting synchronous generator with MgB2 high-temperature superconductor used for both rotor and stator windings.

Cryogenic System Design

The adopted cryogenic system is shown in Fig. 2.6. A design with warm iron and two separate cryostats is selected. The stator cryostat is static, while the rotor cryostat is rotating. A copper electromagnetic shield is placed in between to prevent high-frequency harmonics coming from the stator windings [p2]. In order to reduce the radiation heat load, a radiation shield and a multi-layer insulation (MLI) are installed between the windings and the vacuum walls of the cryostats.

The use of two cryostats simplifies the cryostat design, but it requires a larger magnetomotive force because the magnetic air-gap length is larger than the one that would be obtained with a single cryostat. In addition, the system reliability is improved as any failures occurring in one cryostat system will not affect the other one. Two-stage cryocoolers are selected. The first stage operates at 55 K and is connected to the radiation shield. The second stage is connected to the windings. The operating temperature of the rotor windings is set to 10 K to maximize the DC field. The temperature of the stator windings is set to 20 K to mitigate the effect of the AC losses.

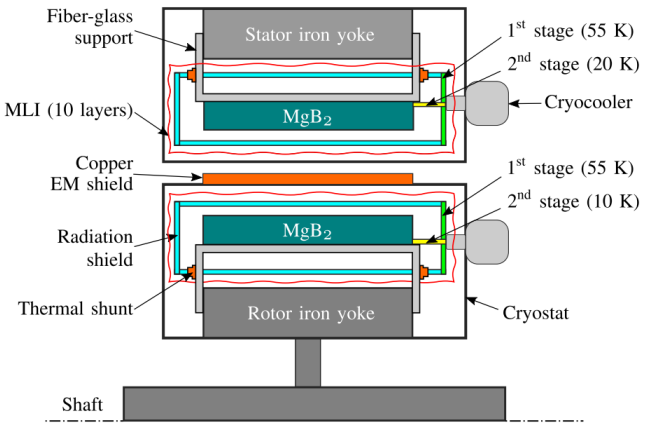

Figure 2.6: EolSupra20 cryogenic design.

Windings Design

The MgB2 conductors are different for the rotor and stator. The rotor windings are double-layer racetrack coils (DLRC). The coils are wound with MgB2 tapes which dimensions correspond to a commercially available conductor from Columbus Superconductors (Fig. 2.7(a)).

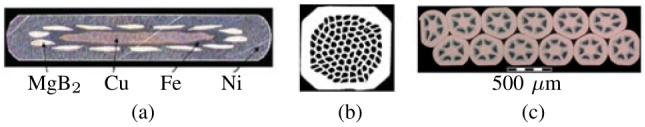

Figure 2.7: Cross section of MgB2 wires and cable. (a) MgB2 tape with 14 filaments by Columbus Superconductors for the rotor windings. (b) MgB2 wire with 91 filaments for the stator windings, reproduced with permission from [140]. (c). A Rutherford cable with two layers of MgB2 wires manufactured by HyperTech Research, reproduced with permission from [141].

The stator windings are double-layer racetrack coils (DLRC). The coils are wound with Rutherford cable made of MgB2 conductors. The advantages of such a cable are high current-carrying capability and low AC losses. Although not yet commercially available, such cable has already been manufactured by Hyper Tech, Inc. (Fig. 2.7(c)) [141]. In order to further reduce the superconductor AC losses (see section 3.5.5), MgB2 conductors with a high number of filaments are used (Fig. 2.7(b)).

Electromagnetic Design

The generator electromagnetic parameterized design is shown in Fig. 2.8. The use of toothless rotor and stator iron cores simplifies the cryostat design with the advantage of reducing the iron loss, the generator mass, and the torque ripple. The large magnetic air-gap is somehow compensated by the large magnetic field that the HTS coils can generate (several tesla).

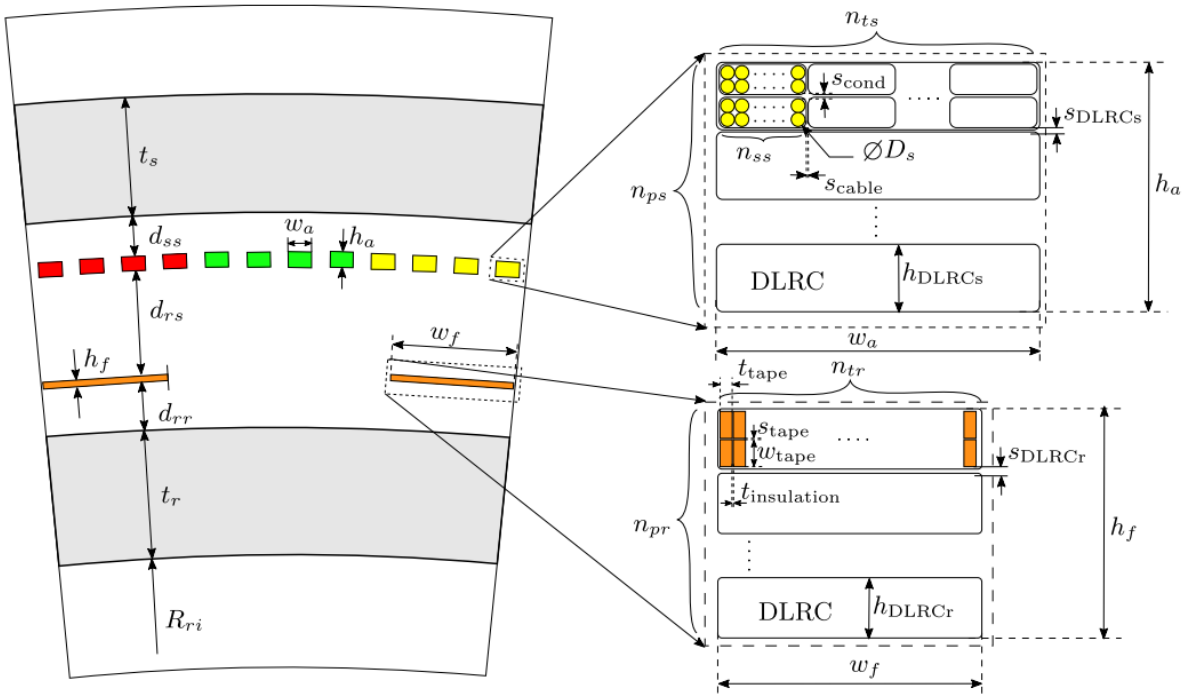

(a)

Figure 2.8: EolSupra20 electromagnetic parameterized design.

2.4.3 State of the art

State of the art on superconducting motors and generators can be found elsewhere [125, 126]. We mention here only the main projects dealing with wind turbine SCSG in Europe:

Ecoswing (2015-2019) [136] focused on the experience gained by the realization of a 3.6 MW demonstrator. Using ReBCO conductor for the rotor winding and copper for the stator windings (partical HTS machine), the machine external diameter decreased from 5.4 m (PMSG) to 4 m. The EcoSwing generator showed a 25% weight reduction compared to the PM generator of the same diameter. It has been assembled and installed on an existing wind turbine tower in Denmark. It produced power during +650 h, reaching 3 MW, but the converter limit was exceeded.

INNWIND (2012-2017) [112] compared many technical solutions for 10 and 20 MW machines, including superconducting machines using ReBCO and MgB2 [127]. They concluded on the excessive cost of ReBCO and on the lower efficiency of MgB2 at 10 MW compared to an innovative magnetically coupled gearbox.

Suprapower (2012-2017) led by Tecnalia [128] considered a 10 MW generator with only the rotor in MgB2. Difficulties in implementation slowed down the project. Only two coils out of the 4 planned for prototype were realized at the end of the project (May 2017) and without the test of the rotating "machine".

2.5 Contributions

2.5.1 EolSupra20

As part of the EolSupra20 project (GeePs, DACM, SATIE), we are studying the feasibility of a 20 MW direct drive fully superconducting synchronous generator (both the rotor and stator windings are superconducting). A first originality is to consider an HTS dynamo for the rotor winding excitation (see section 6.2.1). A second originality is to use magnesium diboride (MgB2). Previous studies often focused on BSCCO or ReBCO conductors, which have the advantage of allowing the use of liquid nitrogen at 77 K but suffer from high costs (they are currently more expensive by 2 orders of magnitude than copper for the same current transported). MgB2, discovered in 2001, seems to be a good alternative. On the one hand, if its production becomes significant, its cost should converge towards the one of NbTi. And its performance already makes it possible to envisage designs at temperatures between 10 K and 20 K [127, 128]. On the other hand, with a critical temperature of 39 K, one cannot use liquid nitrogen but operation without helium is possible.
The objectives of this feasibility study are:

1. Define a suitable generator topology.
2. Estimate the levelized cost of electricity ($LCOE$)
3. Optimize the generator to minimize its $LCOE$.

Define a suitable generator topology

Considering the fact that a MgB2 generator has not yet been demonstrated, we made strong conception choices to reduce the risks. The goal was to propose a design that could be built in the near future. The selected topology has been described above in section 2.4.2.

Estimate the $LCOE$

To estimate the $LCOE$ of a SCSG-based wind energy conversion system, one needs to calculate the initial expenses (tower, foundations, superconductor length), the operating expenses (cooling power) and the net electricity production. We proceed in 3 steps [p11, ic17]:

1. We break down the system into components (Fig. 2.4).
2. For the generator, for which no data is available, we use a circuit coupled 2-D finite element model (FEM) (Fig. 2.9) to calculate the performance indicators: mass, losses, etc.
3. For the other components, for which data is available, we use scaling laws to obtain the masses and the costs. The power electronics loss is calculated by using a scaling law too [175, p.3, eq.(3)].

Note that the use of scaling laws is a common approach to size and estimate the cost of commercially available components. It avoids all the problems that would arise from the multi-physics design and optimization of each component of the system. Plus it inherently takes financial and social aspects into account (e.g. profit margin, or eco-contribution). It has extensively been used in the wind turbine community [177, 178, 179].

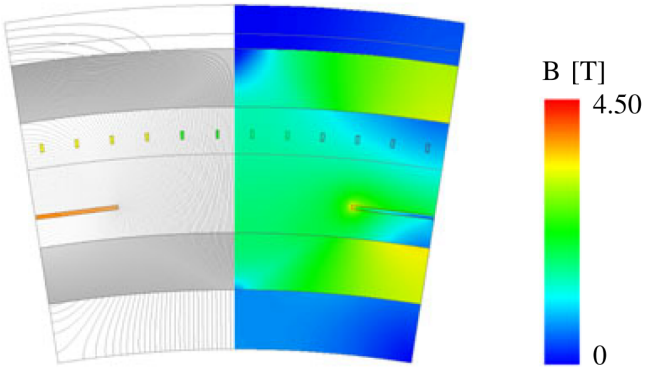

Figure 2.9: Magnetic field distribution of one pole of the EolSupra20 2018 base design (ANSYS Maxwell FEM package).

Optimize the generator

We developed a methodology to optimize the generator with the goal of minimizing the *LCOE*. We argue that this is more adapted that the common approach consisting in minimizing only the generator cost. It makes it possible to account for the impact of the technology change on the whole system, and to compare several technical options. Results are reported below in section 2.6.

Credits

The EolSupra20 project is carried out in collaboration between the laboratory GeePs (CNRS, CentraleSupelec, Univ. Paris-Sud, Sorbonne Univ.), the DACM (CEA Saclay) and the SATIE laboratory (CNRS, Univ. Cergy-Pontoise). The 2018 base design of the EolSupra20 generator was obtained by Trung-Kien HOANG [P1], with the support of the Labex LaSIPS. Many students were involved at different steps (see chapitre 8). The results have been published in [p40, p11, ic21, ic17]. The project has been featured in IEEE spectrum (link).

2.5.2 Current sheet model

The optimization of the EolSupra20 generator was carried out by coupling a 2D magnetostatic finite element model with a stochastic optimization algorithm. This is an accurate but lengthy design method, the finite element model being inherently computing-intensive. To reduce the computing time, a semi-analytical model is being developed: the current sheet (CS) model.

The CS model belongs to the family of "subdomain models" ie. it is based on the formal resolution of Maxwell's equations in each subdomain [142, 143]. Its distinctive feature is to divide the machine into annular subdomains and to model the windings as cylindrical current sheets (Fig. 2.10). The Laplace's equation for the magnetic vector potential $\mathbf{A}$ can then be solved analytically in each subdomain by the classic method of the separation of variables using appropriate boundary and interface conditions. Hugues and Miller pioneered this method in 1977 [144, 145]. At the time, they obtained concise analytical formulas for the field in the rotor core, air gap, stator core and air surrounding the machine. The method was later extended to add the shaft [146, 147, 148], the current sheets space harmonics [149] and the winding thickness [150]. Finally an iterative technique was introduced by Yazdanian *et al.* [146, 147] to account for the nonlinearity of the iron. Despite those improvements, the latest models could not include directly several windings at the same time nor account for the rotation of the rotor.

We tackled this problem by expressing the current sheets not only as a classic sum of sines but as a sum of both sines and cosines. As a result, the proposed model can naturally include both the rotation of the rotor field winding and the time-dependent stator armature windings currents. Being generic and

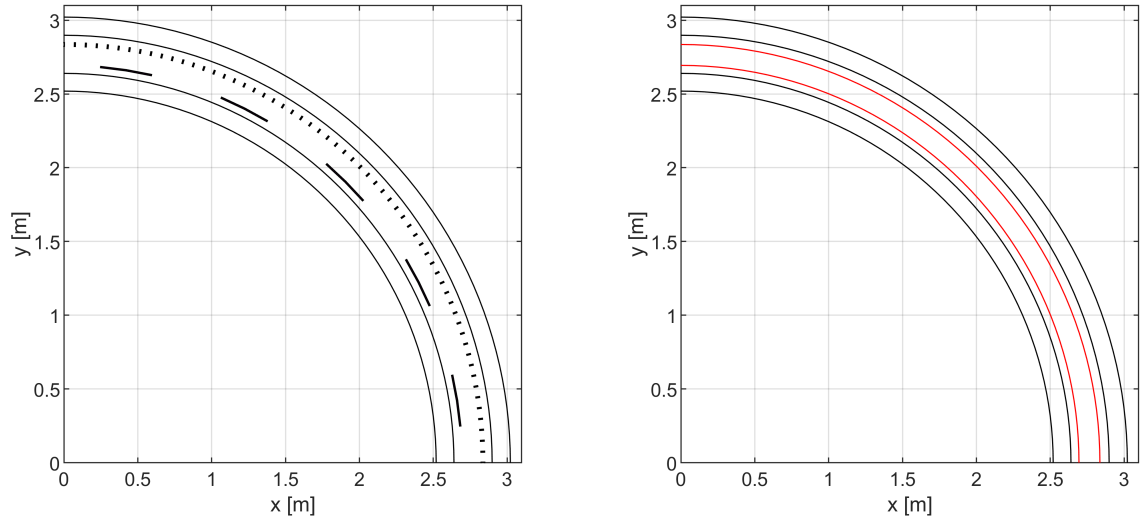

(a) Specific geometry ($\alpha = 0°$)

(b) Generic geometry

Figure 2.10: EolSupra20 2018 base design (a) specific geometry and (b) the corresponding current sheet model geometry. The current sheets are drawn in red.

explicit, the implementation of the resulting system of equations is straightforward [p24]. In addition, an iterative scheme inspired from [146, 147, 151] is used to take into account the nonlinearity of the iron.

Because of its underlying modeling hypotheses, the CS model is naturally adapted to slotless wound rotor electrical machine, such as the EolSupra20's machine. For illustration purpose, we consider here EolSupra20 2018 base design. The result of the CS model are compared to a nonlinear 2-D finite element (FE) model carried out in COMSOL Multiphysics in Fig. 2.11. The agreement between the CS model and the FE model is good, despite the strong saturation of the machine (Fig. 2.9). This validates our implementation of the CS model. Similar agreements were reported for another machine in [p24]. The discrepancy is mainly attributed to the impossibility of modeling the azimuthal variation of the permeability with the CS model. The computation time for the nonlinear current sheet model is roughly 100 ms per iteration, ≤ 15 iterations on an i7-5600 CPU @2.60 Ghz, 16 GB RAM. This is about 5 times faster than the nonlinear FE model, using symmetries to reduce the mesh.

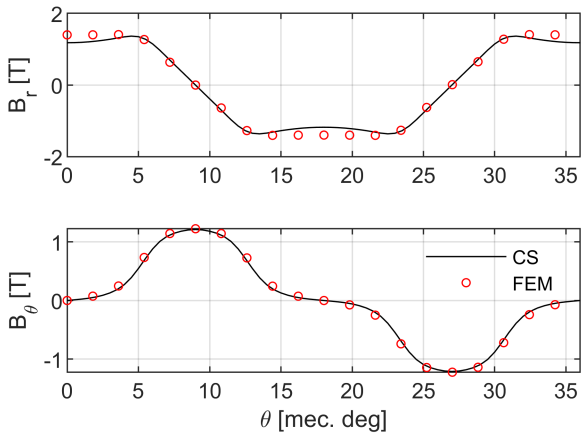

Figure 2.11: Comparison of the air-gap (top) radial and (bottom) azimuthal components of the magnetic flux density for the current sheet (CS) model and the finite element (FE) model (EolSupra20 2018 base design, no load case).

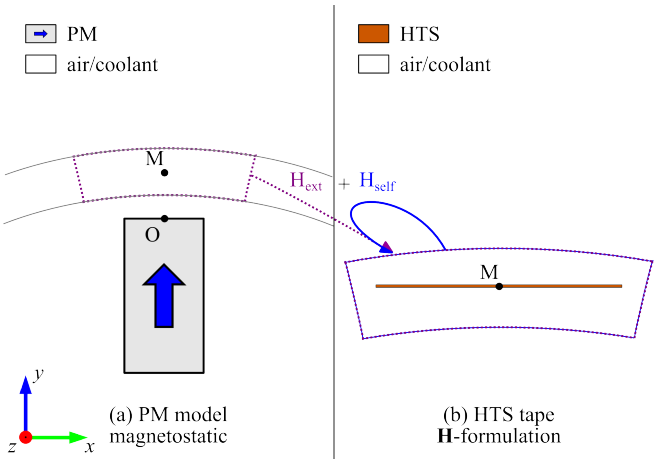

Figure 2.12: Segregated finite-element model for the simulation of an HTS dynamo-type flux pumps: (a) magnetostatic PM model, (b) time-dependent H-formulation HTS wire model.

Credits

The work on the CS model started during the postdoc of Jiling GUO (China Scholarship Council NO. 201707005056, 2017) with the help of Frederic TRILLAUD (UNAM). It is being continued in collaboration with Bastien ROUCARIES (SATIE) and Kien HOANG (Univ. of Science and Technology of Hanoi). Many students were involved at different steps (see chapitre 8). The results have been published in [p24, ic33]. The model is freely available here (BSD-3-Clause license): `https://github.com/lqueval/CS`.

2.5.3 HTS flux pump

A superconducting coil is usually fed by a current source, located outside of the cryostat, via current leads. These feeding method is mature and reliable, but it has drawbacks in terms of weight and losses. A significant fraction of the cooling load of the EolSupra20 base design is actually attributed to the rotor current lead losses (see Table 2.5) [p11].

The HTS flux pump [152, 153, 154] is a promising device to overcome these drawbacks. It can inject large DC supercurrents into a closed superconducting circuit without current leads. It could be used, for example, to energize the field coil of superconducting rotating machines without the need for current leads [155, 156]. This could be a game changer to develop practical superconducting machines. This is what motivated our interest for this technology.

Despite the extensive experimental work carried out to date by other groups, comprehensively understanding the underlying physical mechanism of the HTS dynamo-type flux pumps has proved challenging. A number of different explanations have been proposed to explain this mechanism [158, 159, 160, 161, 162, 163, 164, 165], but quantitatively accurate, predictive calculations have been difficult. It was shown recently in Mataira *et al.* [166] that the open-circuit voltage can be explained well – most importantly, with good quantitative agreement – using classical electromagnetic theory. The DC output voltage obtained from an HTS dynamo arises naturally from a local rectification effect caused by overcritical eddy currents flowing within the HTS wire [157, 158, 159, 160, 166]: a classical effect that has been observed in HTS materials as far back as Vysotsky *et al.* [167].

To further examine and explain the experimental results, as well as optimize and improve flux pump designs, we developed a "segregated H-formulation finite element model". This is a direct adaptation of the model developed in collaboration with Guangtong MA (TPL, Southwest Jiaotong University) to simulate superconducting magnetic bearings for maglev vehicle applications [p13]. The segregated H-formulation model is comprised of a magnetostatic PM model and a time-dependent **H**-formulation HTS tape model. The former is coupled unidirectionally to the latter by applying the sum of the applied field H_{ext} and the self-field H_{self} as a Dirichlet boundary condition on the outer boundary of the **H**-formulation model (Fig. 2.12). To mimic the rotation, H_{ext} is obtained by rotating the field of a static permanent magnet. The self-field H_{self}, created by the supercurrent flowing in the HTS wire, is calculated at each time step by numerical integration of the Biot-Savart law over the HTS subdomain. This avoids the need to model the rotating PM (e.g., using a moving mesh), and also significantly reduces the number of mesh elements in the HTS model.

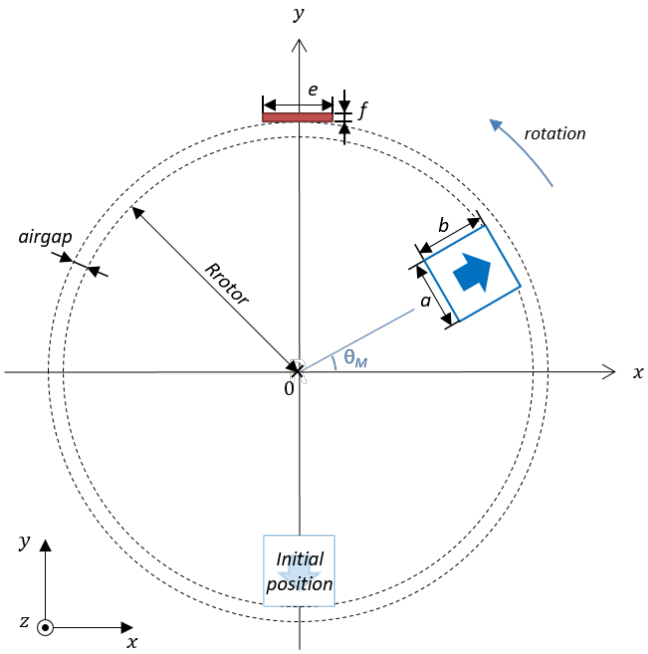

Figure 2.13: Geometry of the HTS dynamo benchmark [p29]. A permanent magnet (PM) rotates anti-clockwise past an HTS tape.

A number of different numerical models have since been published [168, 169]. To compare them, we participated to the definition of a benchmark for the HTS modeling community: the HTS dynamo [p29]. Its geometry is shown in Fig. 2.13. This benchmark has been solved by several groups using different methods: coupled H-A formulation, H-formulation + shell current, segregated H-formulation, minimum electromagnetic entropy production (MEMEP), coupled T-A formulation, integral equation, volume integral equation-based equivalent circuit. Our segregated H-formulation model proved effective when compared to other methods.

Credits

The segregated H-formulation finite element model was initially developed to simulated superconducting magnetic bearings for maglev vehicle applications [p6]. The development and experimental validation was made possible thanks to the extensive work carried out by the team of Guangtong MA at SouthWest Jiaotong University, China. I visited his laboratory several times and built a strong collaboration that led to several communications [p37, p28, p27, p23, p20, p13, p9, ic49, ic36, ic29, ic27, ic26]. The adaptation of the model to the HTS dynamo benchmark has been developed in collaboration with Mark AINSLIE (Univ. of Cambridge). The results have been published in [p34, p31, p29, ic47, ic46, ic42, ic41, ic34].

2.6 Levelized cost of electricity ($LCOE$)

The concept of levelized cost per unit has been widely used to compare the economic competitiveness of various power generation technologies. In that specific context, it is often called "Levelized Cost Of Electricity" ($LCOE$). It represents the average revenue per unit of electric energy produced over the system lifetime required to break even. And it is often expressed in euro per megawatt hour [€/MWh].

Under the hypothesis of section 1.2.5, the $LCOE$ is expressed from (1.8) as,

$$LCOE = \frac{\sum_{t=0}^{T} \frac{CAPEX_t + OPEX_t}{(1+r)^t} - SV}{\sum_{t=1}^{T} \frac{EP_{net,t}}{(1+r)^t}} \tag{2.1}$$

where $CAPEX_t$ is the capital expenses in year t, $OPEX_t$ is the operating expenses in year t, r is the discount rate, $EP_{net,t}$ is the net electric energy produced in year t, T is the system lifetime and SV is

the salvage value.

2.7 A techno-economic assessment of fully superconducting wind turbine generators

2.7.1 Goal and scope definition

Goal: In this section, to complete the discussion, we propose an abbreviated techno-economic assessment of fully superconducting wind turbine generators. We compare an installation using a conventional permanent magnet synchronous generator (PMSG) and an installation using a fully superconducting synchronous generator (SCSG).

Case study: We consider the EolSupra20 case study *et al.* [p11]. The system is a 20 MW wind energy conversion system (WECS) installed on a floating platform. The $LCOE$ is calculated considering only one turbine. As a result, EP_t corresponds to the gross annual energy production (gross AEP). Accounting for the wake effect and the collection and export electrical system losses would give the net annual energy production (net AEP). The parameters of the test case are summarized in Table .

Table 2.2: WECS parameters for $LCOE$ calculation

Parameter	Symbol	Value	Notes
Nominal 3-ph power	P_n	20 MW	-
Nominal voltage [L-L RMS]	U_n	3.3 kV	-
Nominal generator speed [rpm]	rpm	6.3	-
Turbine cut-in wind speed	V_{in}	3 m/s	
Turbine nominal wind speed	V_n	11.4 m/s	
Turbine cut-out wind speed	V_{out}	25 m/s	
Tip speed ratio	TSR	7	[172]
System lifetime	T	20 years	[180, 181, 182]
Discount rate	r	0.1	
Salvage value	SV	0	unknown [173]

Scenario: The wind is not constant and therefore the WECS output power is variable. To account for this, we consider a Weibull distribution having a mean wind speed of 9.7 m/s [171] and a shape parameter equal to 2. EP_t is then assumed to be constant over the years [174].

Optimization problem: We look for the generator sizing that minimizes the $LCOE$. The optimization problem is formulated as [p11],

$$\begin{aligned} \underset{X}{\text{minimize}} \quad & LCOE(X) \\ X = & \{n_{tr}, n_{pr}, J_f, n_{ss}, n_{ts}, n_{ps}, p, L_a, R_{ri}, t_r, t_s\} \\ \text{subject to} \quad & P \geq P_n \\ & U = U_n^{\pm 5\%} \\ & J_f \leq 0.8 J_{cf} \quad \text{at} \ \max B_f \\ & J_a \leq 0.8 J_{ca} \quad \text{at} \ \max B_a \\ & R_{DLRCr} \geq R_{min} \end{aligned} \tag{2.2}$$

where the optimization variables X are (Fig. 2.8): the number of turns (in series) per rotor DLRC (distributed in 2 layers) n_{tr}, the number of DLRC (in series) per rotor winding n_{pr}, the current density in the field's filament J_f, the number of conductor (in parallel) in the Rutherford cable (distributed in 2 layers) n_{ss}, the number of turns of Rutherford cable (in series) per stator DLRC (distributed in 2 layers) n_{ts}, the number of DLRC (in series) per stator winding n_{ps}, the number of pole pairs p, the stack length L_a, the rotor core inner radius R_{ri}, the rotor core thickness t_r, the stator core thickness t_s. P_n is the

nominal output power and U_n is the nominal phase-phase armature voltage. Note that in addition to the constraints on the electric output power P and on the phase-phase armature voltage U, there is a specific set of constraints that depends on the adopted topology and material. The current densities in the field and armature windings must be smaller than the minimum local critical current densities (J_{cf} and J_{ca}) with a 20% current margin. The minimum local critical current densities depend on the local maximum magnetic flux densities (B_f and B_a). Additionally, the last constraint on R_{DLRCr} ensures that the minimum bending radius of the rotor conductor R_{min} is respected. A similar optimization problem is formulated for the PMSG.

2.7.2 Inventory analysis

The system elements are shown in Fig. 2.4. Details about the technical and economic parameters can be found in [p40, p11, ic17].

Benchmark product system: For the permanent magnet synchronous generator (PMSG), we consider a surface-mounted PMSG with double layer stator winding (see section 2.3). The main parameters are summarized in Table 2.3.

Table 2.3: PMSG model parameters

Symbol	Description	Value
q	Number of slots per pole per phase	4
B_r	PM remanent flux density	1.1 T
k_p	Pitch factor	5/6

Proposed product system: For the superconducting synchronous generator (SCSG), we consider a fully superconducting synchronous generator with MgB2 rotor and stator windings (see section 2.4). Note that we use estimates of future technical and economic parameters of MgB2 conductor for this analysis. The main parameters are summarized in Table 2.4.

Table 2.4: SCSG model parameters

Symbol	Description	Value
q	Number of slots per pole per phase [-]	4
w_{tape}	Rotor MgB2 tape width [mm]	3.65
t_{tape}	Rotor MgB2 tape thickness [mm]	0.65
D_s	Stator MgB2 conductor diameter [mm]	0.8
d_{rr}	Distance between outer rotor yoke surface and inner rotor winding surface [mm]	50
d_{rs}	Distance between outer rotor winding surface and inner stator winding surface [mm]	125
d_{ss}	Distance between outer stator winding surface and inner rotor stator yoke surface [mm]	50

2.7.3 Calculation of indicators

We use the technical and economic models presented in section 2.5.1. The optimization is performed by using the multi-objective Particle Swarm Optimization (MOPSO) algorithm [217] with 500 particles and 30 iterations. With a workstation equipped with Intel Xeon 4 core, 3.5 GHz and 16 GB of RAM, one single optimization takes ˜48 hours.

The main parameters of the optimal solution are summarized in Table 2.5. The optimal $LCOE$ for the SCSG-based WECS is 140 $/MWh, to be compared to a $LCOE$ of 152 $/MWh for the conventional PMSG-based WECS. The obtained optimal generator constitutes the EolSupra20 2018 base design [p11]. A detailed analysis shows that thanks to its high power density, the SCSG is not only lighter but cheaper [p40]. Its low weight helps in turn to reduce the turbine top head mass together with the cost of the tower and foundation. This indicates that, for this case study, the SCSG-based WECS could be a competitive solution.

But the results highlighted that, at this stage of the study, a large number of cryocoolers would be required making this solution impractical (Table 2.5). This problem is expected to be mitigated along

with the development of the cryocooler technology. In future works, a thorough consideration of AC losses and cryogenic requirements is needed to solve this problem.

Table 2.5: EolSupra20 2018 base design [p11]

Symbol	Description	Value
	Rotor winding	
-	MgB2 conductor length [km]	37
$J/J_c^{(*)}$	Current density in filaments [A/mm^2]	2276/3294
$\max B_f$	Max. magnetic flux density [T]	4.01
-	First stage (55 K) losses [W]	268
-	Second stage (10 K) losses [W]	37
-	Nb of cryocoolers [-]	8
	Stator winding	
-	MgB2 conductor length [km]	104
$J/J_c^{(*)}$	Current density in filaments [A/mm^2]	3165/4212
$\max B_a$	Max. magnetic flux density [T]	1.72
-	First stage (55 K) losses [W]	929
-	Second stage (20 K) losses [W]	1291
-	Nb of cryocoolers [-]	77
	Machine geometry	
U	Phase-phase voltage [kV rms]	3.2
P	Output power [MW]	20
r_6	Outer stator yoke radius [m]	3.01
M_{gen}	Active and inactive mass [kg]	167512
	Economics	
C_{gen}	Generator cost [$M]	5.81

2.7.4 Interpretation

We would like to use this case study to show how the LCpu can help illustrate a fundamental characteristic of many technical systems. Let's perform the same optimization for different turbine nominal power P_n: from 2 MW to 23 MW with a step of 3 MW. The calculation took 32 days for the two generators and the 8 different nominal power. The results are shown in Fig. 2.14. Note that the model has been improved in between, so the results are slightly different from above paragraph at 20 MW. For each technology the $LCOE$ first decreases with the turbine nominal power then increases. The decreasing trend in the small power region (<7 MW for PMSG) is due to some capital expenses which are independent of P_n. This is the reason why commercial wind turbines are getting bigger and bigger. The increasing trend in the high power region (>15 MW for PMSG) is caused by some components that become particularly heavy. Among them, the blades have a mass that increases rapidly with P_n [ic17]. As a results of this trend, there is an optimal P_n that minimize the $LCOE$ for each technology. It is about 11 MW for PMSG-based WECS, and 17 MW for fully SCSG-based WECS. As a result of these trends, SCSG-based WECS could be more competitive in terms of $LCOE$ than PMSG-based WECS for wind turbines having a nominal power higher than 5 MW.

Beyond the numbers (which are necessarily debatable - see section 6.1.4), the shape of the $LCOE$ curves is probably the most interesting result of this study. We expect to observe similar V-shaped curve for many electrical systems. Below a given power range, fixed costs tend to increase the LCpu. In a given power range, the material is well used and the function is maximized: the LCpu is minimized. And above that power range, technical constraints tend to increase the LCpu. But a technological innovation can "shift" the V-shaped curve. Further research is required to test the hypothesis.

2.8 Summary and Perspectives

In this chapter, we described the work that has been carried out on the techno-economic assessment of superconducting machines for floating offshore wind energy conversion systems. Our efforts have been focused on developing models and tools to study this system.

The results show that the SCSG could be a competitive solution for multi-MW wind turbines. And some challenges were highlighted: cooling system, AC losses, computing time, etc. We shall be dealing

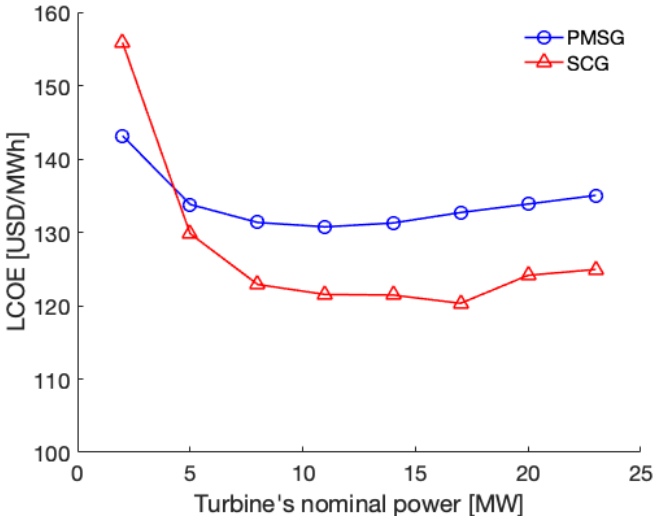

Figure 2.14: Comparison of the optimal $LCOE$ of PMSG- and SCSG-based WECS [p40].

with them over the next few year, with the goal of proposing an updated EolSupra20 base design after that.

It will be challenging to build and commercialize multi-megawatt superconducting wind turbine generators, but with the continuous improvement of superconductors and cryocoolers, such system is likely to grow as a stronger candidate for wind energy and for other applications (electric ship, electric aircraft, maglev train, etc.). Our tools could be adapted to assess the techno-economic potential of these systems.

Chapter 3

Superconducting cables for HVAC underground cable transmission systems

3.1 Context

Most electricity is sent, from power plants to end consumers, first through high voltage transmission lines over long distances and then through medium and low voltage distribution lines over shorter distances. As it moves through that network, some of the energy is lost en route. As a result, only part of the electricity generated reaches the consumers as usable power.

From one country to another, the amount of losses varies considerably. Following Surana and Jordaans [30], "In 2016, aggregate transmission and distribution losses reached 19% in India and 16% in Brazil. But they were over 50% in Haiti, Iraq, and the Republic of Congo. [...] In more developed countries, losses were lower: While the United States experienced 6% losses in 2016, 5% was reported for Germany and Singapore reached 2%."

Greenhouse gas "compensatory emissions" result of the extra electricity required to compensate for transmission and distribution grid losses. Annual compensatory emissions amount to nearly a billion tons of CO2 equivalents worldwide. This is in the same range as the annual emissions of the heavy trucks transport or the chemical industry (Fig. 3.1). Surana and Jordaans [30] surveyed 142 countries, and determined that ∼500 million tons of CO2 could be avoided by improving the efficiency of their transmission and distribution systems. But surprisingly, few countries included transmission and distribution losses in their commitments to reduce their emissions as part of the 2015 Paris Agreement.

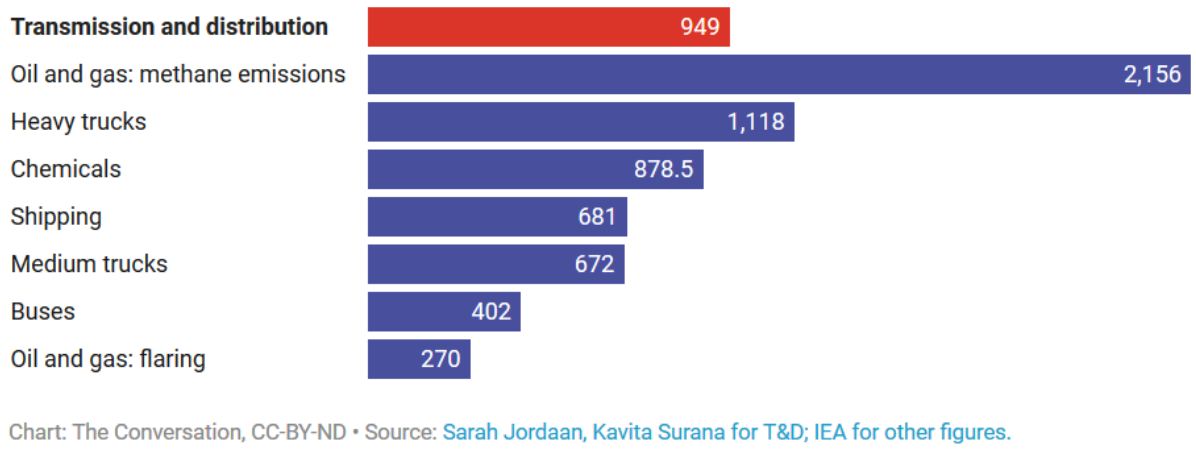

Figure 3.1: Comparison of the annual emissions due to the transmission and distribution grid losses and from some industries [30]. Measured in millions of metric tons of carbon dioxide equivalents.

On the one hand, addressing nontechnical losses is not a straightforward task. This is because their

causes are diverse and often difficult to quantify: hurricanes, war, weak governance, corruption and poverty, etc. On the other hand, technical transmission and distribution losses can be addressed by upgrading existing infrastructure and deploying innovative technologies.

For example, at the transmission level, part of the upgrade is being done using underground cable systems. If today, one generally uses resistive cables; innovative technologies such as high-temperature superconducting (HTS) cables are being tested. They are still at the development stage but they could become competitive solutions.

In this chapter, we describe the work that has been carried out on the techno-economic assessment of HTS cables for high voltage alternating current (HVAC) underground cable transmission systems.

3.2 Overview of an HVAC underground cable transmission system

Consider the HVAC underground cable transmission system shown in Fig. 3.2. The 3-phase overhead line (OHL) is installed on electricity pylons. The 3-phase underground cable (UGC) is installed in trenches. At the transition between the OHL section and UGC section, a "transition station" is needed (Fig. 3.3).

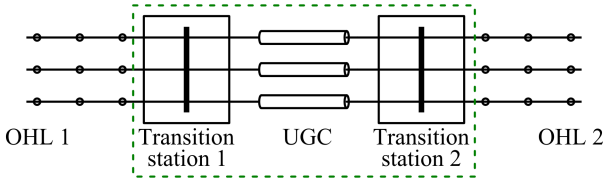

Figure 3.2: HVAC underground cable transmission system overview (OHL = overhead line, UGC = underground cable). The system boundary is delimited by the dotted green line.

Figure 3.3: Transition station of the Kassø-Tjele 400 kV HVAC transmission line in Denmark [74].

This system includes 2 parts that are shown in Fig. 3.4. The transition station part includes 3 types of components: infrastructure, termination and grounding. The underground cable (UGC) section part includes 4 types of components: 3-phase UGC, joint, trench and duct.

To give an idea of the order of magnitude of the quantities involved, we consider the set of parameters of the case study proposed by Kottonau *et al.* [71] and summarized in Table 3.1.

In this chapter, we make the following assumptions:

a) There are several power cable architectures. For high voltage levels, the single core cable configuration is normally used in multiple of 3 to obtain 3-phase systems.

b) For the HTS cable, we consider HTS conductors compatible with liquid nitrogen (LN2) cooling.

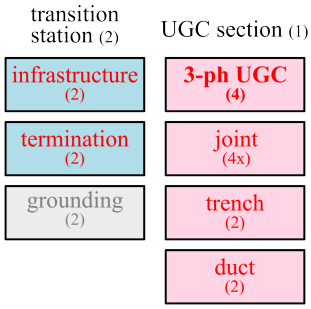

Figure 3.4: HVAC UGC transmission system components. The numbers in parenthesis indicate the number of such component in the system for the case study for conventional technology. The components in red font are directly impacted by the technology shift. The components in gray block are not considered in the following analysis.

Table 3.1: HVAC UGC transmission system parameters

Parameter	Symbol	Value
Nominal active power	P_n	4000 MW
Nominal voltage	V_n	380 kV L-L RMS
Nominal frequency	f_n	50 Hz
Cable length	L_{cable}	3.2 km

3.3 A conventional technology: the HVAC resistive cable

A resistive cable system consists of 2 main components: cable and accessories (joints and terminations). A typical 220 kV (L-N RMS) single core HVAC resistive cable is shown in Fig. 3.5. From the inner to the outer layer, it consists of the following layers:

- **Conductor**: It carries the current in normal and emergency operation. It consists of stranded soft copper or aluminium wires. A "circular compacted conductor" is made of wires wounded up and then compacted. A "segmental compacted conductor" typically consists of 4 to 6 segments made of compacted conductors. The later is usually used for cross-section $\geq$1000 mm^2 to reduce the AC resistance [73]. Protection against water and humidity can be achieved by using swelling powder, or yarns/tapes with water blocking property inside the conductor.
- **Conductor binder**: It fastens the conductor wires together, if required.
- **Conductor screen**: It homogenizes the electric field thus reducing the electric stresses on the conductor outer surface. It consists of an extruded thermoset semi-conducting material.
- **Insulation**: It isolates the flow of current by preventing direct contact between the conductor and the ground, and between conductors. The three main types of insulation are oil-filled cable, mass-impregnated cable and extruded cables [50].
- **Insulation screen**: It homogenizes the electric field thus reducing the electric stresses on the insulation outer surface. It consists of an extruded thermoset semi-conducting material.
- **Water blocking layer**: It prevents the water from penetrating the cable.
- **Metallic screen**: It withstands the required earth fault current during the required duration. It consists of copper or aluminium wires or lead alloy.
- **Longitudinal water blocking layer**: It prevents the screen from longitudinal water penetration. It consists of a non-conductive water blocking tape.
- **Radial water blocking layer**: It prevents the water from penetrating the cable. It consists of a copolymer aluminum tape.
- **Jacket**: It protects the cable from the surrounding mechanical or chemical corrosion. It consists of PE (LLDPE, MDPE, HDPE), PVC or LSOH material sheathed with a semi conductive layer (graphite coating or extruded material).

Note that the cooling is passive. There are many possible layout variations depending on the project requirements.

Figure 3.5: HVAC resistive cable: single core copper conductor, XLPE insulated, copper wire screen and HDPE sheath [73].

3.4 An innovative technology: the HTS cable

3.4.1 Innovation

Power cables is a self-evident application for high temperature superconducting (HTS) technology. The idea is to replace the resistive conductor by an HTS conductor to take advantage of the property of a superconductor to carry more current at near zero resistance.

3.4.2 Description

For the HTS conductor to be in its superconducting state, its must be kept at cryogenic temperature. This is done by placing it in a cryostat and using a cooling system to regulate the temperature. We consider here a cable core cooled with liquid nitrogen (LN2). An HTS cable system consists therefore of 4 main components: HTS cable core, line cryostat, accessories (joints and terminations) and cooling system. A typical single core HTS cable in its line cryostat is sketched in Fig. 3.6.

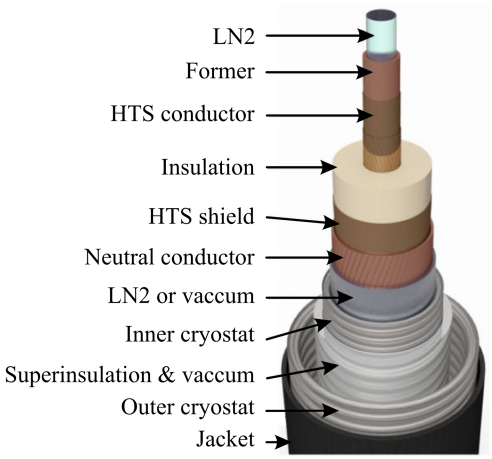

Figure 3.6: HVAC HTS cable: single core corrugated tube former cold dielectric LN2 cooled HTS cable (adapted from [89]).

HTS cable core

The HTS cable core performs the electrical functions (power transport, insulation, magnetic field shielding, neutral conductor). From the inner to the outer layer, it consists of the following layers:

- **Former**: There are several types of former [71]. We consider here a corrugated tube (CT) type. It serves three functions. First it acts as the mechanical support for the other layers. Second it allows the flow of LN2 inside the tube. Third, it may also carry part of the short circuit current.
- **HTS conductor**: It provides a path for the current in normal operation. The HTS conductor layer is composed of several sub-layers of HTS conductors. The conductors are mainly in form of tapes, either bismuth strontium calcium copper oxide (BSCCO) or yttrium barium copper oxide (YBCO). Each sub-layer is composed of several parallel HTS tapes of 2 to 12 mm of width wound around the former with a certain twist angle.
- **Insulation**: It provides electrical insulation between the HTS conductor layer and the outer layers of the cable core. It is often made of Polypropylene Laminated Paper (PPLP) or High-Density Polypropylene (Tyvek) [71].
- **HTS shield**: also called screen. It shields the magnetic field of the cable, therefore reducing the electromagnetic field outside the cable to zero. It is made of a single layer of HTS conductors.
- **Neutral conductor**: It is used both for structural support and as a pathway for currents in emergency operation. It is made of one or several layers of copper tapes.

There are many possible layout variations depending on the project requirements.

Line cryostat

The line cryostat is used for thermal insulation. The goal is to maintain the temperature of the cable core at the target operation temperature. It is usually made of five layers: inner cryostat, superinsulation, vacuum, outer cryostat, jacket. For flexible line cryostat, the inner and outer cryostats are made of corrugated tubes. The superinsulation is wrapped on the outside on the inner cryostat tube and consists of a few dozen layers of aluminum coated polyester foils [71]. The jacket is made of Polyethylene (PE). There are again many possible layout variations depending on the project requirements.

Joints and terminations

Joints are used to connect two HTS cable cores together, to form a long cable. Terminations are used to connect one HTS cable core at cryogenic temperature to the resistive cables at room temperature. Its function is to maintain the cable at its target operation temperature while transferring the current from the cable core to the grid using a current lead. It often connects to the liquid nitrogen pumping system as well. A schematic of this component is shown in Fig. 3.7.

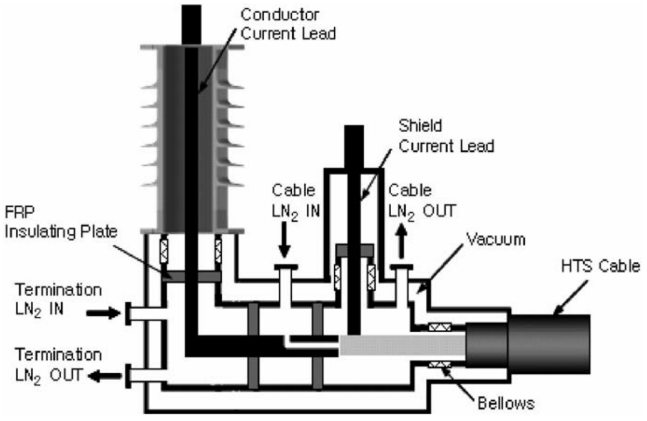

Figure 3.7: Termination of a single core HTS cable [75].

Cooling system

We assume here a liquid nitrogen (LN2) cooling system. There are several options [90]: open cooling systems evaporate LN2 to provide the cooling, whereas closed cooling systems use electricity to re-cool

LN2. Kottonau *et al.* [71] give a detailed explanation of the operation of the closed cooling system shown in Fig. 3.8. It consists of Turbo-Brayton cryocoolers for the primary circuit, and a LN2 tank for inital cool down and backup. For a 3-phase system, the "one-sided cooling concept" is quite common: the LN2 flows in through two phases and returns through the third one. The LN2 in the return path is warmer but the mass flow is doubled. For long cables, "two-sided cooling concept" and/or intermediate cooling stations may be required.

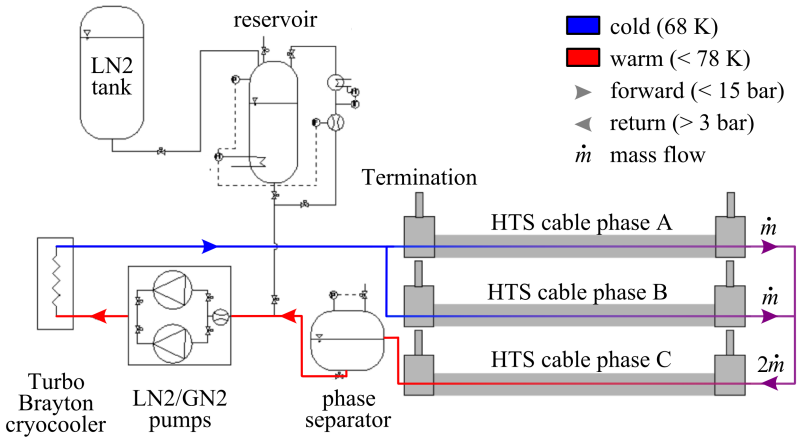

Figure 3.8: Simplified schematic of the cooling system of a LN2-cooled HTS cable system with one-sided cooling concept (adapted from [71]).

The role of the cooling system is to maintain specific temperature and pressure conditions, so that the LN2 remains liquid and circulates properly in the line cryostat. Here the minimum operating temperature is set at 68 K to avoid solidification of the LN2. The maximum temperature is set at 78 K and the minimum pressure at 3 bar to avoid boiling and possible electrical breakdown. The maximum pressure allowed on the inner and outer cryostat is 20 bar. Thus, the maximum operating pressure is set at 15 bar. The operation range is therefore limited by the blue area in Figure 3.9.

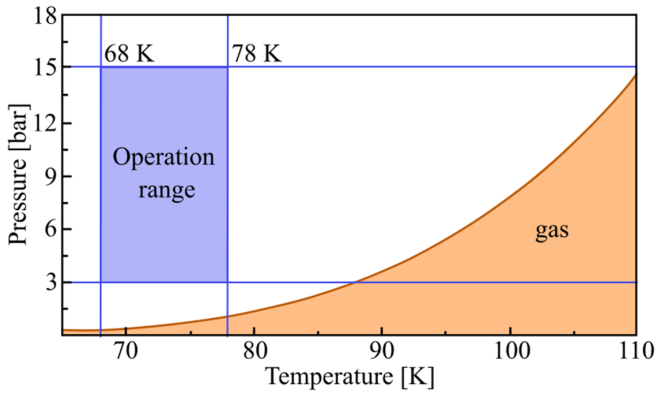

Figure 3.9: Operation range of a LN2-cooled HTS cable [B5].

3.4.3 Advantages and drawbacks

Advantages

- HTS cables have virtually zero resistance under DC condition, allowing theoretically for transmission systems without any Joule losses [76]. But HTS cables show some dissipation under AC conditions...
- HTS cables are able to carry several times the current of a resistive cable having the same outer dimension. It provides a competitive solution for grid upgrade in dense areas.

- For bulk power transmission, the conventional solution is to use a transformer to go from medium to high voltage in order to keep the Joule losses low. HTS cables make it possible to send large power at medium voltage. This reduces the size and volume of the transformers and of the equipments required at both ends of the cable [103].
- HTS cables are actively cooled and thermally independent of the surrounding environment. As a result, an HTS cable system requires a smaller right of way than a conventional UGC system since it does not require a large separation between the cables.
- HTS cables have a reduced environmental impact on their direct surrounding. Since they do not emit any heat, they avoid soil heating. Since they use no oil, there is no risk of leakage. Besides AC HTS cables having HTS shields have zero external magnetic field.
- HTS cables systems are potentially lighter than conventional systems. They could play a role in the realization of next generation all-electric ships and aircraft [77, 78].

Drawbacks

- HTS cables operate at cryogenic temperature. They need cooling units, that impacts the footprint and the cost of the installation.
- HTS cables have no Joule losses but have other electric and thermal losses: superconductor AC losses (see section 3.5.5), dielectric losses, line cryostat losses, termination cryostat losses and current lead losses. Thermal heat losses are load independent. This heat load must be removed from the cryostat by the cooling system. This process is energy-intensive because the efficiency of cryocoolers is low. The reduction of Joule losses can then be counter-balanced by the necessary cooling requirements.
- HTS cables have no black start capability.
- HTS cables require specific cable joints and terminations. Theses accessories are more complex and costly than their conventional counterpart.

3.4.4 State of the art

As shown in Table 3.2, several AC HTS cables have already been successfully tested in the grid. There is a gradual increase in both the nominal current, the nominal voltage and the length. As of today, the cable system with the longest continuous operating time without interruption is the 1 km 40 MVA Ampacity project [84] that was commissioned in Essen in April 2014.

The Figure 3.10 provide a graphic representation of Table 3.2. It outlines that when the nominal voltage exceeds 100 kV, we systematically use single core HTS cables (1-phase 1-cryostat configuration, see section 3.4.2). In addition, it shows that AC HTS cable systems have been demonstrated in grid operation up to 154 kV L-N RMS (275 kV L-L RMS). The necessary technologies are deemed scalable for a voltage of 220 kV L-N RMS (380 kV L-L RMS).

Table 3.2: AC HTS cables in grid operation [B5]

Project	Year	Length	Material	Configuration	V [L-N RMS]	I [RMS]	Temp.	Ref
Carrolton, Southwire C.	2001	30 m	PIT-BSCCO	3-ph 1-cryo	12.4 kV	1.25 kA	70-80 K	[91]
Copenhagen, C. Energy	2001	30 m	BSCCO	1-ph 1-cryo	36 kV	2 kA	79-82 K	[92, 93]
Yunan, China Southern Grid	2004	30 m	BSCCO	1-ph 1-cryo wd	35 kV	2 kA	70-76 K	[94]
Columbus, Ultera	2006	200 m	BSCCO	3-ph concentric	13.2 kV	3 kA	77.6 K	[95, 96]
Albany, NY HTS	2006	350 m	DI-BSCCO	3-ph 1-cryo	34.5 kV	0.8 kA	69-73 K	[97]
LIPA Grid I	2008	600 m	BSCCO	1-ph 1-cryo	138 kV	2.4kA	77 K	[98]
Icheon, LS Cable	2010	410 m	REBCO	3-ph 1-cryo	22.9 kV	1.25 kA	68.8 K	[99, 100]
LIPA Grid II	2011	600m	YBCO	1-ph 1-cryo	138 kV	2.4 kA	77 K	[101]
Yokohama, Sumitomo	2013	250 m	BSCCO	3-ph 1-cryo	66 kV	1.75 kA	69-73 K	[102]
Ampacity, Essen, Nexans	2014	1000 m	BSCCO	3-ph concentric	10 kV	2.3 kA	67 K	[103]
Jeju Island, KEPCO	2015	1000 m	?	1-ph 1-cryo	154 kV	3.75 kA	72 K	[104]

* year = commissioning year, temp. = operating temperature, wd = warm dielectric.

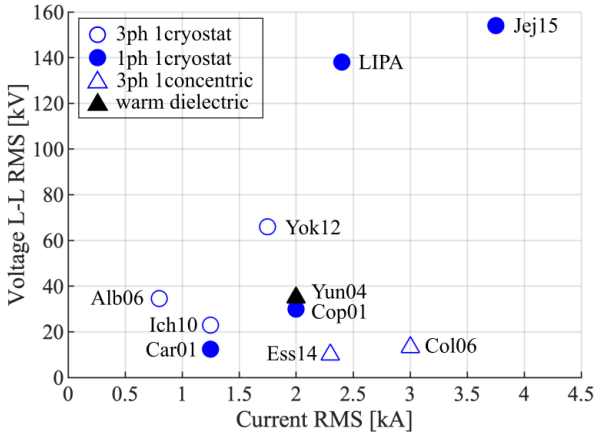

Figure 3.10: AC HTS cables in grid operation [B5].

In the short term, HTS cable systems could be competitive solutions for many applications. This includes industrial high-current grids having a relatively short length, such as aluminum plants. Industrial and urban areas where civil work is expensive (tunnel, bridge), or where space is limited could also benefit from the high power density of HTS cables. In those cases, a short superconducting cable would serve as a "bridge" connecting two resistive lines.

In the long term, superconducting links could transport large amounts of electricity over long distances. In the Best Paths project [88], gigawatt-scale superconducting cables have been investigated. The authors concluded that "thanks to their high efficiency, compact size, and reduced environmental impact, superconducting cables are likely to find higher public acceptance than overhead lines and conventional cables". In addition, they are deemed "technologically mature and cost-competitive for the transmission of large amounts of electricity".

3.5 Contributions

3.5.1 Design and winding of an HTS power cable core

An HTS cable core was designed. It is made of 26 BSCCO high-temperature superconducting tapes (Sumitomo, DIBSCCO, I_c = 115 A (SF, 77 K)) equally distributed in two layers around a stainless steel corrugated tube. Its structure is shown in Fig. 3.11(c). The critical current at 77.8 K is estimated to be larger than 2600 A. A 2-meter long cable was wound in March 2018 in the premises of CIDEC, Servicio Condumex S.A., Querétaro, Mexico (Fig. 3.11). This allowed us to (i) gain valuable insight on the technical constraints for the design and realization of such device, and (ii) have full knowledge about the layout of the cable core to be modeled and tested.

Credits

The design and winding of the HTS power cable core was carried out in collaboration with Frederic TRILLAUD (UNAM), J.J. Perez-Chavez (UNAM) and Petr DOLGOSHEEV (CIDEC).

3.5.2 Design and construction of an HTS power cable DC test station

Despite various successful demonstration projects, including continuous in-grid operation [84], HTS cable systems are still considered as "lacking maturity". One of the reasons slowing down the adoption process is the absence of standard for HTS power cable and their accessories. Indeed, without standard, the installation of a component in the grid is very unlikely.

The community is strongly involved in this standardization. In 2013, the CIGRE Working Group B1.31 published recommendations for the testing of AC superconducting cables, including the measurement of their critical current [85]. Recently, the International Electrotechnical Commission (IEC) published an international standard on the test methods and requirements for AC HTS power cables [86]. Recently, as part of a 3 year national project (2018-2020), Japan launched a national round robin test to characterize HTS cables [87]. The tests are being carried out for short single-core Bi-2223 cables, of

(a) (b)

(c) (d)

Figure 3.11: Realization of an HTS cable at CIDEC, Servicio Condumex S.A., Querétaro, Mexico (Mar. 2018).

length >1 m, operated in liquid nitrogen at 77 K and having a critical current of less than 10 kA. The goal is to propose a standard for the measurement of their DC critical current.

With the support of the French national organization for standardization (AFNOR/UF TC90), we joined the round robin test. To this end, a test station has been developed at GeePs. An overview of the platform is shown in Fig. 3.12. It is composed of several components:

- **DC power supply**: The DC power supply is composed of 4 Sorensen SGX1200 DC power supplies connected in parallel. The installation is able to provide a maximum current of 4800 A at 10 V.
- **Busbars, cables and braidings**: Two 4800 A aluminum busbars are used for the parallel connection of the power supplies. To connect the busbars to the HTS cable connectors, we use 240 mm^2 copper cables and 600 mm^2 copper braidings.
- **Cryostat**: The cryostat has been carved in a polystyrene block. Its internal dimension is 2000 × 200 × 150 mm. It makes it possible to test 2-meter-long cables in a liquid nitrogen (LN2) bath at ∼ 77 K under atmospheric pressure.
- **Nanovoltmeter and thermometer**: To record the voltage, we use a nanovoltmeter Keithley 2182. To record the temperature of the LN2 bath, we use a Graphtec GL 840-WV with a platinum thermocouple.
- **Laptop for the control and acquisition**: A laptop with Matlab is used to control the DC power

supply and the nanovoltmeter, and to record the signals.

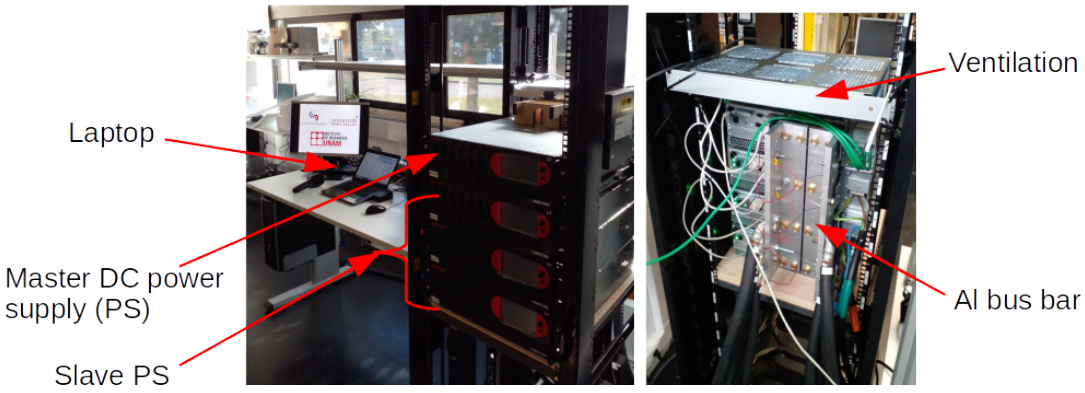

(a) Left: front panels of the DC power supplies and laptop to control the power supply and collect the data. Right: rear of the power supplies showing the aluminium busbars.

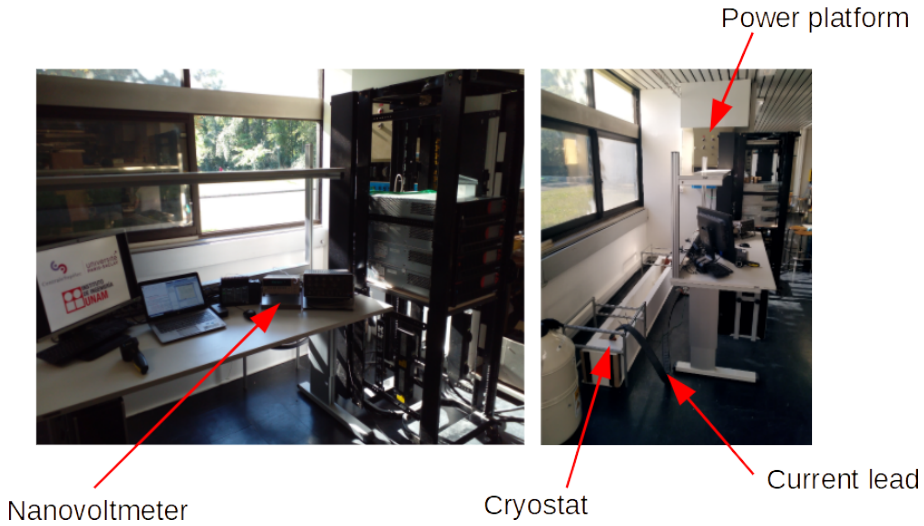

(b) Left: laptop and nanovoltmeter. Right: cryostat hosting the HTS cable and copper cables/braidings.

Figure 3.12: Overview of the HTS power cable DC test station (Jul. 2022).

To complete and expand the capability of this test station, work is being carried out on a number of components as part of student projects (Fig. 3.13): 800 A step down transformer, 1 kA 2-level voltage source converter, low noise high gain signal amplifier for dynamic voltage measurement and quench detection, stainless steel terminal and line cryostat, current lead, etc.

Credits

The development of the HTS cable test station has been carried out in collaboration with Frederic TRILLAUD (UNAM). Many students were involved at different steps (see chapitre 8). Carmen MARTIN-SANZ GARRIDO [B5] wrote her bachelor thesis from this project. I would like to acknowledge the help of Rafael MEDEIROS (GeePs), Didier GROLET (Institut de Physique Nucléaire d'Orsay), José DE FREITAS (GeePs) and Damien HUCHET (GeePs).

(a) 800 A step down transformer

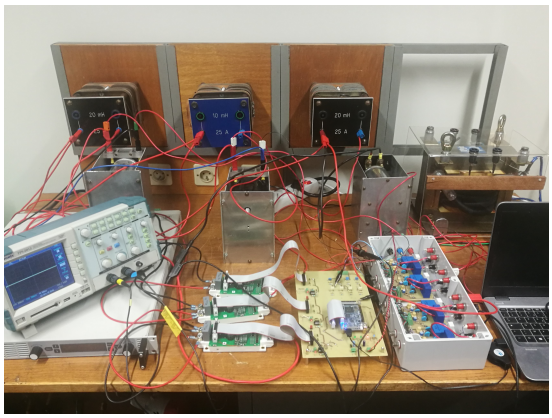

(b) 1 kA 2-level voltage source converter

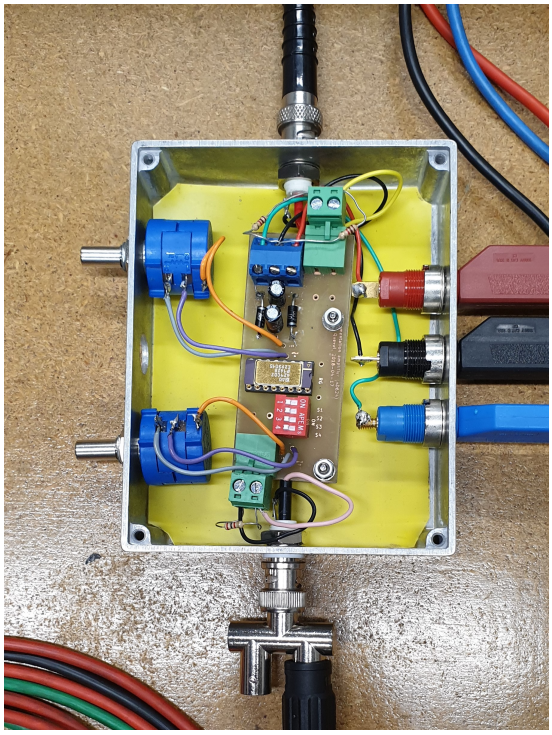

(c) Low noise high gain signal amplifier

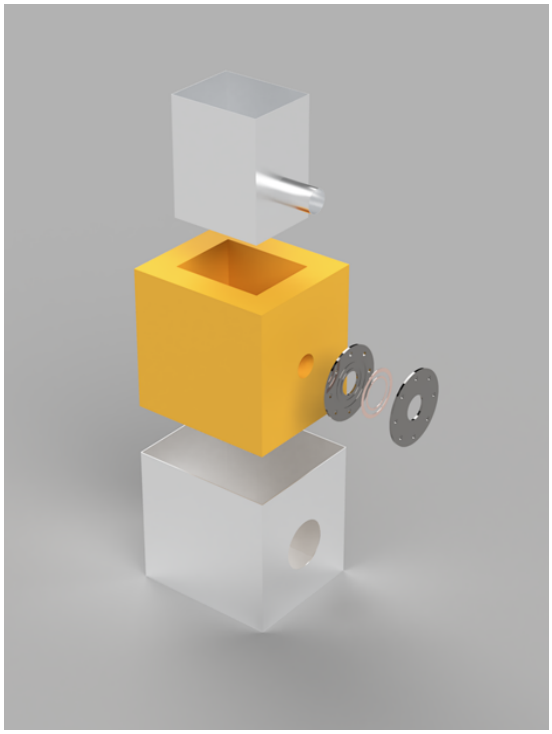

(d) Terminal boxes of the stainless steel cryostat

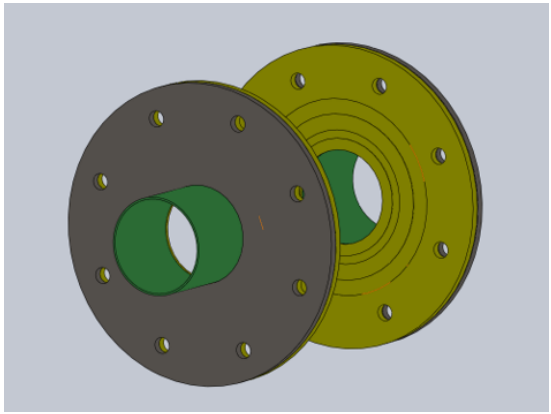

(e) Flange to connect a terminal box with the tube of the cryostat

(f) Current lead soldered to the HTS cable

Figure 3.13: Components for the HTS cable test station.

3.5.3 DC characterization of HTS power cables

Using the HTS power cable DC test station, we measured the V-I characteristic of several HTS power cable cores. To illustrate the kind of data that can be obtained, we report here the results for the BSCCO cable core described in section 3.5.1. It was equipped with voltage taps (179 cm apart on the outer HTS layer), installed in the cryostat and connected to the DC power supply with copper cables/braidings (Fig. 3.14(a)). The current was ramped up by steps of ∼50 A. After each step, we waited 10 s before recording the nanovoltmeter voltage, and the power supply output current. The test stops when the nanovoltmeter voltage reaches a predefined criteria. The results are shown in Fig. 3.14(b). The obtained V-I characteristic presents the expected power law trend,

$$V_{sc} = V_c \left(\frac{I_{sc}}{I_c} \right)^n \tag{3.1}$$

where V_{sc} is the tap-to-tap cable voltage, I_{sc} is the cable current, V_c is the critical voltage (set here at 179 μV assuming a voltage criteria of 1 μV/cm), I_c is the critical current and n is the power law index. The fitting gives $I_c = 2495$ A and $n = 13$. This test confirms that the cable core has not been damaged during winding, and behaves as expected. The measured V-I characteristic is useful to estimate his performances in a real environment, and to validate our numerical models.

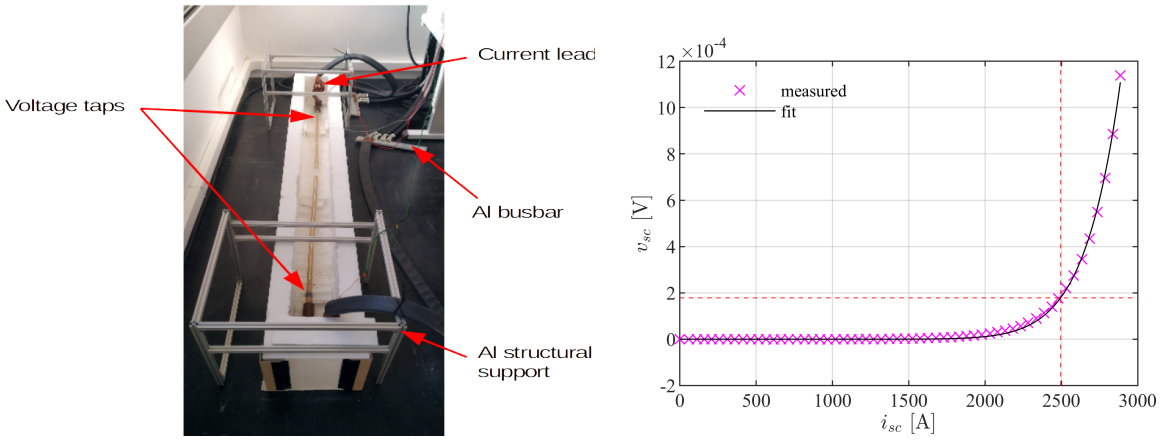

(a) Setup (b) Results

Figure 3.14: Measurement of the V-I characteristics of an HTS BSCCO cable core.

Credits

The DC characterization of HTS power cables has been carried out in collaboration with Frederic TRILLAUD (UNAM). Many students were involved at different steps (see chapitre 8).

3.5.4 HTS cable design framework

Via student projects within the curriculum, we developed a numerical framework to design AC HTS cable system. The methodology is strongly inspired from the one proposed in [89, 71] with some improvements. The design framework is shown in Fig. 3.15. It is made of 4 models that are coupled with each other:

- **Layout model**: The layout model defines the dimensions of the various layers of the cable core and of the line cryostat (see section 3.4.2).
- **Hydraulic model**: The hydraulic model calculates the LN2 pressure distribution along the cable.
- **Losses model**: The losses model calculates the losses of the cable system: superconductor AC losses (see section), dielectric losses, line cryostat losses, termination cryostat losses and current lead losses.
- **Thermal model**: The thermal model calculates the core temperature distribution both in the radial- and axial-direction.

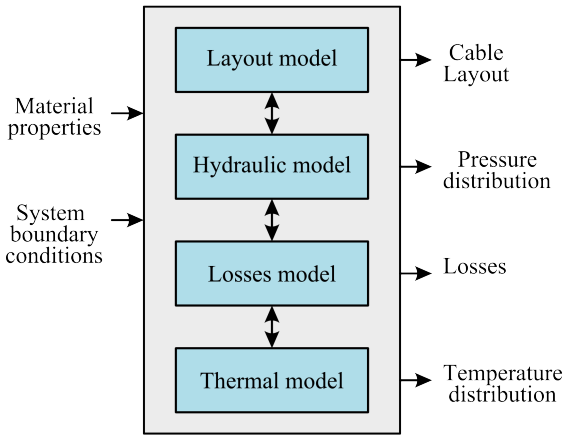

Figure 3.15: HTS cable design framework [B5].

Credits

The development of the HTS cable design framework was done by CentraleSupélec students as part of the curriculum (see chapitre 8). In addition, Lourdes PLATERO DE HEREDIA [B7] and Carmen MARTIN-SANZ GARRIDO [B5] wrote their bachelor thesis based on this project.

3.5.5 AC characterization of HTS tapes

When they carry AC currents or when then are subjected to AC fields, HTS conductors are subject to power losses. These losses, called AC losses, can cause problems with regard to cryogenic stability and overall efficiency. Understanding and management of such losses is, therefore, of paramount importance for practical applications of superconductors (including HTS cables).

We carried out extensive measurements of transport AC losses in various HTS tapes, with and without magnetic substrate, up to 10 kHz. Experimental data revealed that the classical description of transport AC losses in HTS tapes is incomplete in some aspects when transport currents in the kilohertz range are considered. More specifically, above a certain "transition frequency" the AC losses per cycle no longer increase with the frequency as the theory predicts. Using a finite element model to allow for loss separation, we find that this phenomenon is caused by a combination of several factors that appear only above the transition frequency: the hysteresis and ferromagnetic losses per cycle are no longer independent of the frequency, while the eddy current losses per cycle no longer increase proportionally to the frequency.

Credits

The AC characterization of HTS tapes was carried out in collaboration with Guangtong MA from Southwest Jiaotong University in China, as part of the PhD thesis of Pengbo ZHOU. It was partially financed by Campus France. The results have been published in [ic30, p21, p19].

3.6 Levelized cost of transmission of electricity ($LCOTE$)

The concept of levelized cost per unit can be used to compare the economic competitiveness of various power transmission technologies. In that specific context, we call it "Levelized Cost Of Transmission of Electricity" ($LCOTE$). It represents the average revenue per unit of energy transmitted over the system lifetime required to break even. It is expressed here in euro per megawatt hour [€/MWh].

Under the hypothesis of section 1.2.5, the $LCOTE$ is expressed from (1.8) as,

$$LCOTE = \frac{\sum_{t=0}^{T} \frac{CAPEX_t + OPEX_t}{(1+r)^t} - SV}{\sum_{t=1}^{T} \frac{ET_t}{(1+r)^t}} \tag{3.2}$$

where $CAPEX_t$ is the capital expenses in year t, $OPEX_t$ is the operating expenses in year t, r is the discount rate, ET_t is the electric energy transmitted in year t, T is the system lifetime and SV is the salvage value.

3.7 A techno-economic assessment of HTS HVAC cables

3.7.1 Goal and scope definition

Goal: In this section, to complete the discussion, we propose an abbreviated techno-economic assessment of HTS HVAC cables. We compare an installation using conventional HVAC copper cables and an installation using HVAC HTS cables.

Case study: We consider the test case proposed by Kottonau *et al.* [71]. The system is a 4 GW 380 V HVAC underground cable link having a length of 3.2 km. The parameters of the test case are summarized in Table 3.3.

Table 3.3: HVAC UGC transmission system parameters

Parameter	Symbol	Value	Notes
Nominal active power	P_n	4000 MW	
Nominal voltage	V_n	380 kV L-L RMS	[71]
Nominal power factor	$\cos\varphi_n$	0.85	
Nominal frequency	f_n	50 Hz	
Cable length	L_{cable}	3.2 km	[71]
System lifetime	T	40 years	[71]
Cost of electricity	C_{elec}	60 €/MWh	[D4]
Discount rate	r	0.041	[71]
Salvage value	SV	0	unknown

Scenario: The cable loading (operating current) is not constant, and usually well below the cable nominal current. To account for this, we use the concept of "annual load factor" [71]. As a result, the energy transmitted ET_t is a function of the annual load factor that is set here equal to 0.8.

Optimization problem: We look for the HTS cable sizing that minimizes the $LCOTE$. The optimization problem is formulated as [B7],

$$\begin{aligned} \underset{X}{\text{minimize}} \quad & LCOTE(X) \\ X = & \{DN, \alpha, w\} \\ \text{subject to} \quad & T(r)_{min} \leq T(r,z) \leq T(r)_{max} \\ & P(0)_{min} \leq P(0,z) \leq P(0)_{max} \end{aligned} \tag{3.3}$$

where the optimization variables X are: the former normalized diameter $DN \in \{32, 40, 50\}$, the HTS tape twist angle $\alpha \in [10, 45]$ and the HTS tape width $w \in \{2, 3, 4, 6, 12\}$. The constraints on the temperature T and on the pressure P ensure that the HTS cable stays within the operating region (Fig. 3.9). The corresponding optimization problem is formulated for the conventional resistive cable.

3.7.2 Inventory analysis

The system elements are shown in Fig. 3.4. Details about the technical and economic parameters can be found in [71].

Benchmark product system: For the copper cable system, we consider four 3-phase circuits (12 cables) in parallel. We assume single core HVAC copper cables (see section 3.3). The use of 12 cables is necessary because each cable can carry only 1800 A. The cable sizing, adopted from the case study, is considered already optimal. The main parameters are summarized in Table 3.4.

Table 3.4: HVAC copper cable parameters

Parameter	Symbol	Value	Notes
Ampacity	$I_{cable,r}$	1800 A/core	[71]
Nominal voltage	V_n	220 kV L-N RMS	[71]
nb of cables	n_{cable}	12	4× 3-ph circuits [71]
Conductor cross section		2500 mm2	[72]
AC resistance @90°C	r_{cable}	0.0136 Ω/km	at 90^{o}C [72]
Inductance	l_{cable}	0.64e-3 H/km	[72]
Capacitance	c_{cable}	0.23e-6 F/km	[72]

Proposed product system: For the HTS cable system, we consider two 3-phase circuits (6 cables) in parallel. We assume HVAC HTS cables with a single core (see section 3.4.2) and a closed cooling sytem with one-sided cooling concept (Fig. 3.8). The use of only 6 cables is made possible because each HTS cable can carry up to 3600 A (Table 3.2). Note that we use estimates of future technical and economic parameters of YBCO HTS conductor for this analysis. The main parameters are summarized in Table 3.5.

Table 3.5: HVAC HTS cable parameters

Parameter	Symbol	Value	Notes
Ampacity	$I_{cable,r}$	3600 A/core	[71]
Nominal voltage	V_n	220 kV L-N RMS	[71]
nb of cables	n_{cable}	6	2× 3-ph circuits [71]
Flow rate of LN2 at inlet	$\dot{m}_{inlet}$	0.9 kg/s	[71]
Temperature of LN2 at inlet	T_{inlet}	68 K	[71]
Pressure of LN2 at inlet	P_{inlet}	15e5 Pa	[71]

3.7.3 Calculation of indicators

We use the technical and economic model described in section 6.2.1 [71][B7, B5]. Note that the $CAPEX_t$ include the following costs: HTS cable core, line cryostat, cable accessories (joints and terminations), cooling system, civil engineering and installation. The $OPEX_t$ include the cost of losses but neglects the maintenance costs (lack of data). The losses include the superconductor AC losses, the dielectric losses, the line cryostat losses, the termination cryostat losses and the current lead losses.

The optimization is performed by using the multi-objective Particle Swarm Optimization (MOPSO) algorithm [217] with 100 particles and 100 iterations. With a laptop equipped with Intel(R) Core(TM) i7-8665U CPU @ 1.90GHz and 32 GB of RAM, the optimization takes ∼4 hours.

Table 3.6: Case study optimal results

	HVAC copper cables	HVAC HTS cables
Former normalized diameter DN [mm]	na	50
HTS tape twist angle α [deg]	na	10.2
HTS tape width w [mm]	na	2
$LCOTE$ [€/MWh]	0.092	0.081

The results of the optimization are summarized in Table 3.6. The optimal $LCOTE$ for the HVAC HTS cable system is 0.081 €/MWh, to be compared to a $LCOTE$ of 0.092 €/MWh for the conventional HVAC copper cable system. This indicates that, for this case study, the HTS cable system could be a competitive solution.

3.7.4 Interpretation

We would like to use this case study as a support to discuss how uncertainties can affect the LCpu, and what could be done to make the method more robust.

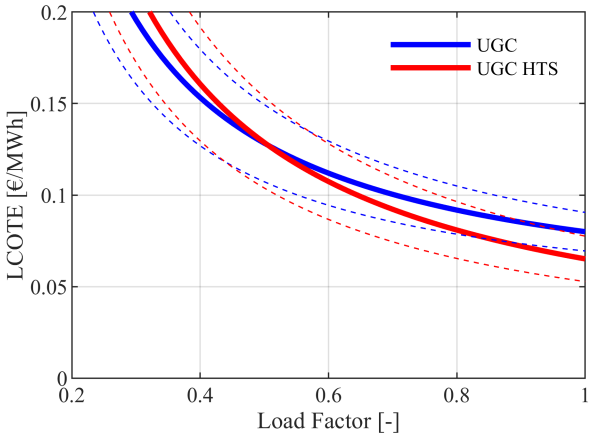

Figure 3.16: Comparison of the levelized cost of transmission of electricity ($LCOTE$) as a function of the annual load factor, for a conventional HVAC underground cable system (UGC) and an HTS cable system (UGC HTS). The dashed lines show the $LCOTE$ interval.

Uncertainty on usages

The traditional engineering task is to optimize a system according to its anticipated usage, typically a deterministic projection of demand. This is what we did here by setting the annual load factor to 0.8. This value becomes questionable as we look 40 years into the future: customer preferences, competition on the energy market and even political events might drive changes in usage.

This can be studied by running a parametric study. A comparison of the systems $LCOTE$ as a function of the annual load factor is shown in Fig. 3.16. For low annual load factors, the conventional copper cable system is the most competitive. This is due to the high CAPEX of the HTS cable and to the load-independent losses (mainly cryostat losses) [B7]. For annual load factors larger than 0.5, the HTS cable system becomes the most competitive. The high CAPEX of the HTS cable system is compensated by the reduction of the Joule losses. The expected usage is therefore of great importance for the decision on the type of cable system.

Uncertainty on costs

Uncertainties on costs make it a difficult task to perform a relevant techno-economic analysis. This is even more true when evaluating the potential of innovative technologies, for which there is no historical data. This point is discussed in more depth in section 6.

One possibility is to take this uncertainty into account by considering cost intervals. We illustrate this by using an estimation of the minimal and maximal CAPEX of each component [71] when calculating the CAPEX of each system. The resulting $LCOTE$ interval has been added in Fig. 3.16 (dashed lines). It shows that, considering uncertainty on CAPEX, the $LCOTE$ intervals of the two systems overlap. Depending on the actual cost at the time of construction, one system may become clearly more competitive than the other. But this cannot be guaranteed with the current cost. The decision maker should then adjust the risk to the desired level of exposure.

3.8 Summary and perspectives

In this chapter, we described the work that has been carried out on the techno-economic assessment of HTS cables for HVAC underground cable transmissions systems. The efforts span both the experimental part and the theoretical part.

The development of an HTS power cable DC test station, unique equipment of this kind in France, has been carried out between 2018 and 2022. The equipment is being used as part of an international

effort around standardization of HTS cables. Beyond this, it opens the door to new research projects involving high currents.

The proposed techno-economic analysis is a first assessment of the potential of HTS technology for HVAC underground power transmission. It is a concatenation of the results of various student projects that were carried out between 2016 and 2022 in CentraleSupelec. To be relevant, such analysis should be completed to include a proper design of the HTS cable core (account for magnetic field), an improved estimation of the CAPEX distribution (cable, cryostat, pumps, etc.) and of the OPEX (losses, cooling power, maintenance, etc.).

Chapter 4

Cryo-MMC for HVDC converter stations

4.1 Context

High voltage direct current (HVDC) lines have many advantages. First, DC links are the only solutions for transporting electricity underwater over long distances, and are therefore used to connect wind farms far from the coast [32, 42]. Second, some renewable energy sources are intermittent. It becomes important to be able to transport electricity over large distances in order to smooth production, which HVDC links make it possible to do economically [33, 34]. Third, the large penetration of renewables changes power flows. Indeed, the existing network was designed to transport power from centralized power plants to consumption centers. Since renewable energy sources are often located in areas with a sparse network, flows are modified with consequences for stability. However, HVDC lines make it possible to control the power flows, and thus to improve the stability of the network [34, 35]. Fourth, countries are strengthening existing networks and their interconnections to increase the reliability of the electricity system and to facilitate energy exchanges in a liberalized energy market. DC connections here again offer technical and economic guarantees [35].

To date, HVDC systems are mainly point-to-point links [36, 45]. But eventually, the multiplication of HVDC systems implies their interconnection [35]. It will form a transnational transmission power grid, that is often called "Supergrid".

HVDC grids are connected to the AC grids at several points via AC/DC converters. Among the many topologies of converters proposed for HVDC applications [37], the Modular Multilevel Converter (MMC) is currently state of the art for power ratings under 2000 MW [D4]. It has many advantages [38, 39, 40, 41]: low switching frequency, quasi-sinusoidal AC voltage ie. small size filters, modularity, high reliability, etc. But this is a valuable asset, so any improvement is welcome.

4.2 Overview of an HVDC converter station

We consider the HVDC converter station shown in Fig. 4.1. The AC/DC converter is an half-bridge modular multi-level converter (HB-MMC).

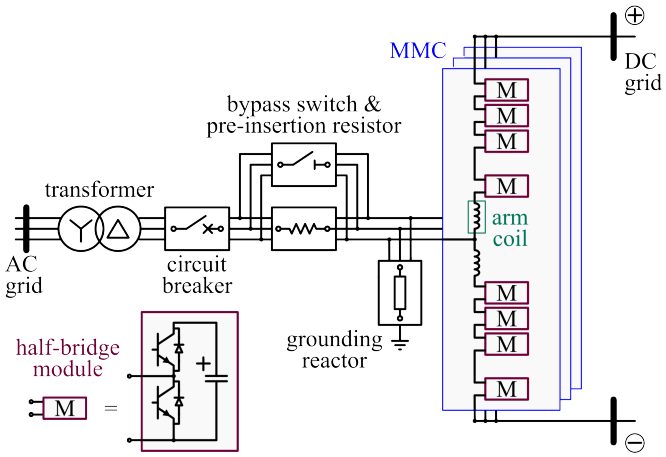

Figure 4.1: Overview of an HB-MMC-HVDC station.

This system includes 3 parts that are shown in Fig. 4.2. The AC side part includes 4 types of components: transformer, 3-phase AC line/cable, AC circuit breaker and bypass (BP) switch & pre-insertion (PI) resistor. The MMC part includes 6 types of components: arm coil, half-bridge (HB) module, cooling plant, infrastructure, control and grounding. The DC side part includes 1 type of component: DC line/cable.

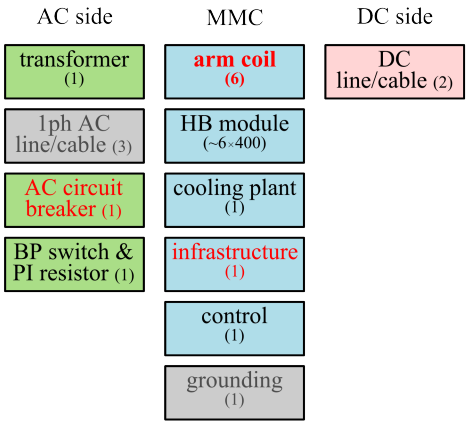

Figure 4.2: Components of an HB-MMC-HVDC station. The numbers in parenthesis indicate the number of such component in the system. The components in red font are directly impacted by the technology shift. The components in gray block are not considered in the following analysis.

To give an idea of the order of magnitude of the quantities involved, we consider a reference HB-MMC station, inspired from the CIGRE TB832 [51]. Its main parameters are summarized in Table 4.2. Photos of such station are shown in Fig. 4.4.

Quantity	Symbol	Value
Rated Active Power [MW]	P_{nom}	1000
Rated Reactive Power [MVAr]	Q_{nom}	300
Rated DC Voltage [kV]	V_{dc}	±320
Grid Voltage L-L RMS [kV]	U_g	400

Table 4.1: Main parameters of the reference HB-MMC station [D4].

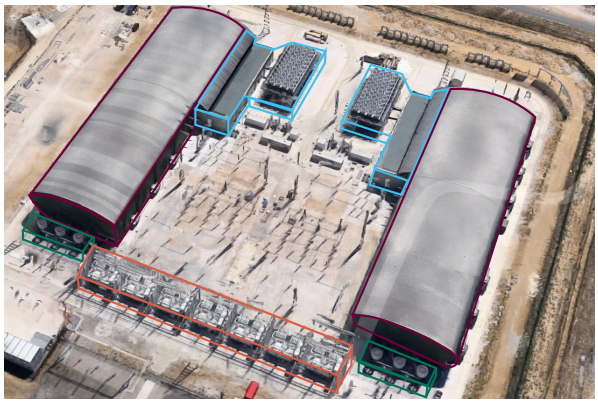

(a) Aerial view. Source: Google Maps.

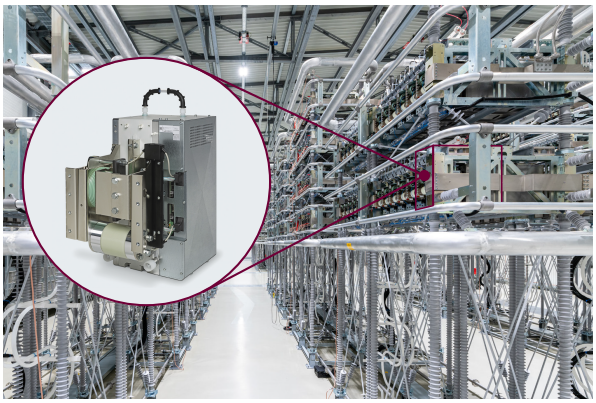

(b) Valve building and HB modules. Source: [52].

Figure 4.3: Inelfe Baixas 2×1 GW ±320 kV HB-MMC-HVDC station [D4].

4.3 A conventional technology: the dry-type air-core arm coil

The arm coils of GW-class MMC are dry-type air-core coils [57, p. 96]. A schematic view is proposed in Fig. 4.4(a). The winding is made up of several concentric layers. Each layer is a solenoid wound with aluminum wires which are insulated with insulating tapes or films and encapsulated in a fiberglass epoxy composite. Glass-fiber sticks are put between the layers to create the required radial spacing to allow for natural convection air cooling.

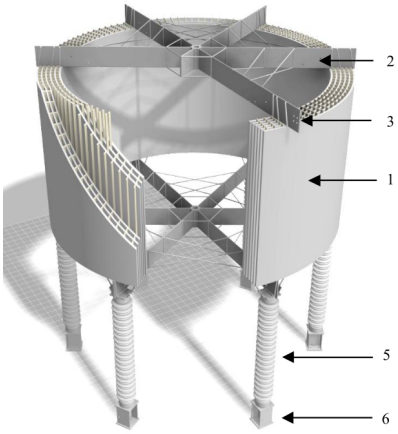

(a) Schematic [58]. (1 - winding, 2 - spider, 3 - terminal, 4 - glass fiber duct stick, 5 - insulator, 6 - mounting bracket)

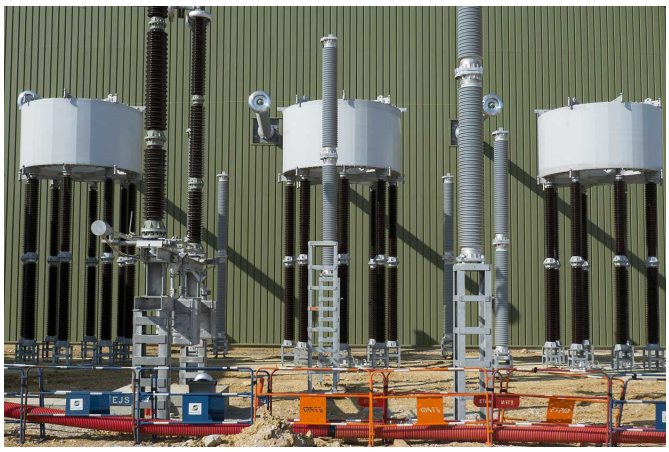

(b) Arm coils of a 1 GW and ±320 kV HB-MMC. Source: https://www.inelfe.eu.

Figure 4.4: Dry-type air-core coil.

The breakdown of an HB-MMC-station capital cost, weight, and losses are shown in Fig. 4.5. Despite being seemingly minor components, the arm coils account for up to 4% of the cost, 9% of the losses and 42% of the weight of the MMC [53].

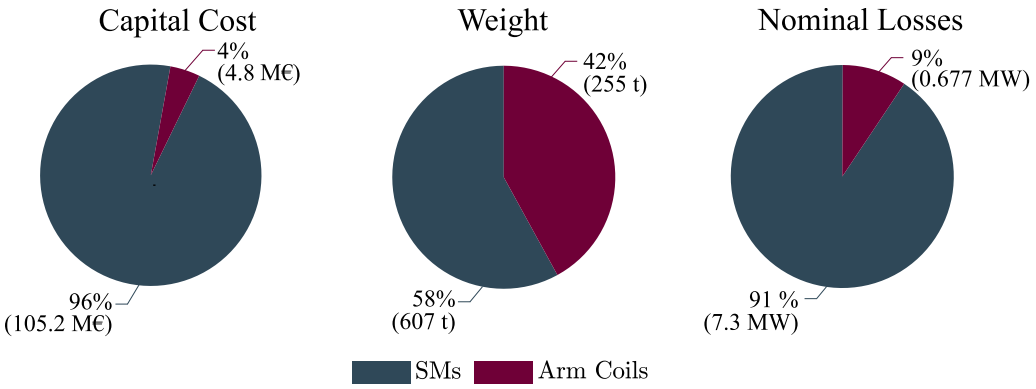

Figure 4.5: Breakdown of the capital cost, weight, and losses for the reference MMC [D4]. "SMs" includes the HB-SMs, the valve building, the cooling plant, and control.

4.4 An innovative technology: the coupled HTS arm coil

4.4.1 Innovation

Since the arm coils represent a non-negligible part of the cost, losses, and weight of an HB-MMC station, we focused our efforts on their design.

First, we proposed to magnetically couple the arm coils of the HB-MMC [55]. It is expected that a direct-coupling reduces the size and weight of the arm coils, thereby decreasing the footprint of the MMC-HVDC station. This point is particularly important for offshore applications.

Second, we proposed to replace the conventional dry-type air-core arm coils with high-temperature superconducting (HTS) arm coils [56]. It is expected that it will allow us to reduce the losses of the arm coils, thereby increasing the efficiency of the MMC-HVDC station. In addition, it should provide a DC fault current limitation function to the HB-MMC, by behaving like a superconducting fault current limiter. By limiting the fault currents, the constraints on the converter and on all of the associated equipment of the MMC-HVDC station will be reduced. This could simplify the design of the DC-circuit breakers too [54].

The resulting topology is an HB-MMC with directly-coupled HTS arm coils (Fig. 4.6) that we called "cryo-MMC".

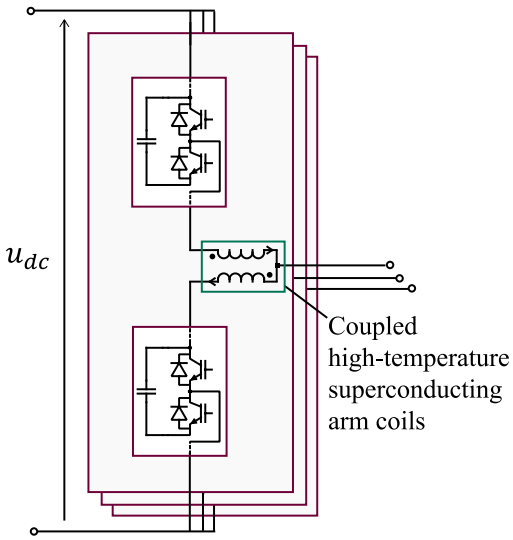

Figure 4.6: Cryo-MMC topology [D4].

4.4.2 Description

The coupled HTS arm coils are shown in Fig. 4.7. Both arm coils are located in the same cryostat, cooled down in an LN2 bath. A set of coupled HTS arm coils is composed of several HTS pancake coils

connected in series and parallel, to obtain the required self and mutual inductance (see details in [D4]). Each HTS pancake coil is made by co-winding the HTS tape with a corrugated spacer. The support structure is full of holes to favor the circulation of the LN2. The connectors are made of copper.

We assume liquid nitrogen (LN2) as the coolant, either right below the LN2 boiling temperature of 77 K or subcooled at 65 K. The study of R-type superconducting fault current limiters in [59] pointed out that a subcooled operation temperature of 65 K yields a most economical solution than at 77 K.

Unlike 1G tapes fabricated using an Ag matrix, an excellent electrical conductor, 2G HTS tapes are much more resistive in the event of quench and are thus more suitable for current limiting applications [60, 61]. Therefore, we adopt a 2G HTS tape to wound the pancake coils.

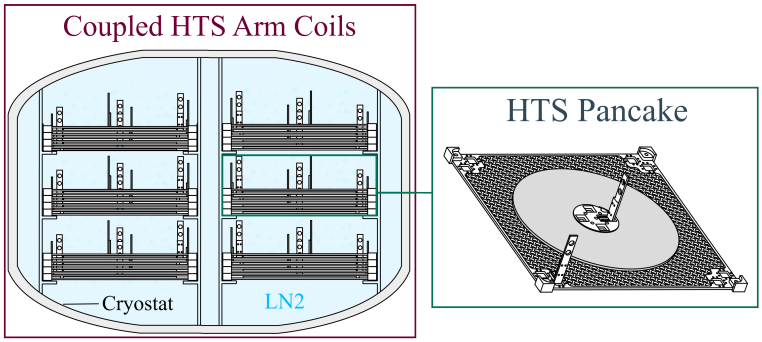

Figure 4.7: Overview of coupled HTS arm coils [D4].

We consider a single refrigeration system for all the HTS arm coils. We adopt the hybrid architecture [62] illustrated in Fig. 4.8. It uses a cryocooler as the primary source for refrigeration and one open-cycle LN2 buffer tank as a backup. This configuration provides the high reliability required for in-grid operation while avoiding the high costs of cryocooler redundancy.

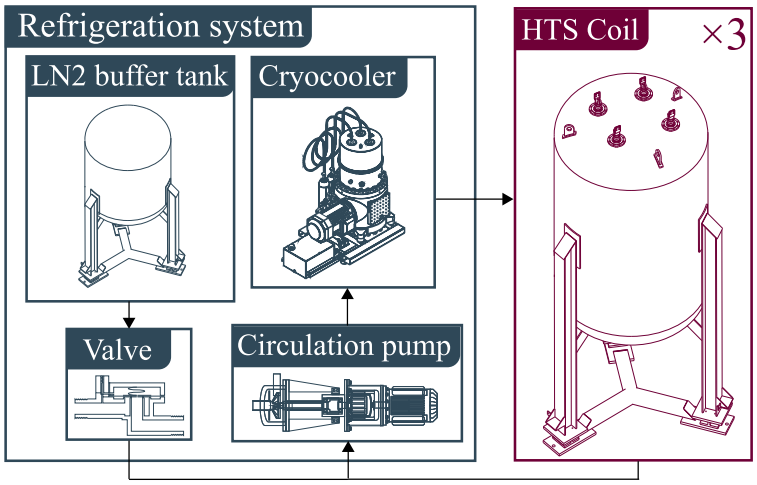

Figure 4.8: Overview of the coupled HTS arm coils refrigeration system [D4].

4.4.3 State of the art

To our knowledge, we are the first group to work on the cryo-MMC concept. The technology is still at a low technology readiness level (TRL) but it could progress rapidly. This is because the modular multi-level converter (MMC) is already widely adopted for high voltage (HV) power grid applications, including long distance power transmission and offshore wind power. And the construction of the coupled HTS arm coil of the cryo-MMC can benefit from feedback from successful superconducting fault current limiter projects [66, 67, 68, 69]. The industrialization of the cryo-MMC would require a joint effort between two industries: HVDC power electronic converter manufacturers and superconducting equipment manufacturers.

4.5 Contributions

4.5.1 Models for the sizing of modular multi-level converters

Due to its topology, the modeling of the MMC is quite complex. Numerical models are often slow, which makes them unsuitable for sizing at the design stage. This is why we have been looking for models that are able to estimate the converter steady-state variables with a reduced computational burden and low error.

Integral based MMC model

Integral based modeling is a powerful tool: it gives closed-form analytical expressions for some variables that can be evaluated efficiently. But due to the complexity of the MMC topology, many simplifications are necessary. In particular, the arm equivalent resistance R, the arm inductance L and the circulating current are often neglected. But experimental results obtained with our MMC prototype showed that these hypotheses are not always acceptable [chap. 1, D2].

In this context, we extended the commonly used integral based model and we clarified the hypotheses behind it. Among others, expressions for the circulating and DC currents have been developed and compared with the one that can be found in the literature. It allowed us to analyze the module capacitor voltage ripple as a function of R and L, but without circulating current only [chap. 3, D2].

AA-SSTI $\Delta\Sigma$ MMC model

To overcome the limitations of the integral based model, we derived an averaged-arm steady state time invariant (AA-SSTI) $\Delta\Sigma$ MMC model in $dq0$ frame. It is derived from the time-dependent differential equations of the averaged-arm model, truncating them at the second harmonic and writing them in two rotating reference frames at the fundamental frequency and at the second harmonic using the $dq0$-transformation. By eliminating the time dependence of the equations, the SSTI $\Delta\Sigma$ model obtains the steady-state response of the system through sparse-matrix inversion. This considerably shortens the simulation time.

Using this model, first we analyzed the module capacitor average voltage and the module capacitor voltage ripple as a function of R and L, with and without circulating current [chap. 4, D2].

Second, we developed a detailed PQ diagram of the MMC [chap. 5, D2]. In addition to the conventional AC current limit, DC current limit and modulation index limit, we added several internal limits: IGBT current, arm rms current and module capacitor voltage and current ripple. The PQ diagram corresponding to our prototype is shown in Fig. 4.15. The results have been confirmed by numerical simulation using a detailed Matlab Simulink SimPowerSystems model. This tool could be used to optimize the sizing of the components of the MMC considering its operating area, and to assess the impact of different parameters on the MMC performance.

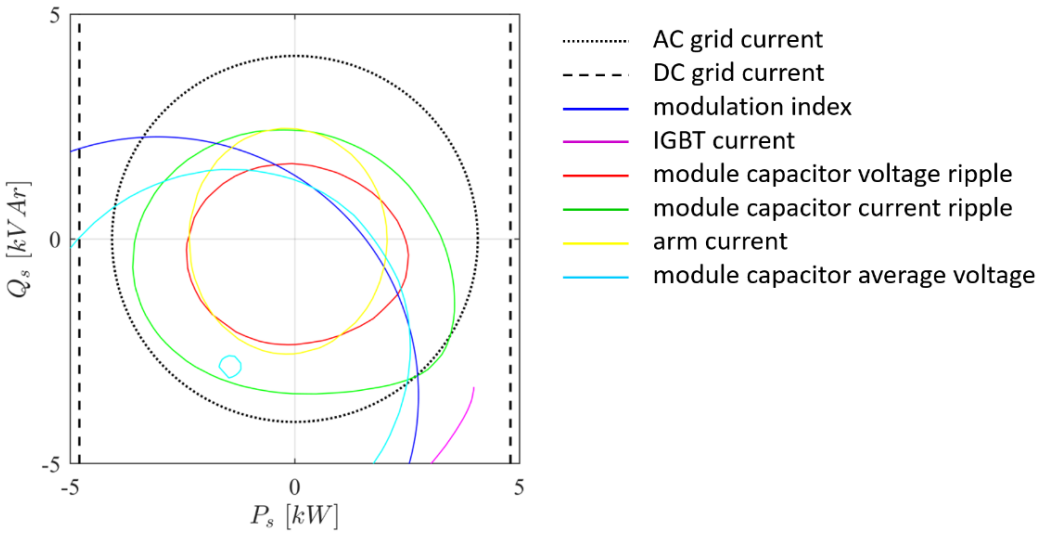

Figure 4.9: PQ diagram of our MMC prototype with external and internal limits [D2].

DA-HSS $\Delta\Sigma$ MMC model

More recently, we proposed a detailed-arm harmonic state-space (DA-HSS) $\Delta\Sigma$ MMC model in *abc*-frame [chap.II, D4]. The time dependence of the equations is eliminated by transposing the converter equations from the time domain to the frequency domain using the HSS decomposition of linear time-periodic (LTP) systems [Appendix A, D4]. It allows one to model the converter behavior up to any frequency, accounting for the harmonics generated by any arbitrary modulation technique, by simply increasing the harmonic order of the HSS decomposition.

This tool was used to design the arm dry-type air-core coils of an HB-MMC with uncoupled and directly-coupled arm coils [chap.III, D4]. We demonstrated that directly-coupled arm coils can be designed with different objectives: keep a similar weight and size while improving the performances (reduced conversion losses, reduced DC-fault current), or reduce the size while keeping similar performance (Fig. 4.10).

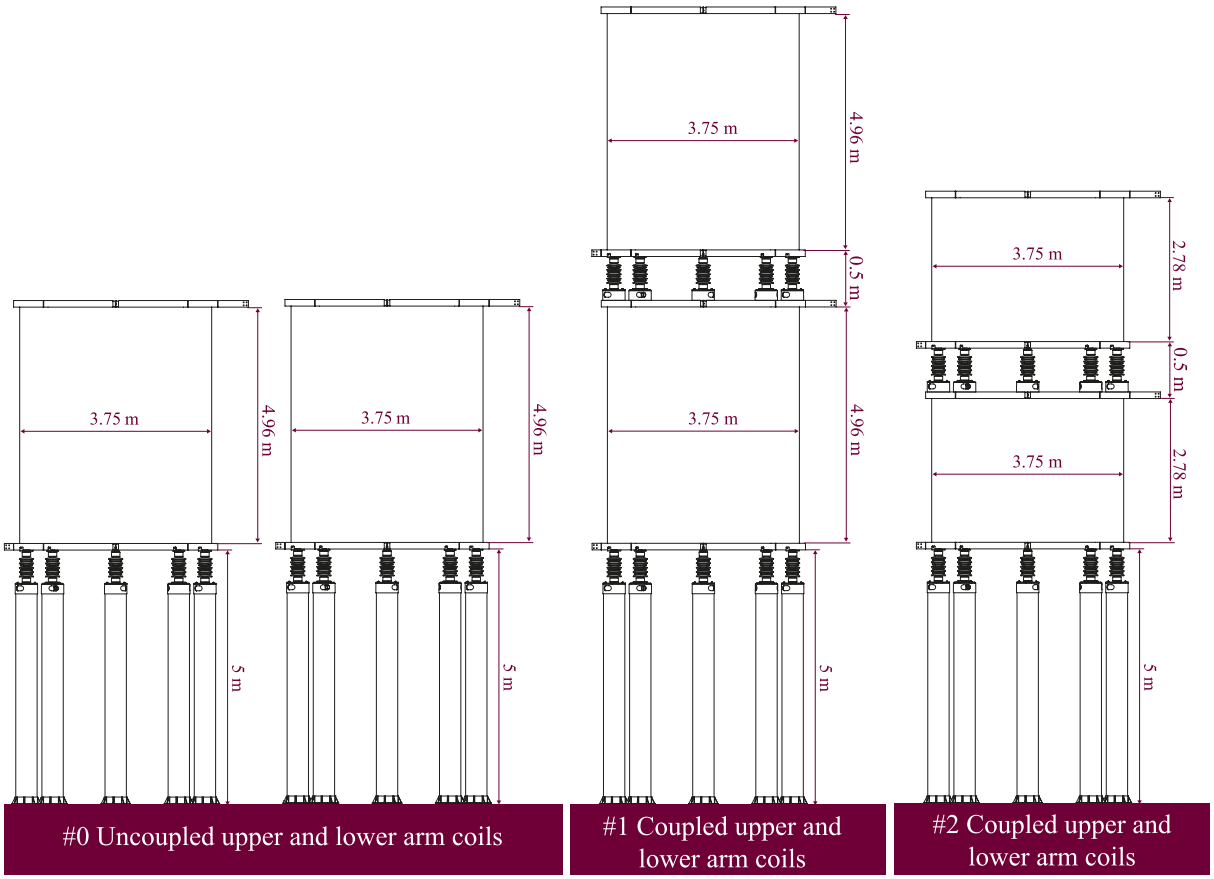

Figure 4.10: Comparison of uncoupled and coupled dry-type air-core MMC arm coils [D4]. #0 reference design, #1 same size but improved performances, #2 reduced size but same performances.

4.5.2 Design and construction of a full-bridge modular multi-level converter

A 3-phase 6-level full-bridge MMC prototype has been designed and built in several stages.

First stage

In the framework of the PhD thesis of Davi JOCA (Universidade federal do Ceará & Université Paris-Saclay, funding Erasmus Mundus SMART2) [D1], 16 full-bridge modules (Fig. 4.11), 4 arm controllers and one master controller were built. They were assembled to obtain 4 MMC arms having 4 modules and 1 arm controller each. Indeed, the goal of the visit of Davi to the GeePs was to realize an experimental proof of concept of an original topology that was initially proposed by his home laboratory. This converter, called "AC-DC interleaved MMC with medium frequency transformer", is intended for the connection of microgrids to the medium voltage grid. The schematic is shown in Fig 4.12(a) and the prototype is shown in Fig. 4.12(b).

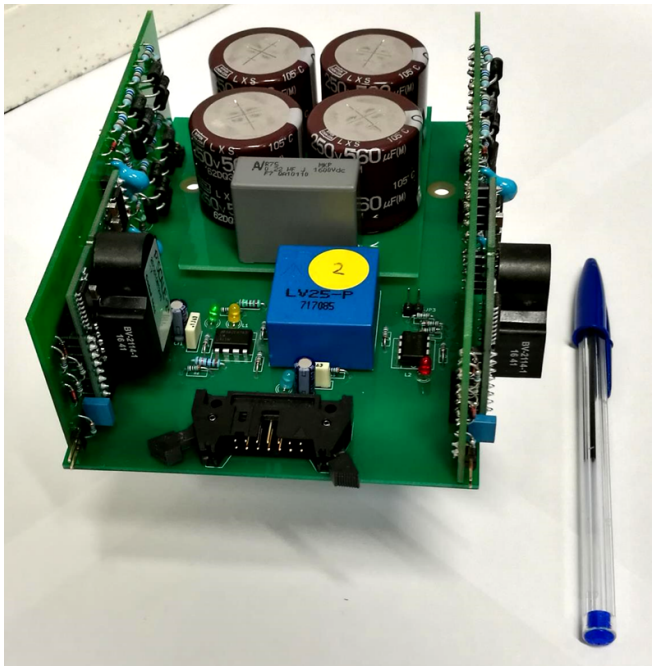

Figure 4.11: MMC full-bridge module, designed and realized at GeePs [D1].

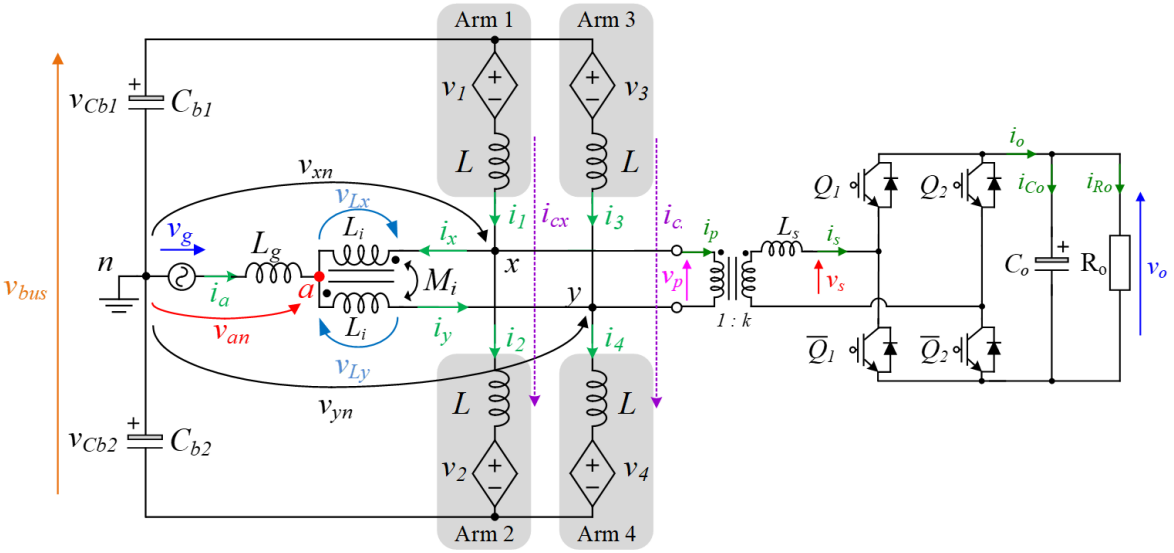

(a) Schematic

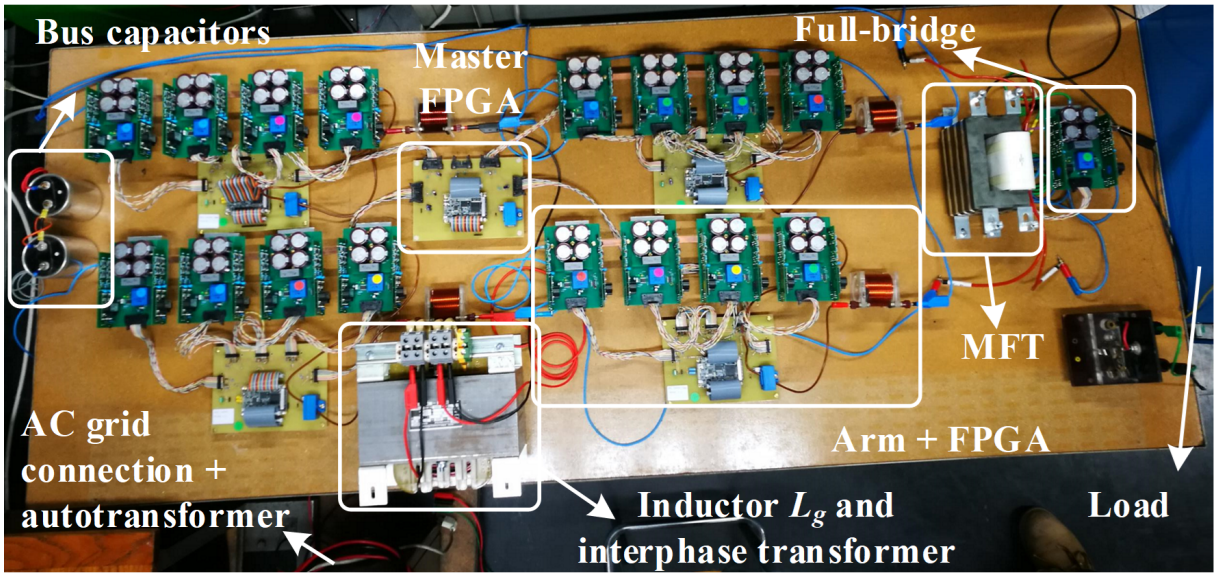

(b) Prototype

Figure 4.12: AC-DC interleaved MMC with medium frequency transformer (Davi JOCA, Jun. 2018) [D1].

Second stage

In the framework of the PhD thesis of Bogdan DZONLAGA (Université Paris-Saclay, funding MESR) [D2], 14 extra full-bridge modules, 2 extra arm controllers and one improved master controller were built. The total of 30 modules were assembled to obtain 6 MMC arms having 5 modules and 1 arm controller each. The schematic is shown in Fig 4.13(a) and the prototype is shown in Fig. 4.13(b).

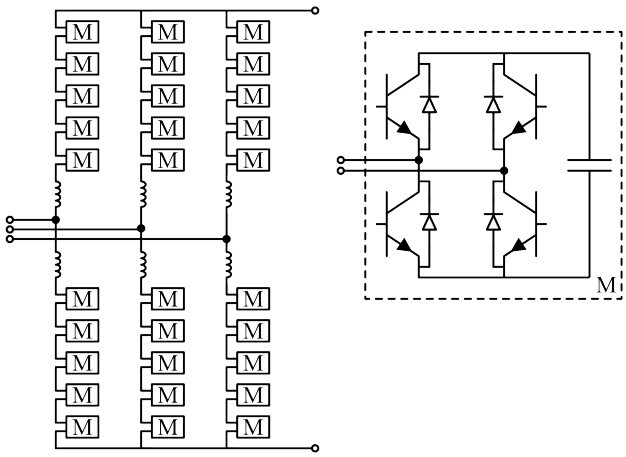

(a) Schematic

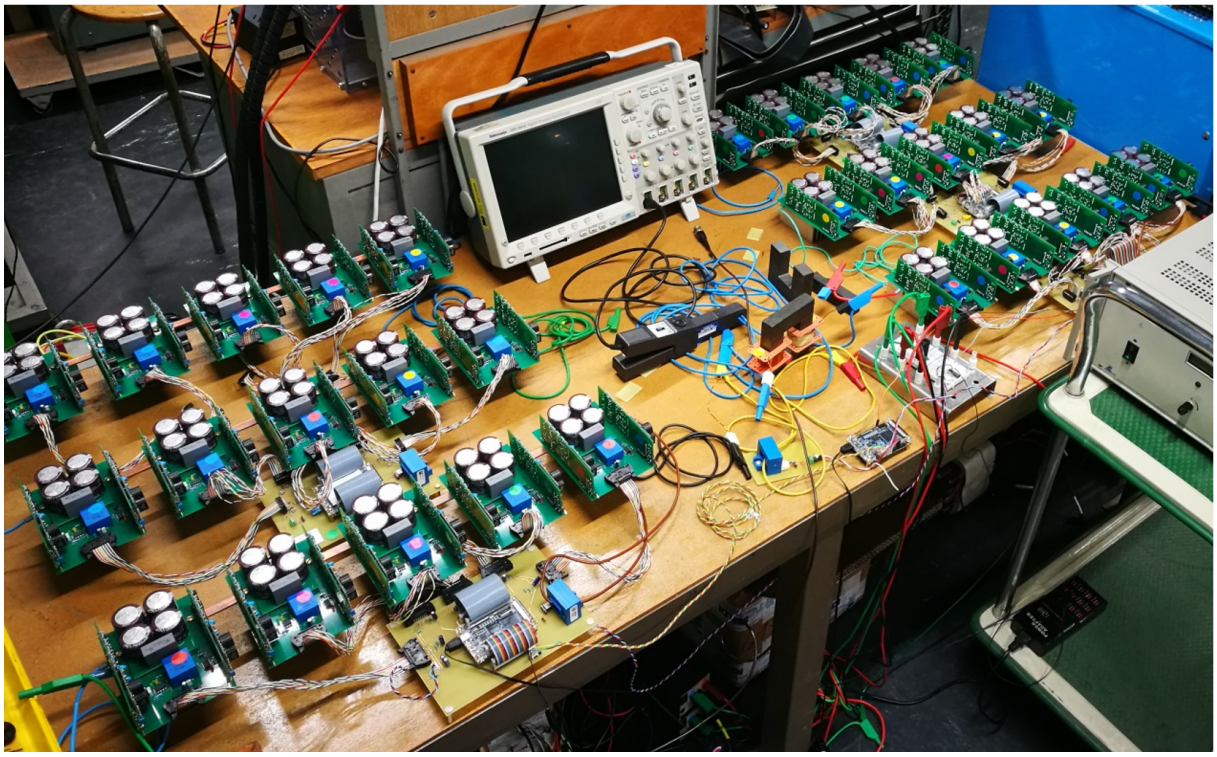

(b) Prototype

Figure 4.13: 3-phase 6-level full-bridge MMC (Bogdan DZONLAGA, Dec. 2019) [D2].

Third stage (ongoing)

The next stage will be to connect the FB MMC to the GeePs multi-terminal DC experimental test grid (Fig. 4.14). To do so, the power converter will be integrated in an electric cabinet with additional safety protections and suitable interfaces. This will flatten the learning curve of handling the device, and allow us to host external researchers for short periods.

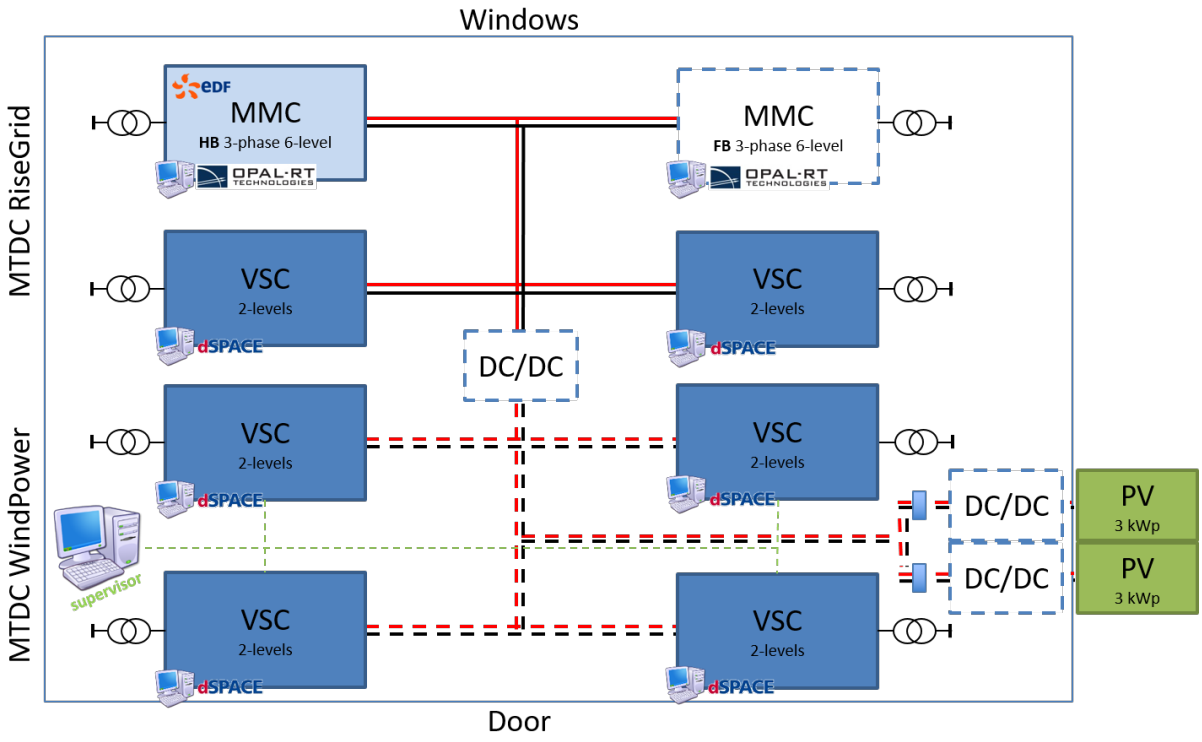

Figure 4.14: GeePs multi-terminal DC experimental test grid (Apr. 2020).

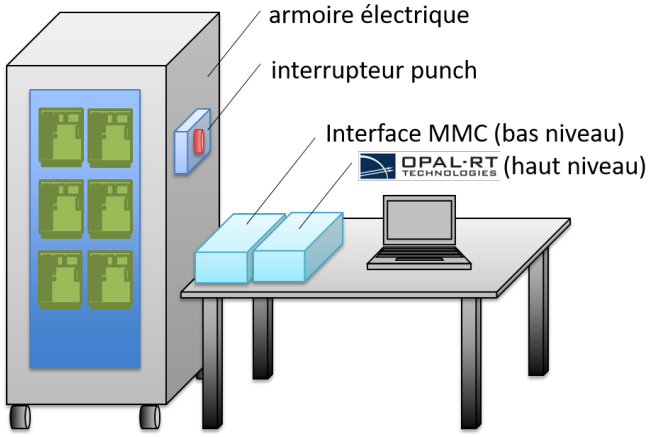

Figure 4.15: Illustration of the MMC platform being constructed.

Credits

Davi JOCA [D1] and Bogdan DZONLAGA [D2] spent countless hours building the converter as part of their thesis. We acknowledge the help of José DE FREITAS (GeePs), Damien HUCHET (GeePs), Richard BELJIO (GeePs) and Amir ARZANDE (GeePs).

4.5.3 Design and construction of a cryo-MMC

In the framework of the PhD thesis of Rafael MEDEIROS (Université Paris-Saclay, funding Cifre EDF R&D), we designed, built, and tested the world's first laboratory-scale HB-MMC with directly-coupled HTS arm coils (cryo-MMC).

We designed, wound, and successfully tested eight inductive HTS pancake coils. They can be connected in series and stacked to obtain the uncoupled or directly-coupled HTS arm coils. Each pancake coil is made of 47 m of 1G BSCCO tape and has an inductance of ∼1.2 mH (Fig. 4.16). We measured

their V-I characteristic in a liquid nitrogen bath at 77 K. The coil critical currents were between 140 and 155 A, denoting that the conductor was not degraded during winding.

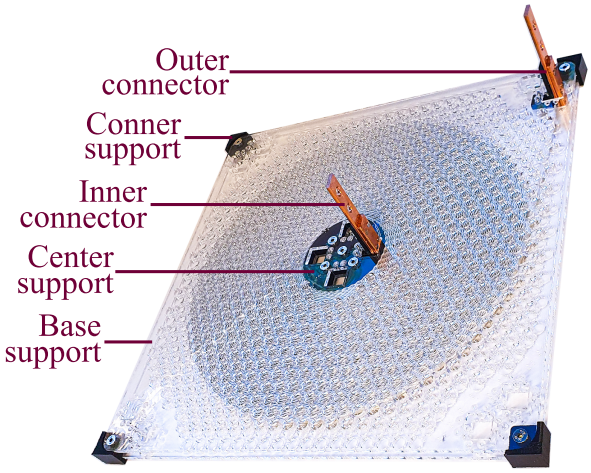

Figure 4.16: HTS pancake coil (Rafael MEDEIROS, Mar. 2022) [D4].

Two stacks of 5 HB modules, that were designed and built as part of the Ph.D. thesis of Gilbert Bergna [63] and the postdoc of Nikola Stankovic [64], were updated so that they could be used in this project. They were assembled with the coils to obtain a 1-phase HB-MMC. The prototype was operated in open loop using an OP 5600 real-time target for the low level control (nearest-level modulation and capacitor voltage balancing). It operated as expected, in inverter mode for a DC voltage of 150 V up to 760 W. The normalized arm coils losses were ten times lower for the cryo-MMC compared to the HB-MMC with uncoupled copper arm coils. The schematic is shown in Fig. 4.17(a) and the prototype is shown in Fig. 4.17(b).

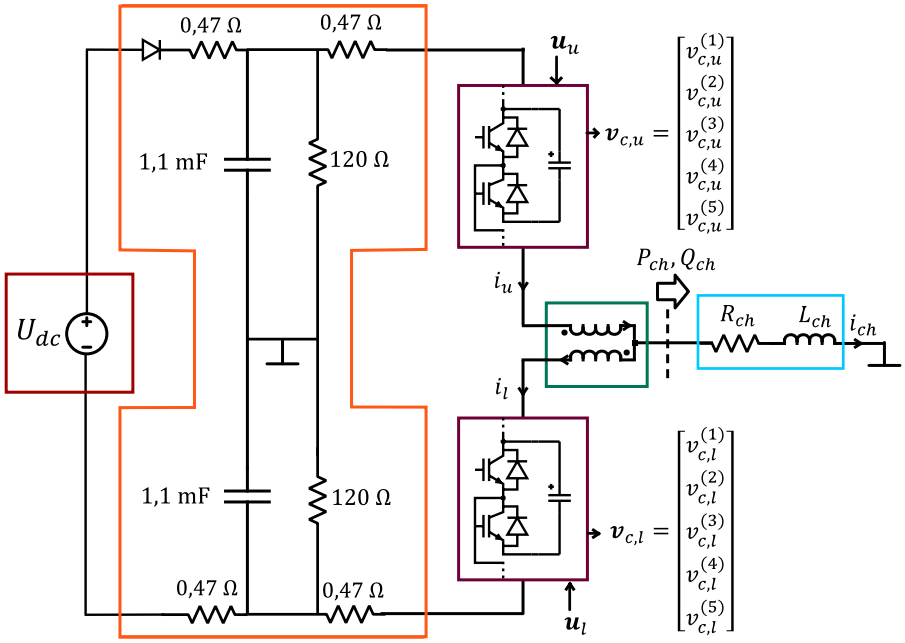

(a) Schematic

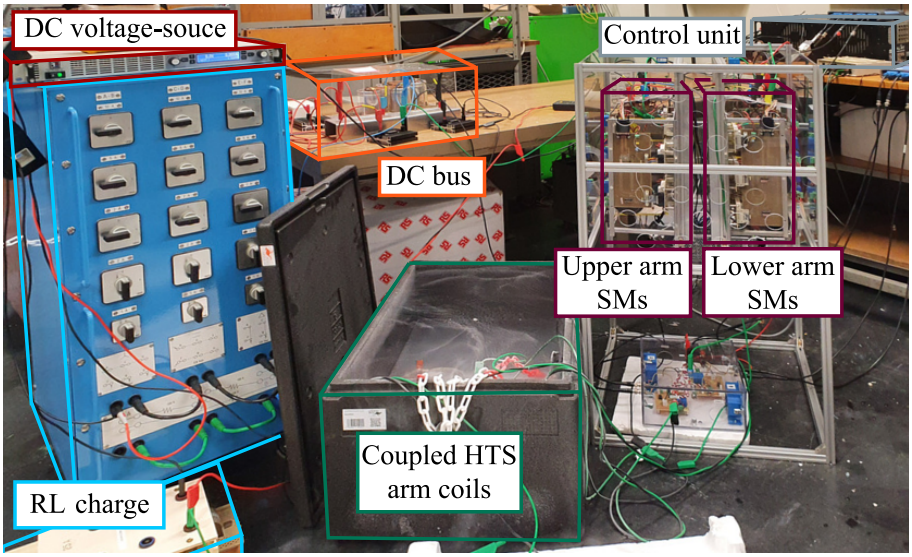

(b) Prototype

Figure 4.17: 1-phase 6-level cryo-MMC (Rafael MEDEIROS, Mar. 2022) [D4].

To assess the technical feasibility of the concept, we extrapolated this design to the reference 1 GW ±320 kV HB-MM station [chap.IV, D4]. Considering directly-coupled HTS arm coils operating at 65 K, we computed the cryo-MMC steady-state and transient performances in normal and fault operation conditions. It confirmed that directly-coupled HTS arm coils can help reducing the conversion losses (a reduction of 8%) while providing an effective fault current limitation (a reduction of 80%). Note that the weight and the volume of coupled HTS arm coils (including the refrigeration system) is greatly reduced too (a reduction of 76% and 82% respectively).

Credits

Rafael MEDEIROS [D4] worked hard on this converter as part of his thesis. Many students were involved at different steps (see chapitre 8). We acknowledge the help of José DE FREITAS (GeePs), Damien HUCHET (GeePs), Richard BELJIO (GeePs) and Amir ARZANDE (GeePs).

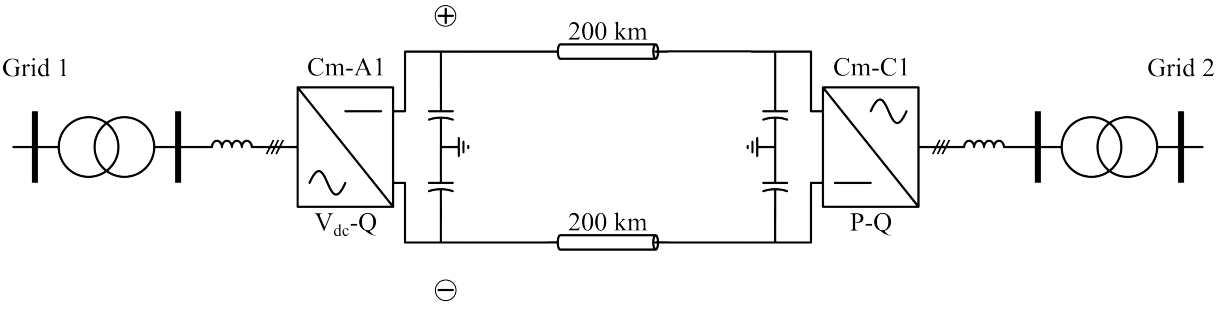

(a) circuit of the HVDC link

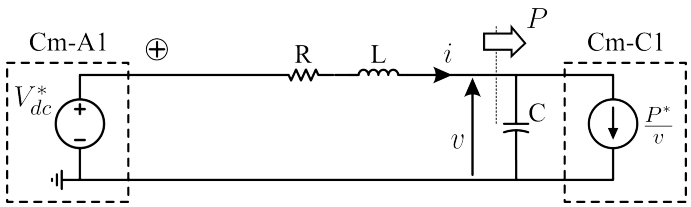

(b) equivalent circuit of the positive pole

Figure 4.18: CIGRE B4 DC grid test system DCS1.

4.5.4 Superconducting power filter (ScPF)

While looking at the potential of HTS coils to provide fault current limitation to an HB-MMC, we naturally investigated superconducting fault current limiters [ic20, p22]. A fault current limiter is designed to provide over-current protection during fault conditions. But outside of fault condition, the asset is left unused. Could it provide another functionality? If yes, this might increase industry's interest in the technology and accelerate its spreading. These consideration lead us to propose a new device referred to as "superconducting power filter" (ScPF). It aims at increasing the stability of HVDC grids by adding a current-dependent resistance to the grid.

Concept

To clarify the concept, we consider an HVDC link. Fig. 4.18 shows the CIGRE B4 DC grid test system DCS1 together with the equivalent circuit of the positive pole (assuming balanced operation and ideal controllers). The constant voltage source models the DC side of the HVDC converter Cm-A1 operating in Vdc-Q mode. The RLC elements model the HVDC cable (and the DC capacitor of the 2-level VSC). The power-controlled current source (power load) models the DC side of the HVDC converter Cm-C1 operating in P-Q mode. Because the power load behaves like a negative resistance, it reduces system damping and can lead to instability. The topic has been extensively addressed in the literature (see [105] for example). The approximated expression for the stability condition of the DC grid of Fig. 4.18 is recalled here,

$$P^* \leq \frac{RC}{L} V_{dc}^{*2} \tag{4.1}$$

In practice, the control loops modify the dynamics of the equivalent circuit, making it difficult to calculate precisely the stability limit. But this expression is useful to illustrate that above a given power reference P^*, the system becomes unstable. To increase the stability limit, one could, for example, increase the DC grid equivalent resistance R [106]. But in nominal operation, the power losses would increase. This issue can be solved by using a superconducting power filter (ScPF). This is a non-inductive superconducting coil that behaves as a current-dependent resistance. In nominal operation for which the critical current I_c of the device is much larger than the operating current i, there is virtually no losses. However during unstable operation, the operating current oscillates approaching I_c, the device resistance increases and damps the fluctuations to reach a new stable point of operation. The operation of the device is actually closely related to the one of a resistive fault current limiter (r-ScFCL), but here the superconductor is expected to remain in the superconducting state during transients, with the option of providing timely over-current protection if required.

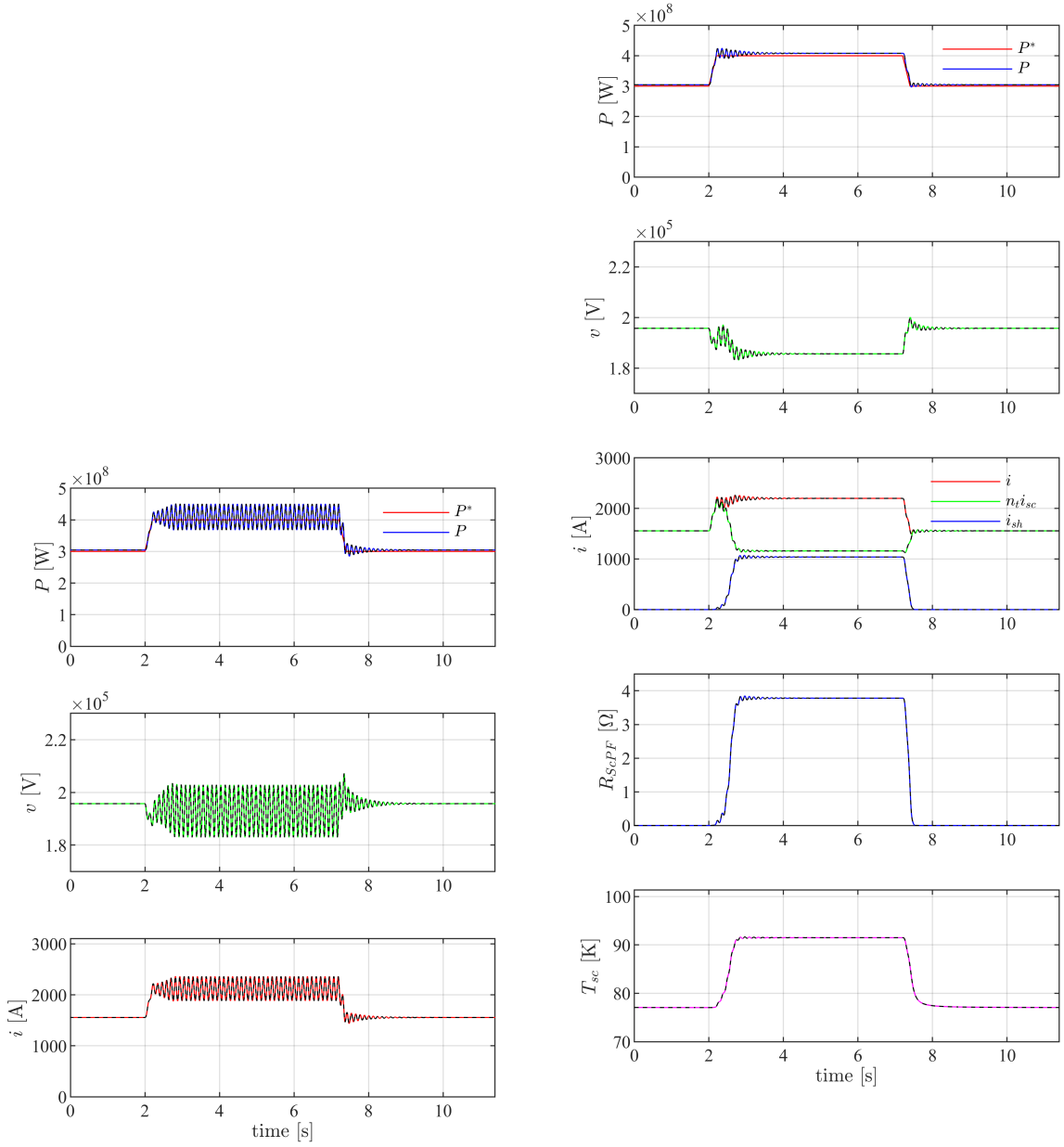

(a) without ScPF

(b) with ScPF

Figure 4.19: Stabilization of an HVDC grid using a ScPF. The continuous lines mark the signals of the positive pole. The dashed lines mark the signals of the negative pole. The active power reference ramp rate is 500 MVA/s per pole.

Numerical analysis

We simulated the impact of introducing a ScPF in the HVDC system DCS1, which was modified in order to decrease its stability [ic39]. The results of the simulation without ScPF are shown in Fig.4.19(a). We observe that the DC voltage starts oscillating when the active power transfer P increases. The stability limit was found to be around 350 MW per pole for this test case.

We now insert one ScPF in series with each cables. The ScPF is modeled using a thermo-electric lumped-parameter model [p22] that allows us to realistically represent the dynamic response of the superconductor. The results of the simulation with ScPF are shown in Fig. 4.19(b). When the power

reference increases above the stability limit, the current going through the ScPF becomes larger than the device critical current $i > n_t I_c$, both its resistance R_{ScPF} and its temperature T_{sc} increase. This is because the superconductor starts to enter its resistive state thereby dissipating active power. The current now flows simultaneously through the superconductor and through the shunt $i_{sh} > 0$. Following Equation (4.1), the stability limit is higher thus explaining the stabilization of the DC grid. When the power reference goes back bellow the stability limit, the temperature decreases and the superconductor resistivity falls back to zero.

This demonstrates that the ScPFs are providing the stabilization function. In addition, this shows that the ScPFs can recover their superconducting state in few tens of milliseconds after the transient, since they operated around their critical current without thermal runaway (quench).

Towards an experimental proof of concept

A laboratory scale experimental setup is being assembled to back up the numerical results. The DC test grid is constituted of an ideal constant DC voltage source and a controlled power load connected through a RLC filter in series with a superconducting power filter (Figure 4.20). The ideal DC voltage source emulates the HVDC converter operating in Vdc-Q mode. The controlled power load emulates the HVDC converter operating in P-Q mode.

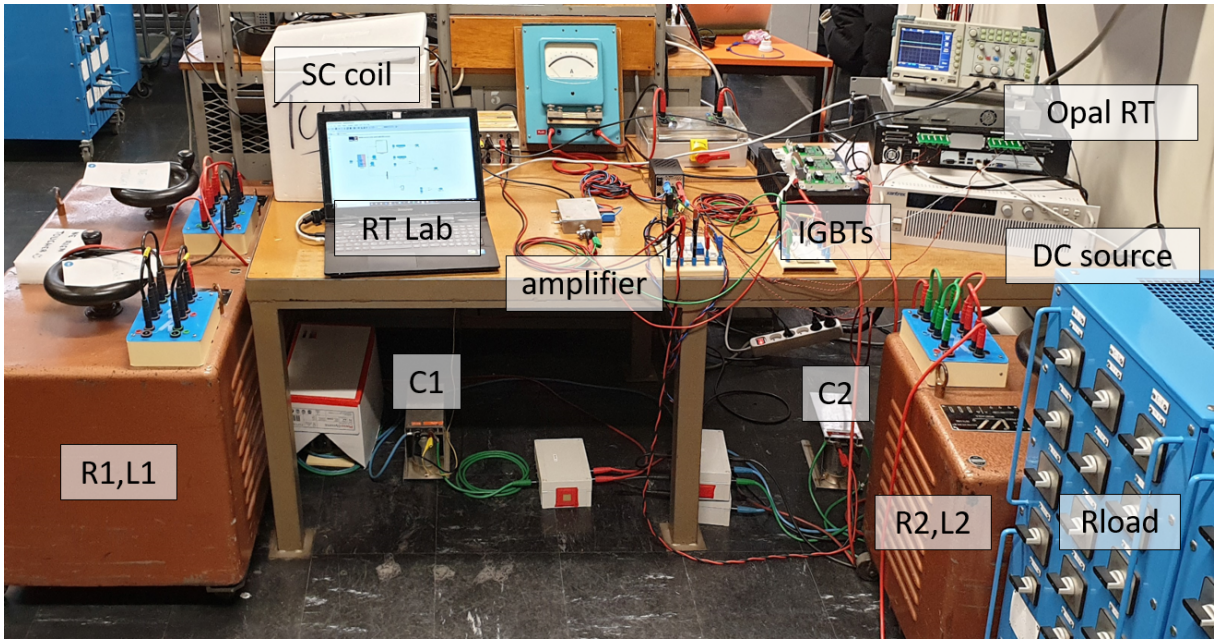

Figure 4.20: DC test grid for the proof of concept of the ScPF.

Several ScPF prototypes have been realized with different HTS conductors. The one shown in Fig. 4.21(d) has been wound with 2 m of ReBCO HTS coated conductor manufactured by SuNAM (Korea). The one shown in Fig. 4.21(e) has been wound with 5 m of BSCCO HTS conductor manufactured by Sumitomo (Japan). Fig. 4.21(g) shows our final prototype: an industrial scale ScPF wound with 100 m of BSCCO. The IV curve of a BSCCO prototype measured in liquid nitrogen at 77 K is plotted in Fig. 4.22. The measured critical current obtained for the usual 1 µV/cm criteria is 175 A, which is similar to the datasheet value. This demonstrates that the superconductor has not been damaged during winding. The next step is to connect the ScPF to the DC test grid to confirm experimentally the functionality.

(a) 1st prototype (b) 3rd prototype (c) 3rd prototype

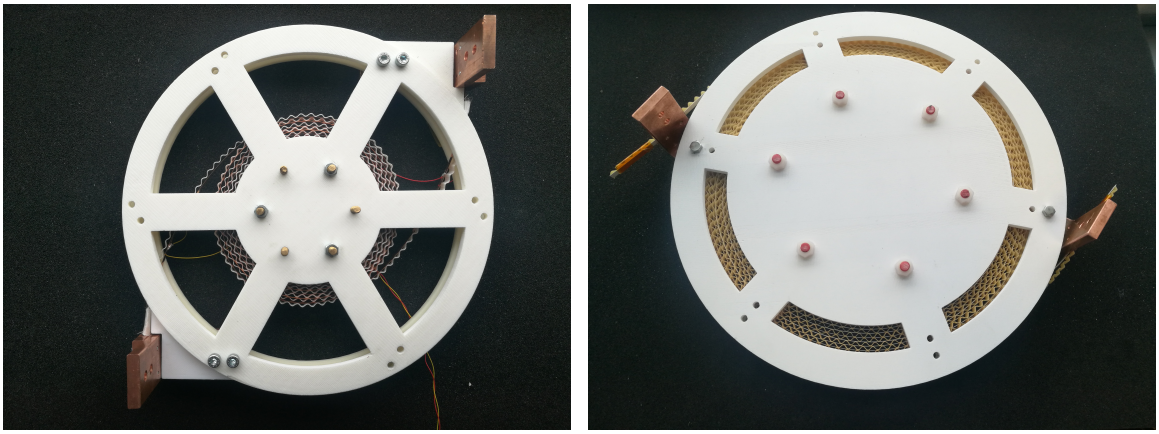

(d) ReBCO prototype (e) 3rd prototype

(f) 5th prototype (g) 5th prototype

Figure 4.21: Winding of the ScPF prototypes at GREEN Laboratory, Nancy (Jan. 2020-Apr. 2021).

Credits

The development of the ScPF is being carried out in collaboration with Bruno DOUINE (GREEN, Universtié de Lorraine) and Frederic TRILLAUD (UNAM) with the financial supports of the company RTE (research contract in 2019-2020) and SEEDS (Appel à projets internes 2019). Many students were involved at different steps (see chapitre 8). We acknowledge the help of Isabelle SCHWENKER (GREEN), Michel POLICE (GeePs) and Damien HUCHET (GeePs). The results have been published in [p36, p35, p32, ic55, ic53, ic45, ic44, ic43, ic38, ic35, ic22, ic16] and [nc33, nc29, nc27, nc12, nc9].

4.5.5 Set up of a PHIL platform

To facilitate prototyping and testing of electrical equipments, we set up a Power Hardware-in-the-Loop (PHIL) platform. PHIL simulation uses a real-time simulator to compute a model of a given system in real time and to send the power signals from the model to a physical system connected to the simulator. Power

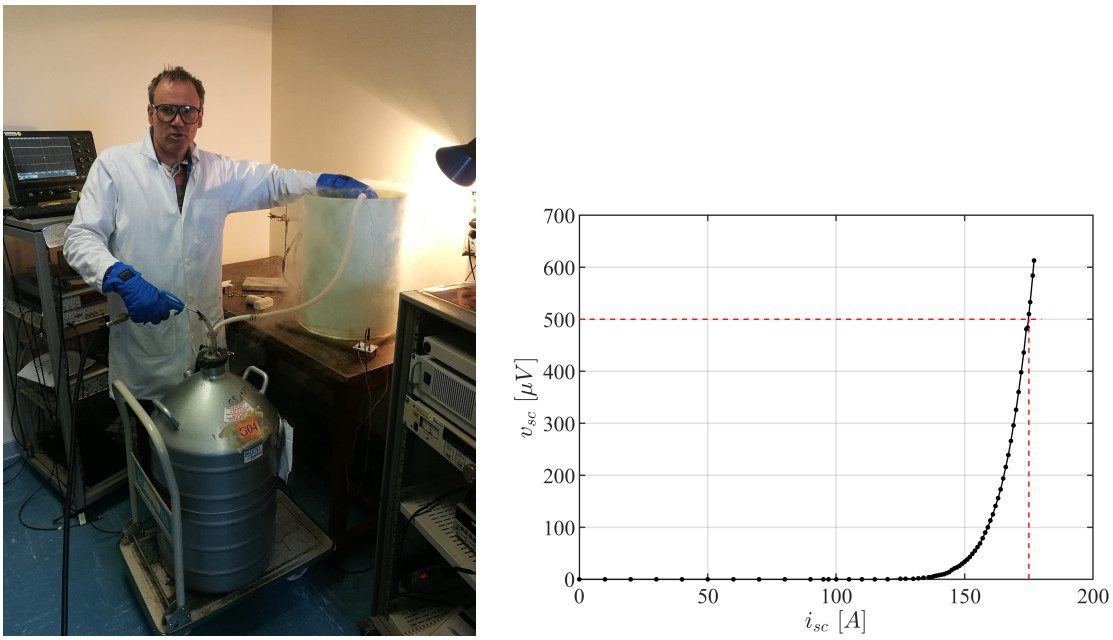

(a) Measurement

(b) IV curve of the ScPF shown Fig. 4.21(e)

Figure 4.22: DC characterization of a ScPF prototype.

amplifiers are inserted between the real-time simulator I/Os and the physical system. This enables us to test multiple systems, including power converters, electrical machines and PV load, while also benefiting from high-fidelity simulation that provide great flexibility and safety.

An overview of our PHIL platform is shown in Fig. 4.23. It consists of a real-time computer (Opal RT 4510) and a 3-ph real-time amplifier (3x 3.3 kVA). The current test capabilities of our platform (2022/09):
- 4 quadrant operation
- 3-ph AC+DC arbitrary waveforms $\leq$ @2 kHz
- 24 A, 220 V L-L, 3$\times$ 3.3 kVA

Credits

The installation has been carried out by Frédéric REYMOND-LARUINA [D6] as part of his PhD thesis. Many students were involved at different steps (see chapitre 8). We acknowledge the help of José DE FREITAS (GeePs), Damien HUCHET (GeePs), Richard BELJIO (GeePs) and Amir ARZANDE (GeePs).

4.6 Levelized cost of conversion of electricity ($LCOCE$)

The concept of levelized cost per unit can be used to compare the economic competitiveness of various AC/DC power conversion technologies. In that specific context, we call it "Levelized Cost Of Conversion of Electricity" ($LCOCE$). It represents the average revenue per unit of energy converted over the system lifetime required to break even. It is expressed in euro per megavolt-ampere hour [€/MVAh] [65].

Under the hypothesis of section 1.2.5, the $LCOCE$ is expressed from (1.8) as,

$$LCOCE = \frac{\sum_{t=0}^{T} \frac{CAPEX_t + OPEX_t}{(1+r)^t} - SV}{\sum_{t=1}^{T} \frac{EC_t}{(1+r)^t}} \tag{4.2}$$

where $CAPEX_t$ is the capital expenses in year t, $OPEX_t$ is the operating expenses in year t, r is the discount rate, EC_t is the electric energy converted in year t, T is the system lifetime and SV is the salvage value.

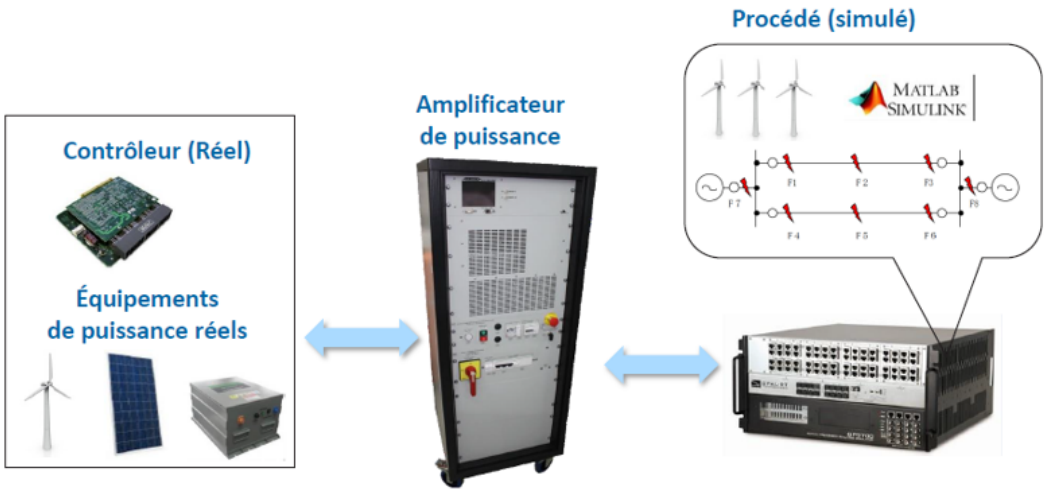

(a) Schematic

(b) Our setup

Figure 4.23: Overview of the GeePs PHIL test platform (June 2022).

4.7 A techno-economic assessment of the cryo-MMC

4.7.1 Goal and scope definition

Goal: In this section, to complete the discussion, we propose an abbreviated techno-economic assessment of the cryo-MMC. We compare an installation using a conventional MMC and an installation using a cryo-MMC.

Case study: We consider the reference HVDC converter station described in section 4.2. The system is a 1 GW ±320 kV HB-MMC HVDC station. The main parameters of the test case are summarized in Table 4.2.

Scenario: To account for the converter downtime, the energy converted EC_t is multiplied by an utilization factor that is set here equal to 0.95 [D4].

Table 4.2: HVDC transmission system parameters

Quantity	Symbol	Value	Notes
Nominal active power	P_n	1000 MW	
Nominal reactive power	Q_n	300 MVAr	
Nominal DC voltage	V_{dc}	±320 kV	
Nominal grid voltage L-L RMS	U_g	400 kV	
System lifetime	T	40 years	[D4]
Cost of electricity	C_{elec}	60 €/MWh	[D4]
Discount rate	r	0.041	[71]
Salvage value	SV	0	unknown

Optimization problem: We look for the HTS arm coil sizing that minimizes the $LCOCE$. The optimization problem is formulated as,

$$\begin{aligned} \underset{X}{\text{minimize}} \quad & LCOCE(X) \\ X = & \{N_p, N_s, T_{op}\} \\ \text{subject to} \quad & L \geq L^* \\ & K \geq K^* \end{aligned} \tag{4.3}$$

where the optimization variables X are: the number of HTS modules in parallel N_p, the number of HTS modules in series N_s and the operating temperature $T_{op} \in [65, 75]$. The constraints on the self inductance L and on the coupling coefficient K ensure that the MMC has the required performances. A similar optimization problem is formulated for the MMC.

4.7.2 Inventory analysis

The system elements are shown in Fig. 4.2. Details about the technical and economic parameters can be found in [D4].

Benchmark product system: For the conventional MMC, we consider dry-type air-core uncoupled coils (see section 4.3). The required self inductance is 51.6 mH. The arm coils are obtained by winding a suitable number of turns in series and in parallel, to meet the required arm coil nominal current and inductance. The main parameters are summarized in Table 4.3.

Table 4.3: HB-MMC parameters

Parameter	Symbol	Value	Notes
Arm coil nominal current	$I_{coil,n}$	1750 A	[Tab. IV.5, D4]
Required arm coil self inductance	L^*	51.6 mH	[Tab. IV.5, D4]
Required arm coil coupling coefficient	K^*	0	uncoupled

Proposed product system: For the cryo-MMC, we consider directly-coupled HTS arm coils (see section 4.4.2). The required self inductance is 27.3 mH for a coupling factor ≥ 0.6. It was demonstrated in [chap.III, D4] that a MMC with such directly-coupled arm coils has smaller arm coils than the reference MMC but similar steady-state performances. We assume that the HTS arm coils are obtained by connecting a suitable number of "HTS modules" in series and in parallel, to meet the required arm coil nominal current and inductance. Note that we use present technical and economic parameters of YBCO HTS conductor for this analysis, and that some parameters were obtained from our prototype. The main parameters are summarized in Table 4.4.

4.7.3 Calculation of indicators

For the MMC part, we use the technical models presented in section 4.5.1. For the other system elements, details about the technical and economic models can be found in [D4]. The optimization is performed manually.

Table 4.4: Cryo-MMC parameters

Parameter	Symbol	Value	Notes
Arm coil nominal current	$I_{coil,n}$	1750 A	[D4]
Required arm coil self inductance	L^*	27.3 mH	[D4]
Required arm coil coupling coefficient	K^*	≥ 0.6	direct coupling [D4]
Operating temperature	T_{op}	65 - 75 K	
HTS tape width	w_t	12 mm	[D4]
HTS tape critical current	I_c	401.2 A	SF, 77 K [D4]
HTS module dimensions		$40 \times 40 \times 8$ cm^3	from prototype [D4]
HTS module weight		4.85 kg	from prototype [D4]
HTS module self inductance	L_m	6.6 mH	[D4]
HTS module self resistance	R_m	124.6 $\mu\Omega$	[D4]
HTS module coupling coefficient	K_m	0.8788	from prototype [D4]
HTS module critical current	$I_{c,m}$	377 A	SF, 65 K [D4]
HTS module current margin		20%	[D4]

Table 4.5: Case study optimal results

	Conventional MMC	cryo-MMC
Nb HTS modules in parallel N_p [-]	-	6
Nb HTS modules in series N_s [-]	-	25
Operating temperature T_{op} [K]	RT	65
$LCOCE$ [€/MVAh]	1.107	1.087

The results of the optimization are summarized in Table 4.5. The optimal $LCOCE$ for the cryo-MMC is 1.087 €/MVAh, to be compared to a $LCOCE$ of 1.107 €/MVAh for the conventional MMC. This indicates that, for this case study, the cryo-MMC could be a competitive solution.

4.7.4 Interpretation

We would like to use this case study to discuss how the *LCpu* can help to apprehend the complexity of sizing a complex system. This can be illustrated by plotting the $LCOCE$ as a function of the operating temperature. The result is shown in Fig. 4.24. For the sake of discussion, we have plotted the $LCOCE$ from 47 to 77 K, but to avoid solidification of the LN2 the operating temperature must actually stay above 65 K (green area). The $LCOCE$ has a distinct "Chinese temple roof" shape.

This is because there is a trade-off that impacts both the CAPEX and the OPEX. On the one hand, the lower the temperature, the higher the HTS tape critical current. It means that less HTS tape is required to obtain a given coil. As a result, the lower the temperature the lower the CAPEX. The number of modules in parallel being a natural number, the CAPEX has a "staircase" shape. On the other hand the lower the temperature, the lower the cryocooler efficiency. It means that more electric power is required to remove each watt of losses from the cryogenic environment. As a result, in first approximation, the lower the temperature the higher the OPEX. This can be seen by the gradient of each staircase step.

The use of the $LCOCE$ makes it easy, from our point of view, to visualize such trade-off and to account for its economic impact on the life-cycle.

4.8 Summary and perspectives

In this chapter, we described the work that has been carried out on the techno-economic assessment of cryo-MMC for HVDC converter stations. The efforts cover both the experimental and the theoretical part.

The design and construction of a full-bridge MMC converters and of a cryo-MMC, have been carried

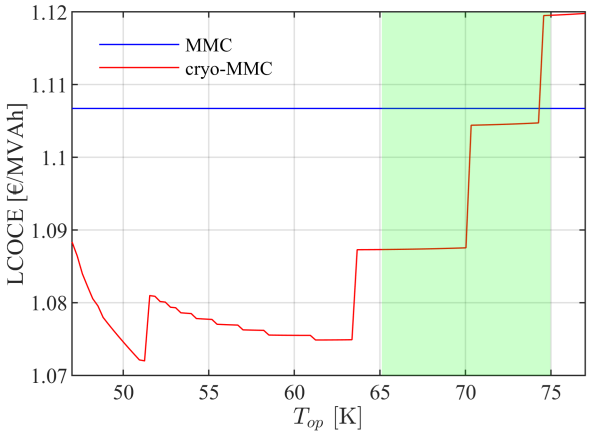

Figure 4.24: Levelized cost of conversion of electricity ($LCOCE$) as a function of the operating temperature for the cryo-MMC.

out between 2016 and 2022. The in-house development of a power converters allows us to have full control on their design, to test original ideas and to repair them easily. This is a characteristic trait of our research group. We aim to keep developing this competence, while improving our prototyping speed using our PHIL platform.

Our theoretical work is mainly focused on the optimal design of the passive elements of a converters via the development of fast models for the sizing. The techno-economic analysis shown here could be expanded and integrated to our design routine. The goal would be to size power converters that are optimal considering their life-cycle.

Chapter 5

SAUREA's motor-pump for photovoltaic water pumping systems

5.1 Context

In sub-Saharan Africa, more than 300 million people do not have access to safe drinking water and most of them live in rural areas. The most common alternatives for water extraction in low-income rural areas of developing countries are gathering water from an open well with a bucket and a rope, and hand pumps [184]. Water from open wells is usually not potable because it is exposed to contamination through mud [185], and can cause diseases such as diarrhea and trachoma [186, 187]. Contrarily to open wells, hand pumps can provide water suitable for drinking as they extract water from aquifers and they are sealed to prevent contamination [185]. However, as for open wells, the pumped flow rate is limited by human strength, water extraction is hard and time consuming, which is responsible for significant queuing time [188, 189, 190]. Finally, hand pumps do not allow to reach deep aquifers (typically groundwater levels deeper than 50 m [191]) and require regular maintenance due to moving parts [185].

In comparison to the alternatives described above, electrified water pumping systems appear as promising for providing water for domestic use (drinking, cooking, personal hygiene and laundry). Indeed, despite their higher initial cost [184], they allow to reach deeper aquifers and they provide higher flow rates. Consequently the water collection and queuing time is strongly reduced, which gives more free time for other activities [192, 193]. In addition, they allow to lower the hardness of water collection [192, 193].

Nevertheless, a deficient access to improved water sources is generally correlated to no access to electricity [194, 195]. In this context, the most common energy sources for electrified water pumps in off-grid areas are photovoltaic energy and diesel [M4]. Despite their higher capital cost [184, 193, 196], photovoltaic water pumping systems (PVWPS) have become competitive in comparison to diesel pumps in off-grid rural areas in terms of life cycle cost [197, 198]. In several cases, they are even more economically viable [196, 199]. However, the high capital cost still represents a challenge for financing PVWPS. Another key advantage of PVWPS in comparison to diesel pumps is their long lifetime [196, 200, 201] and their reduced maintenance needs [196, 202, 203], which is particularly important in rural areas [204]. Moreover, PVWPS do not emit toxic fumes [206] and are less noisy [205], reducing their effect on the local operator. In regions with suitable solar resources, and with appropriate planning, off-grid PVWPS can therefore provide significant contributions to closing the water access gap.

5.2 Overview of a photovoltaic water pumping system

We consider the PVWPS shown in Fig. 5.1, which is a common architecture for domestic water access [183][p33]. The architecture of a PVWPS for irrigation would be different. Note that the motor, the power electronics DC/AC converter and the pump are integrated into a single casing; the assembly is called "motor-pump".

The PV array generates electricity that is fed to the motor-pump. The motor-pump pumps water from the borehole to the water tank. Depending on the water level in the tank, the float switch sends a signal to the controller to start/stop the motor-pump. The inhabitants collect water at the fountain. Note that there is no energy storage system: the motor-pump is stopped when there is no sunshine. The water tank acts as a storage system.

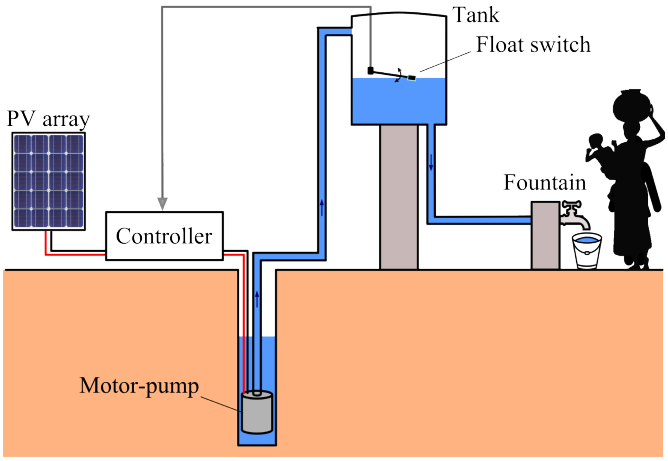

Figure 5.1: Overview of a photovoltaic water pumping system.

This system includes 3 parts that are shown in Fig. 5.2. The electric part includes 4 types of components: PV array, DC cable, motor-pump and float-switch. The hydraulic part includes 6 types of components: borehole, pipe, tank, fountain, fountain tap and water meter. The construction part includes 3 types of components: PV array structure, wire fence and signpost.

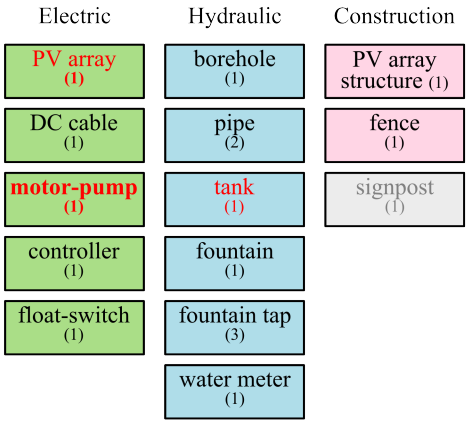

Figure 5.2: Components of a photovoltaic water pumping system. The numbers in parenthesis indicate the number of such component in the system. The components in red font are directly impacted by the technology shift. The components in gray block are not considered in the following analysis.

To give an idea of the order of magnitude of the quantities involved, we consider the set of parameters of the PVWPS installed in the village of Gogma, which are summarized in Table 5.1 [D3].

5.3 A conventional technology: the submersible PV motor-pump

Conventional PVWPS use either a DC motor directly connected to the PV array (Fig. 5.3(a)) [211] or an AC (brushless) motor connected to the PV array through a DC/AC converter (Fig. 5.3(b)) [212]. The later solution is widely adopted since the DC/AC converter can track the maximum power point of the PV array and operate efficiently the AC motor. A typical example of this architecture is the Grundfos SQFlex submersible PV motor-pump shown in Fig. 5.4. It consists of the following elements:

- **PV array**: It converts the solar energy into electrical energy. It consists of one or several PV modules depending on the requirements.
- **Motor-pump**: It is installed in the borehole, submerged in water.

Table 5.1: Main parameters of Gogma's photovolatic water pumping system

Parameter	Symbol	Value	Notes
Number of users	-	∼280	
Static water level	H_{bs}	-4 m to -10 m	water level in the borehole when there is no pumping, varies with time [p25]
PV array peak power	$P_{pv,p}$	620 Wp	STC [p.66, D3]
Motor-pump reference	MP	SQFlex 5A-7	[p.36, D3]
Tank volume	V_t	11.4 m^3	[p.36, D3]

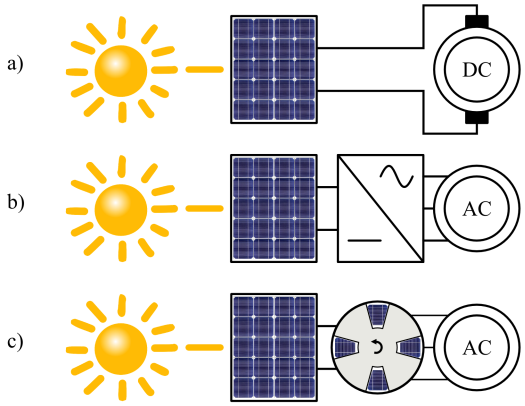

Figure 5.3: (a) PV cells + DC motor, (b) PV cells + DC/AC converter + AC motor, (c) SAUREA's photovoltaic transistor inverter-fed switched reluctance motor.

  - **DC/AC converter**: It has 2 functions. First, it converts the electrical energy from DC to AC. Second, it follows the Maximum Power Point (MPP) of the PV array.
  - **AC motor**: It converts the electrical energy into mechanical energy. For the SQFlex, it is a permanent magnet synchronous motor with segmented stator, operating at 3000 rpm for helical pumps and 3600 rpm for centrifugal pumps.
  - **Pump**: It converts the mechanical energy into hydraulic energy. For the SQFlex, it is either an helical rotor pump for large heads and low flows, or a centrifugal pump for low heads and large flows.
  - **Casing**: It protects the motor-pump from the surrounding mechanical or chemical corrosion. It is made of stainless steel.
- **Controller**: It is used to turn on/off the motor-pump manually or automatically (when the tank is full).

5.4 An innovative technology: SAUREA's PV motor-pump

5.4.1 Innovation

Alain COTY invented in 2012 a new motor drive, that we called the "photovoltaic transistor inverter-fed switched reluctance motor (PVT inverter-fed SRM)" (Fig. 5.3(c)). The specificity of this motor drive is that it is able to convert light energy into mechanical energy using PV cells, but without the need of any brushes or other power electronics. This could make it more affordable and reliable than conventional motor drives, and give it a competitive advantage for fully autonomous applications requiring thousands of operating hours without maintenance, like water pumping in rural areas. The technology is now being developed and commercialized by the company SAUREA, and is therefore called SAUREA's PV motor-pump in the following. A PVWPS with SAUREA's motor and a piston pump is shown in Fig. 5.5.

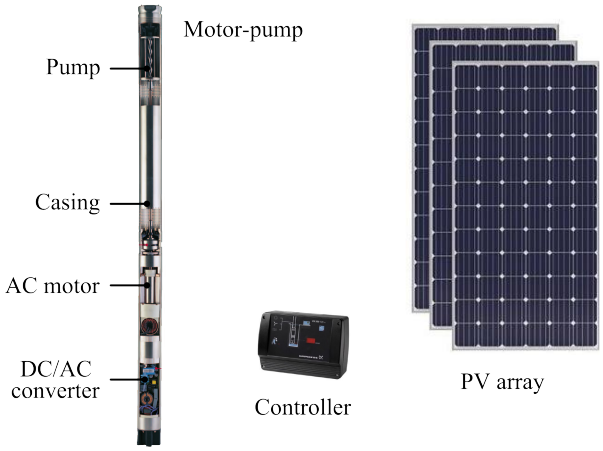

Figure 5.4: Submersible PV motor-pump: sectional view of the Grundfos SQFlex submersible motor-pump, its controller and a photovoltaic array (adapted from [210]).

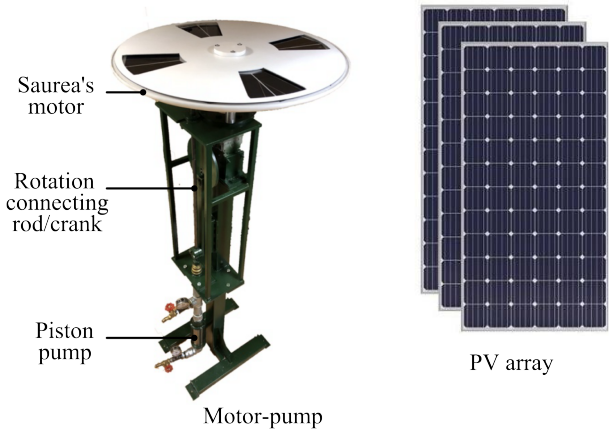

Figure 5.5: SAUREA's PV motor-pump: view of SAUREA's motor driving a piston pump and fed by a photovoltaic array.

5.4.2 Description

A "photovoltaic transistor inverter-fed switched reluctance motor" (Fig. 5.3(c)) is a solar-powered switch reluctance motor drive. The expression "photovoltaic transistor (PVT)" is used to designate a conventional photovoltaic cell used as a light-controlled power transistor. To obtain a motor drive, a set of PVTs controls the current fed from an external DC power source to the motor phases. The control is achieved by modulating the sunlight hitting the PVTs using a shutter driven by the motor rotor. If the external DC source is a solar panel, the resulting system is able to convert light energy into mechanical energy, without the need of any brushes or other power electronics components. This architecture was first proposed in [214], and analyzed in [p8, ic13].

To explain the operation of photovoltaic cells used as photovoltaic transistors, we adopt the convention shown in Fig. 5.6 with the understanding that the symbol represents a photovoltaic transistor (and not a phototransistor). The classical operation quadrant of a photovoltaic (PV) cell is quadrant II (generator). If we operate the PV cell in quadrant I, it can be used as a light-controlled transistor (PVT). Indeed from Fig. 5.6, for a given polarization $0 < v < v_{br}$, the current i is approximately equal to the short circuit current i_{sc}. And i_{sc} is approximately proportional to the product of the normal solar irradiance I_{sol} by the normalized illuminated surface S_{pv}. Therefore, one can control the PVT current by varying I_{sol} or S_{pv} .

Let's now have a look at the working principle of a photovoltaic transistor inverter-fed switched reluctance motor. For simplicity's sake, we consider here a simplified 3-phase SRM [215] having 3 stator teeth and 2 rotor teeth (SRM 3/2 without back yoke). The aim is not to introduce an optimal system,

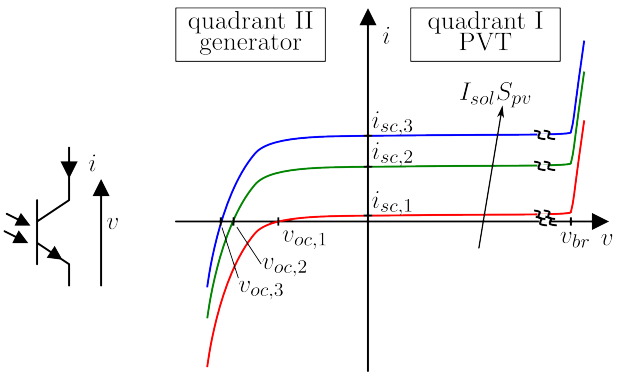

Figure 5.6: Photovoltaic transistor convention and idealized current-voltage curves for various $I_{sol}S_{pv}$. v_{oc} is the open-circuit voltage (∼0.6 V). v_{br} is the breakdown voltage (10-30 V). i_{sc} is the short-circuit current.

but to demonstrate the operating principle. The adopted inverter topology has one switch per phase, where each switch is a PVT (Fig. 5.7). The optical control of the PVT is obtained by using a shutter that is mechanically connected to the rotor, and that rotates synchronously with it. The DC voltage source could be replaced by a solar PV source for autonomous operation. A step-by-step operation of the PVT inverter-fed SRM is shown in Fig. 5.7.

5.4.3 Advantages and drawbacks

In SAUREA's motor, the DC/AC conversion from the PV array to the AC machine is performed optically by a mechanical shutter instead of brushes or power electronics. This offers several advantages. First, considering that the cost of the power electronics is usually substantial, SAUREA's motor could be inexpensive. Second, it potentially requires little maintenance and could therefore have a low life cycle cost.

On the other hand, SAUREA's motor have inherent limitations. The output power is directly limited by the number of PV cells that can be installed in the area swept by the shutter (imposing a mechanical constraint). Moreover there is no motion control possibility, and so its efficiency is relatively low. But this could be offset by the declining cost of the PV cells.

Finally other considerations should be taken into account, such as the absence of permanent magnets, the facility of recycling, etc.

5.4.4 State of the art

The technology is being developed by SAUREA since 2016. From 2020 SAUREA has commercialized the MPA100, a PVT inverter-fed SRM able to deliver 120 W at 1000 rpm. From 2022 SAUREA has commercialized the MPA200, a PVT inverter-fed SRM able to deliver 250 W at 500 rpm. Several commercial systems have been installed for water pumping (Fig. 5.8) and ventilation, in France and abroad. More information at `www.SAUREA.fr`.

5.5 Contributions

5.5.1 Turning Sun into Water

Installation and monitoring of a PVWPS for domestic water access

In the framework of the project "Turning Sun into Water", we raised funds and coordinated the installation of a PVWPS for the domestic water consumption of the inhabitants of Gogma, a rural community of Burkina Faso (Figure 5.9(a)). Gogma's PVWPS has a conventional submersible PV motor-pump. The first reason for installing this PVWPS was to improve our understanding of the system and of the local

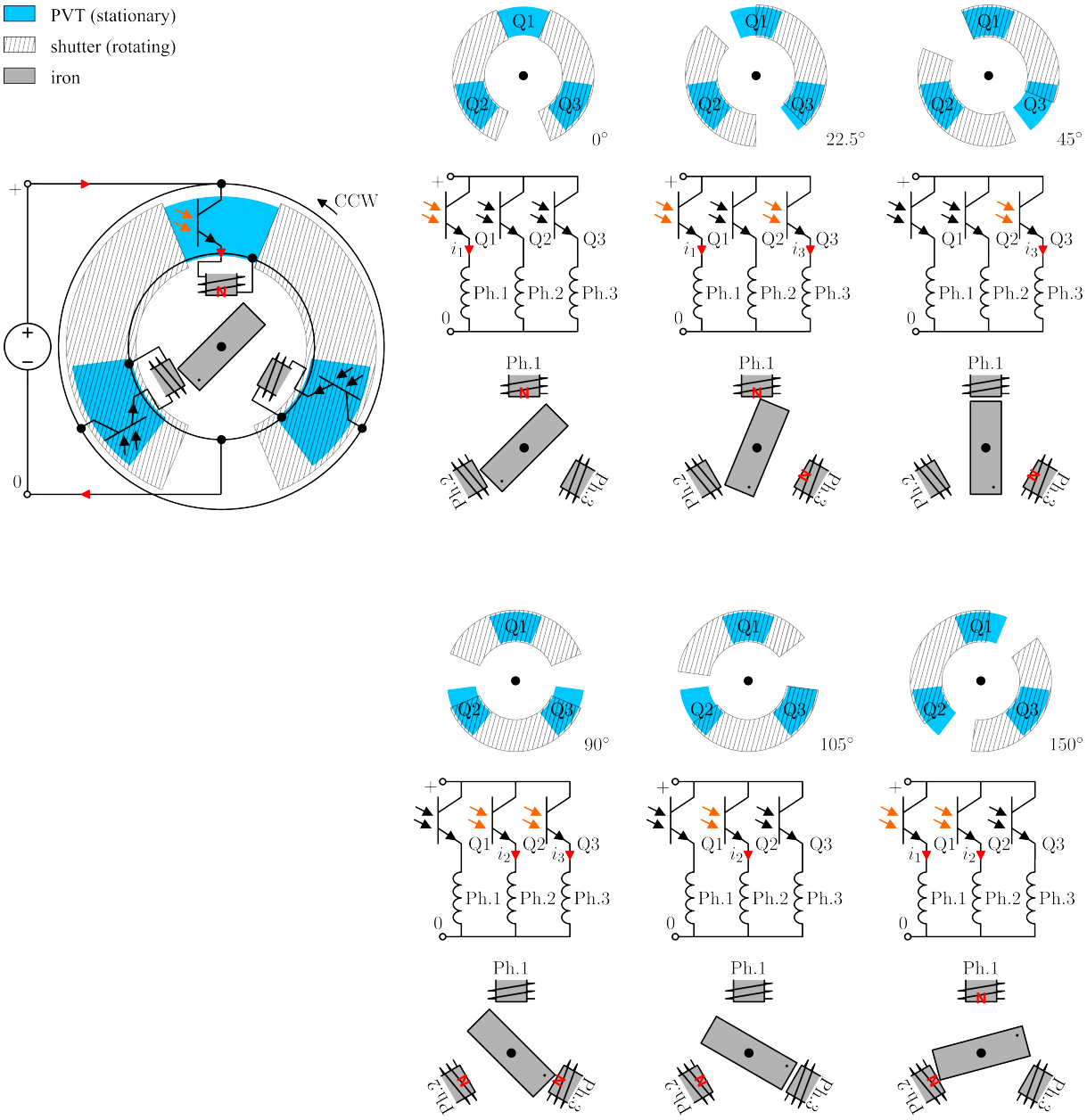

Figure 5.7: PVT inverter-fed SRM, overview and details of the operating principle (simplified magnetic circuit) [p8]. For an SRM 3/2, the PVT angle θ_{PV} and the shutter aperture angle θ_s are selected to be 45 degrees so that there is no generator (breaking) torque during operation. Assuming the rotor initial angle is between -15 and 15 degrees, the shutter lets the light hit PVT Q1. PVT Q1 is conducting, a current i_1 magnetizes the armature coil Ph.1. This causes the rotor to rotate in the counterclockwise direction to reduce reluctance. This rotation lets progressively the light hit PVT Q3. As a result, a current i_3 magnetizes the armature coil Ph.3. After a 45 degrees rotation, the shutter blocks the light on PVT Q1. The current i_1 goes to zero, as well as the armature coil Ph.1 magnetization. But PVT Q3 is still conducting: the magnetization of the armature coil Ph.3 causes the rotor to go on rotating in the counterclockwise direction. Similarly PVT Q2 becomes conducting, and allows the magnetization of Ph.2 by the current i_2. After a 105 degrees rotation, the shutter blocks the light on PVT Q3. The current i_3 goes to zero, as well as the armature coil Ph.3 magnetization. PVT Q2 maintains the rotation till the light hit again PVT Q1. Thus, a positive torque is generated continuously.

practices. The second reason was to gather real-world technical and socio-economic data to calibrate and validate our models.

(a) COVED Saint-Florentin (Dec. 2021). (b) Voies Navigables de France écluse n°76S (Jul 2021).

Figure 5.8: PVWPS with SAUREA's motor and a piston pump.

The installation started in September 2017. The borehole was drilled in November 2017. The PVWPS was installed between December 2017 and January 2018. On January 14th 2018: the PVWPS was opened for consumption to the inhabitants. The water collected at the fountain is used for 4 types of domestic uses: drinking, cooking, personal hygiene a nd laundry. Most of the users take water back home for drinking, cooking and personal hygiene and do the laundry next to the fountain (Figure 5.9(c)). A video of the village and of the PVWPS is also available at: `https://youtu.be/VrjM0edKVsI`. Table 5.1 summarizes the features of the PVWPS.

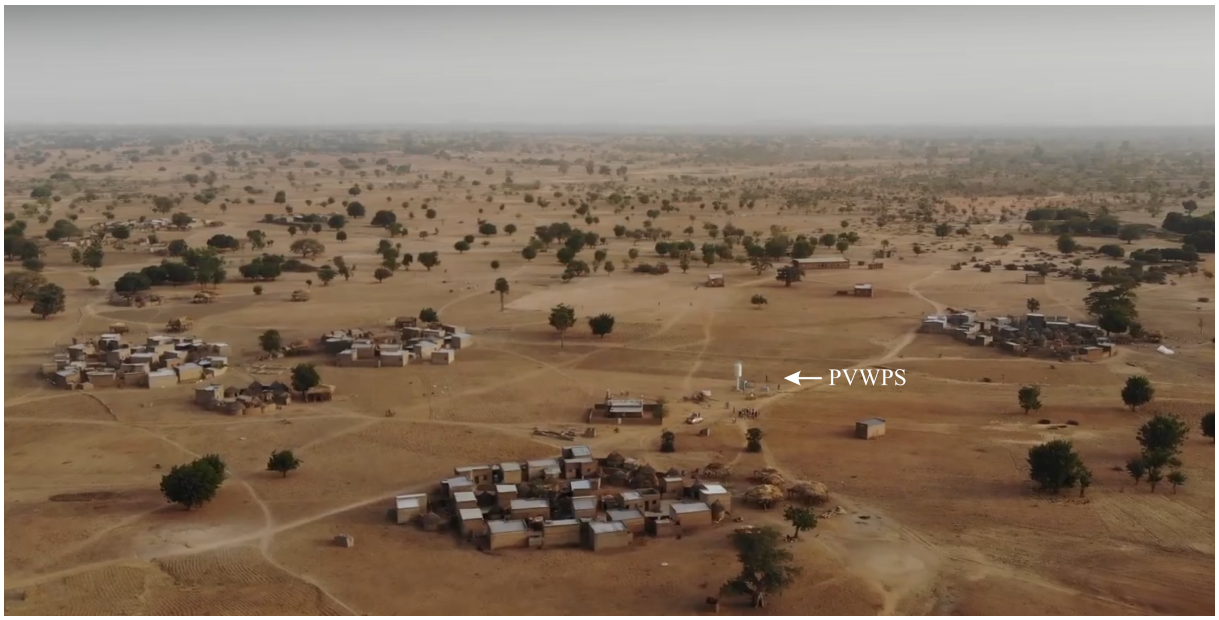

(a) View of the village.

(b) The departure of Matthias.

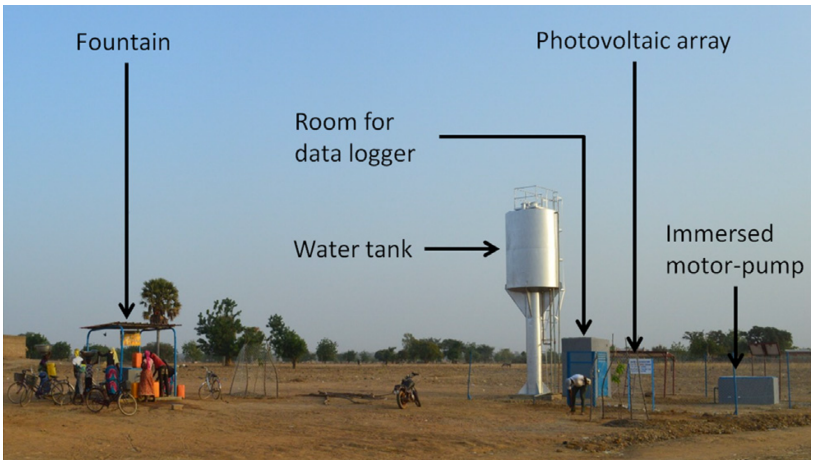

(c) View of the PVWPS

Figure 5.9: The photovoltaic water pumping system of Gogma [p26], Burkina Faso (Jan. 2018).

In Gogma, since September 2017, we have been collecting technical and socio-economic data covering several disciplines (Table 5.2): energy systems, social sciences, geography, hydrology and geophysics. Note that the PVWPS is monitored continuously since January 2018 thanks to a data logger that we developed (Fig. 5.10). This data logger was conceived with the idea of minimizing its cost in order to encourage its use for monitoring other PVWPS. The cost of the monitoring should be a small fraction of the cost of the system. In February 2019, an independent hydrostatic pressure sensor was installed to measure the water level in the borehole.

Table 5.2: Summary of the data collected in Gogma

Data	Description	Period
Observations	On-field observations on living conditions and water access	since Sep 2017
GIS	GPS positions of the households, water sources, important points of the village (shops, mosques, church, etc.)	Sep 2017
Geophysics	Detection of the presence of water along 4 profiles of 150 m long each by using electromagnetic methods	Sep 2017
Account books	The account book of a water source keeps track of users and costs	Oct 2017 – Jun 2018
Household surveys	Survey on the living conditions and water access Survey before installation: Survey after installation:	 Oct 2017 Oct 2018
Hydrology	4 step pumping tests and 1 long pumping test	Nov 2017
Water quality	1 physico-chemical test at the PVWPS bacteriological test at all the water sources for domestic water access	Nov 2017 Feb 2018
Monitoring	Irradiance on the plane of the PV array, ambient temperature, PV array temperature, PV array voltage, PV array current, pumped flow rate, collected flow rate, Water level in the borehole	since Jan 2018 since Feb 2019

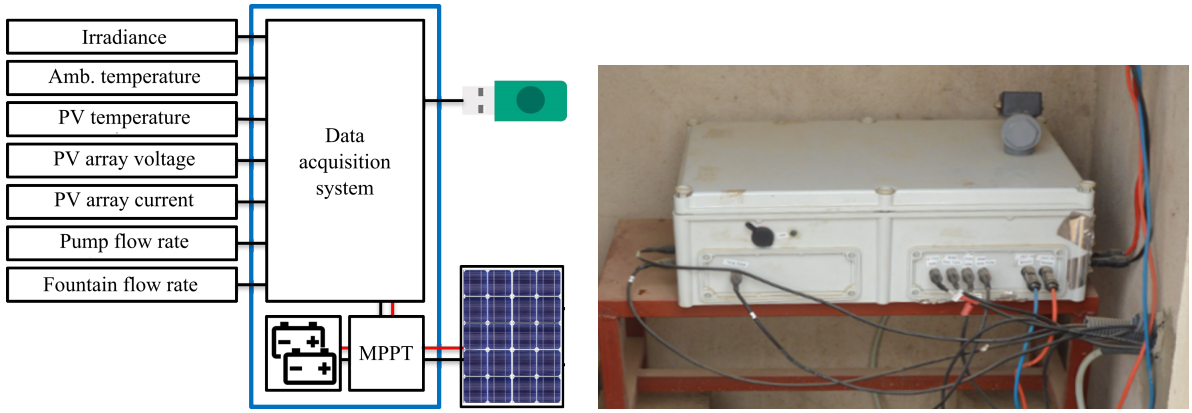

Figure 5.10: Data logger developed for the monitoring of the PVWPS of Gogma. It is powered by external PV modules (different from the ones of the PVWPS) and the recorded data are collected via a USB stick. The data logger collects and records the data with a time step of 2.2 s.

To our best knowledge, it is the first time that experimental measurements have been collected on a PVWPS for domestic water access in a rural village and on a PVWPS located in sub-Saharan Africa. Our long term goal is to monitor Gogma's PVWPS during its whole lifetime. This unique database, that is being created, will allow us to study the performance, the sustainability and the socio-economic impact of photovoltaic water pumping in sub-Saharan Africa and for domestic water access.

Beyond that, this database can also be used for other studies related to photovoltaic systems in rural villages in sub-Saharan Africa. For instance, we used it to train machine learning tools with the aim of detecting cleaning interventions on photovoltaic modules [p26] (collaboration with IFSTTAR).

Interdisciplinary model of a PVWPS in view of its optimization

In the framework of the PhD thesis of Simon MEUNIER (Université Paris-Saclay in co-supervision with Imperial College London and Université Cergy-Pontoise, funding IDI-IDEX), a methodology for

the optimal design of PVWPS for domestic water access in rural villages was proposed. The aim is to determine the sizings of the PVWPS and its positions in the village that minimize its life-cycle cost and maximize its positive socio-economic impact (e.g. use of water of better quality, decrease in the distance to collect water).

To do so, the first step was to build a model that relates the optimization variables, which are associated to the sizing and the position of the PVWPS, to the objective functions of the optimization, which are the life-cycle cost of the PVWPS and its socio-economic impact. An overview of the PVWPS interdisciplinary model is shown in Fig. 5.11. It is made of 4 models that are coupled to each other [D3]:

- **Demand model**: This is an econometric model which predicts the water sources where the households wish to go after installation of the PVWPS from the position of the PVWPS in the village and the water sources where the households go before installation of the PVWPS. To the best of our knowledge, it is the first model that predicts the water demand profile at water sources of a rural village.
- **Technical model**: From the solar resource and the groundwater resource, it simulates the different stages of the energy conversion chain within the PVWPS. This model has been validated by extensive comparison with the measurements from Gogma's PVWPS [p17, p30]. Sure to delight water pumping aficionados, we propose a new validation on Fig. 5.12). This technical model allows to identify the households that can effectively go to the PVWPS (water consumption) among the households that wish to go to the PVWPS (water demand).
- **Impact model**: It evaluates the socio-economic impact associated with the changes in water source between before and after the installation of the PVWPS. The socio-economic impact is quantified thanks to a combination of several indicators identified from the theory of change: water quality, extraction easiness, water cost [p18], distance household-source and WASH (water, sanitation and hygiene) diseases.
- **Economic model**: It determines the life-cycle cost *LCC* of the PVWPS from its sizing. It relies on cost functions obtained by fitting data collected through surveys and quotations.

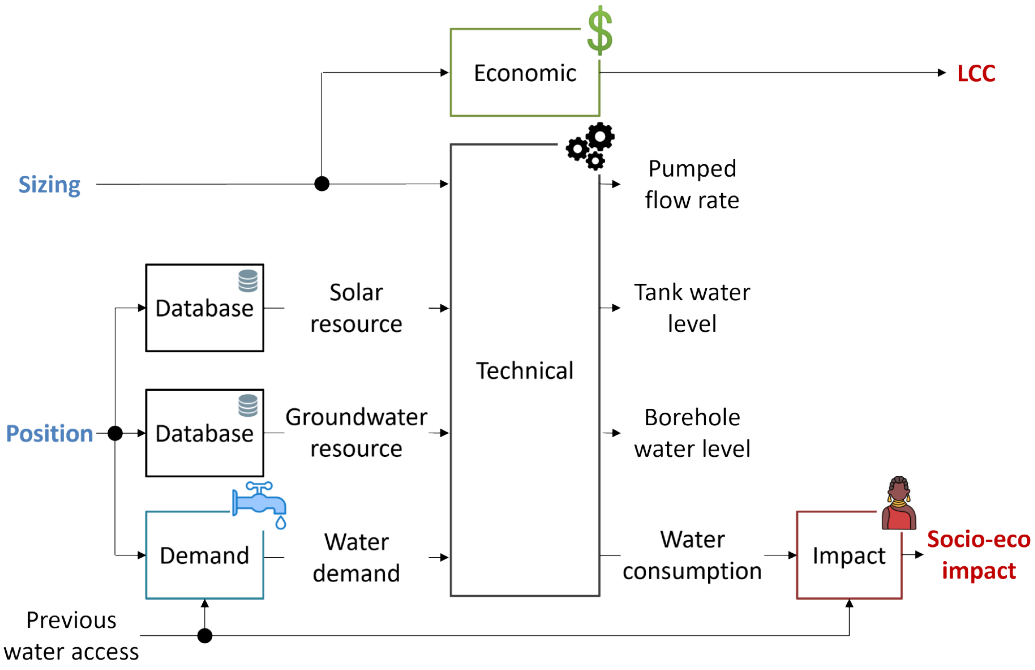

Figure 5.11: Block diagram of the PVWPS interdisciplinary model.

The first main originality of the proposed method is the introduction of the position of the PVWPS in the village as an optimization variable. This is particularly relevant given the extent of many rural villages in sub-Saharan Africa and the high number of water sources that are available to the inhabitants. The second main originality is the inclusion of the socio-economic impact as an objective function of the optimization. Indeed, governments and institutions that finance these systems aim at maximizing their positive socio-economic impact.

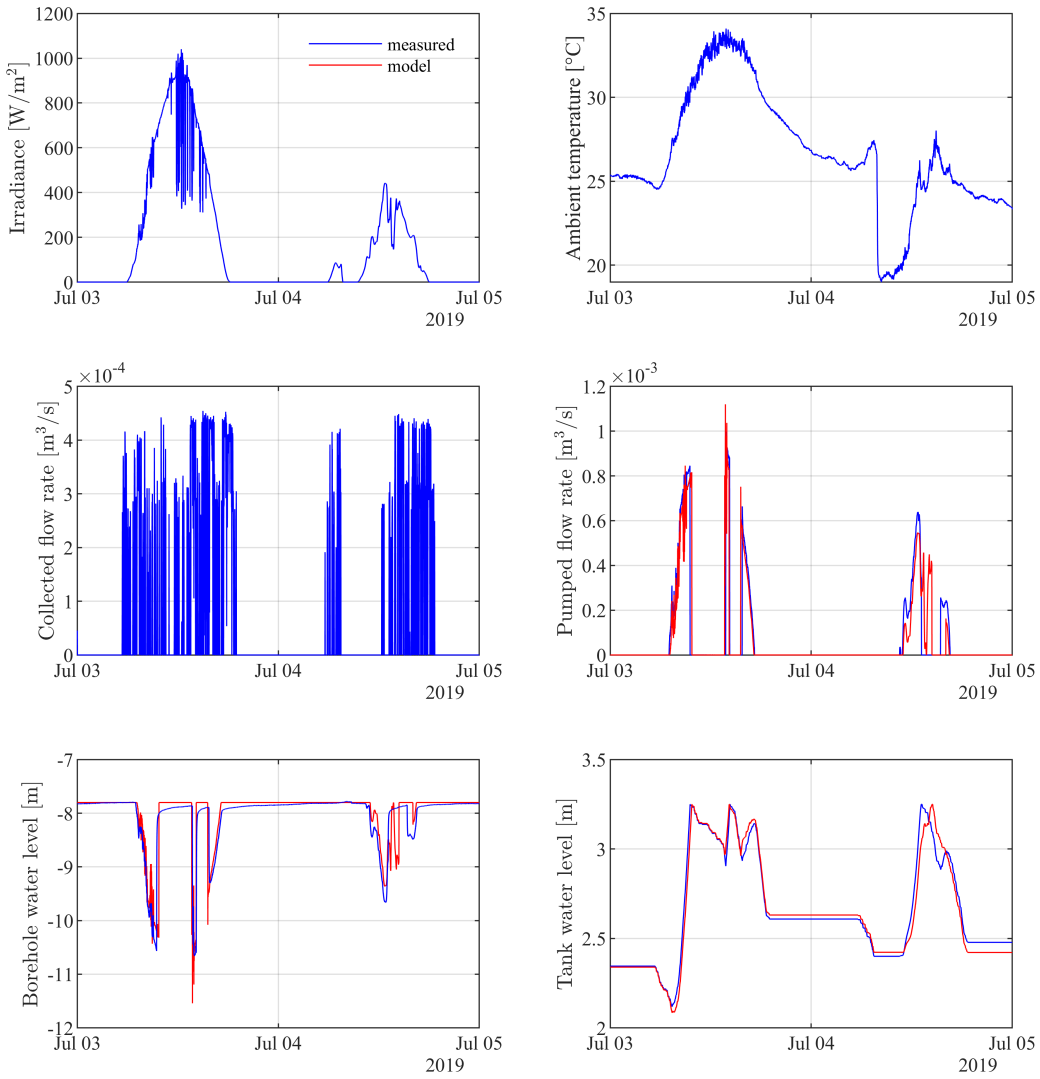

Figure 5.12: Sample of Gogma's experimental data and of the corresponding simulation results. The input of the model are the irradiance, the ambient temperature and the collected flow rate. The output of the model are the pumped flow rate, the borehole water level and the tank water level. Quiz: What happens late morning on the 4th of July?

First steps towards groundwater sustainability

As electrified pumping systems provide the opportunity to extract larger volume of water than hand pumps, increased attention has to be paid to the effect of pumping on groundwater resources in order to preserve groundwater sustainability [191]. The data collected in Gogma allowed us to develop and validate borehole models [p25, M6] (collaboration with Standford Univ.).

Comparison of water tank and battery storage for PVWPS

In order to be able to fulfil the water needs and to deal with the variability of the climatic conditions, a storage component is always required in PVWPS for domestic water use. The two mains possibilities for providing storage are: storing electrical energy produced by the PV array in batteries, or storing pumped water in a tank. Using Gogma as a case study, we compared tank and battery storages for photovoltaic water pumping [p33, M7] (collaboration with Imperial College London). Our method consisted of mod-

eling and optimizing each system separately and comparing the optimization results in terms of life cycle cost and impact on water resources in particular. The sustainability of batteries in this environment was further evaluated in [M12] (collaboration with Imperial College London).

Credits

The project Turning Sun into Water started in 2017 as a support for the PhD thesis of Simon MEUNIER (Université Paris-Saclay in co-supervision with Imperial College London and Université Cergy-Pontoise, funding IDI-IDEX) [D3]. He has done more than anyone, no doubt.

The design and installation of the PVWPS was carried out by the company DargaTech [209], based in Ouagadougou and specialized in photovoltaic systems. The funding was provided by a crowdfunding campaign organized by the association Eau Fil du Soleil [207, 208] and a donation from the NGO Respublica. The installation was coordinated in France by Simon MEUNIER and in Burkina Faso by Matthias HEINRICH who took a year off from the ENS Rennes, and spent 7 months on-site with DargaTech.

The datalogger has been developped in collaboration with Lionel VIDO (SATIE, University of Cergy-Pontoise) with the help of Anne MIGAN (GeePs), Damien HUCHET (GeePs) and Richard BELJIO (GeePs). Many students were involved at different steps (see chapitre 8). The installation of the hydrostatic pressure sensor was coordinated by Thomas VEZIN who took a year off from École Polytechnique, and spent 4.5 months on-site with DargaTech. The data are being collected since then through the intermediary of DargaTech. We acknowledge the help of Arouna DARGA (GeePs) and Severin DARGA (DargaTech).

The sizing methodology was developed by Simon MEUNIER in collaboration with Juidth CHERNI (Imperial College London, UK), Lionel VIDO (SATIE, Université Cergy-Pontoise), Philippe DESSANTE (GeePs), Arouna DARGA (GeePs) and Claude MARCHAND (GeePs). The borehole hydrology model was developped by Thomas VEZIN and Anne CHARPENTIER [M6] in collaboration with Peter KITANIDIS (Stanford University), with some inputs from student (see chapitre 8). The demand model builds on the related MSc thesis of Vitali CAPLAIN [M3] with the help of Dale MANNING (University of Colorado). The economic model builds on the related MSc thesis of Elvire ANDRE DE LA FRESNAYE [M4].

The results have been published in [p17, p18, p25, p26, p30, p33, p39], [ic28, ic31, ic32, ic40] and [nc14, nc15, nc16, nc17, nc18, nc19, nc23, nc24, nc25, nc26].

5.5.2 Modeling of a SAUREA's motors

SAUREA provided us a PVT inverter-fed SRM prototype. In order to understand the complex interaction between the photovoltaic transistors and the SRM, we developed a numerical model. The modeling difficulty lies in correctly taking into consideration the SRM nonlinearity, the high level of integration, and the uncommon dynamic operation of the PV cells in PVT mode. We built a test bench (Fig. 5.13(a)) and carried out extensive measurement campaigns to validate this model. A comparison of the experimental and simulated torque-speed curves is shown in Fig. 5.13(b).

Credits

I carried out this work during my postdoc under the supervision of Lionel VIDO (SATIE, Université de Cergy-Pontoise), in collaboration with Bernard MULTON (SATIE, ENS Rennes) and Raimund GOTTKEHASKAMP (Lab of electrical machines, Hochschule Düsseldorf) with the financial support of the University of Cergy-Pontoise (The University of Cergy-Pontoise Postdoc Fellowship, 2014) and SAUREA. We acknowledge the help of Alain COTY (SAUREA), Isabelle GALLET-COTY (SAUREA), Gilles COTY (SAUREA) and Abasse BOUKARI (SATIE, Université de Cergy-Pontoise). The results have been published in [p8], [ic10, ic11, ic13] and [nc5, nc8].

5.5.3 Creation of SAUREA

The technology is now being developed and commercialized by SAUREA, a startup that I cofounded in 2016. I am on the board of SAUREA and I participate to its scientific committee. It's been a challenging and exciting adventure, with a lot of world "firsts" (Fig. 5.14). SAUREA owns 5 patents protecting its technology. It won 6 innovation awards, including the prix i-Lab of Bpifrance in 2015 and the "Prix du Public" of EDF Pulse in 2019. After extensive R&D work, SAUREA commercialized its first motor in 2020. Since then the product line has expanded to cover a wider power range (up to 250 W) and more

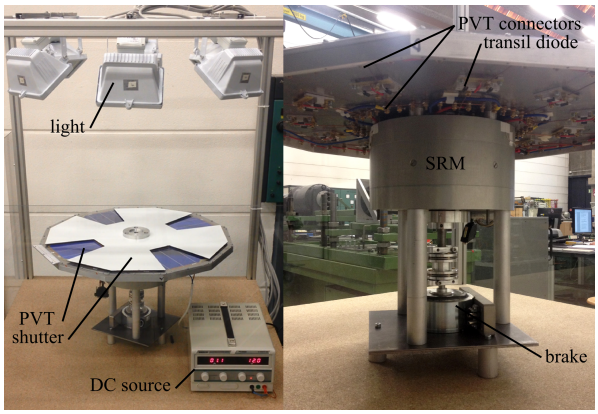

(a) Prototype on its test bench. The halogen lamps emulate the sun while the brake emulates the mechanical load.

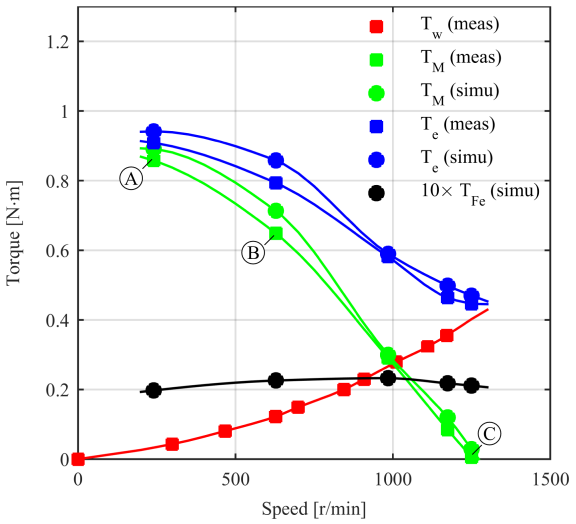

(b) Experimental and simulated torque-speed curves for $\theta_0 = 30^o$ under a mean illumination $I_{sol} \simeq 600$ W/m^2. T_w is the friction torque (bearings, windage and shutter), T_M is the output mechanical torque, T_e is the electromagnetic torque. T_{Fe} is the torque associated with iron loss.

Figure 5.13: PVT inverter-fed SRM prototype [p8] (2015).

applications. Since 2020, it has installed several commercial systems for water pumping and ventilation, in France and abroad.

In the short term, with the increase of the performance of the system and the decrease of its cost, the motor SAUREA could become competitive for off-grid mechanical applications requiring thousands of operating hours without maintenance: ventilation, oxygenation of breeding and cultivation basins, water circulation for aquaculture, etc. More information at `www.SAUREA.fr`.

5.6 Levelized cost of water ($LCOW$)

The concept of levelized cost per unit can be used to compare the economic competitiveness of various water pumping technologies. In that specific context, we call it "Levelized Cost Of Water" ($LCOW$). It represents the average revenue per unit of water pumped over the system lifetime required to break even. It is expressed here in dollar per cubic meter [\$/m^3].

Under the hypothesis of section 1.2.5, the $LCOW$ is expressed from (1.8) as,

$$LCOW = \frac{\sum_{t=0}^{T} \frac{CAPEX_t + OPEX_t}{(1+r)^t} - SV}{\sum_{t=1}^{T} \frac{WP_t}{(1+r)^t}} \tag{5.1}$$

where $CAPEX_t$ is the capital expenses in year t, $OPEX_t$ is the operating expenses in year t, r is the discount rate, WP_t is the water pumped in year t, T is the system lifetime and SV is the salvage value.

5.7 A techno-economic assessment of SAUREA's photovoltaic motor-pump

5.7.1 Goal and scope definition

Goal: In this section, to complete the discussion, we propose an abbreviated techno-economic assessment of SAUREA's photovoltaic motor-pump. We compare an installation using a conventional submersible PV motor-pump and an installation using SAUREA's PV motor-pump.

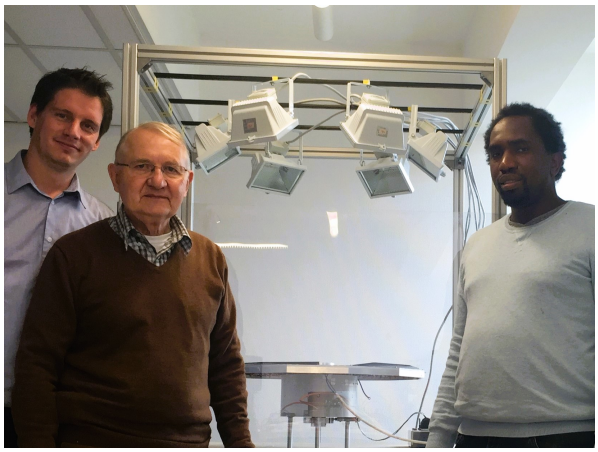

(a) First testbench at SATIE in 2015.

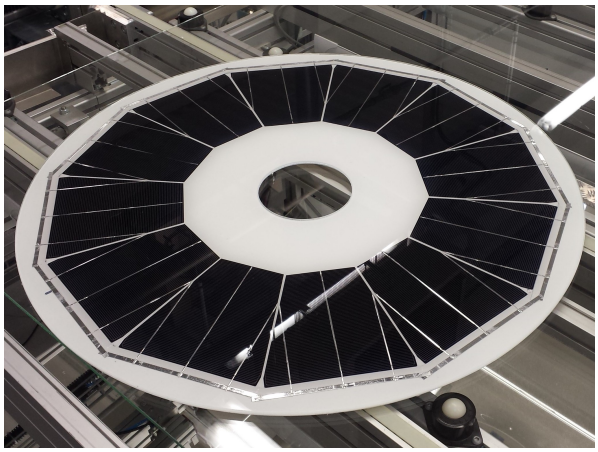

(b) First industrial PVT assembly in 2015.

(c) First PVWPS with SAUREA's motor and a centrifugal pump in 2016.

(d) First PVWPS with SAUREA's motor and a mini-Volanta piston pump in 2019.

Figure 5.14: SAUREA: from the prototype to the commercial product.

Case study: We consider the test case of the PVWPS of Gogma (see section 5.5.1). The real system is a PVWPS for the domestic water consumption of 280 villagers. But SAUREA's PV motor-pump is not powerful enough to pump water for 280 people. So, to perform the comparison, we divide the measured collected flow rate at Gogma's PVWPS by a factor 3. This is similar to sizing a PVWPS for 3 times less users (*i.e.* 93 users in this case). The parameters of the test case are summarized in Table 5.3.

Table 5.3: Case study PVWPS parameters

Parameter	Symbol	Value	Notes
Number of users	-	~93	
Static water level	H_{bs}	-4.9 m	[Tab I, D3]
System lifetime	T	20 years	[Tab I, D3]
Discount rate	r	0.056	[Tab I, D3]
Salvage value	SV	0	unknown

Scenario: We consider 2 time series (irradiance, collected flow rate) measured at Gogma (see section 5.5.1). The first one lasts from May 16th to May 29th 2018 and is representative of the dry season. The second one lasts from July 29th to August 11th 2018 and is representative of the wet season.

Optimization problem: We look for the PVWPS sizing that minimizes the $LCOW$. The optimization

problem is formulated as [D3],

$$\begin{aligned} \underset{X}{\text{minimize}} \quad & LCOW(X) \\ X = & \{MP, V_t\} \\ \text{subject to} \quad & H_t(t) > 0 \text{ m}, \forall t \\ & H_b(t) > -20 \text{ m}, \forall t \\ & TDH(t) < H_{p,max}(MP), \forall t \end{aligned} \tag{5.2}$$

where the optimization variables X are: the PV array peak power $P_{pv,p}$, the motor-pump reference MP, and the water tank volume V_t. The constraint on the water level in the tank H_t ensure that the tank always has water so that the water needs of the inhabitants are fulfilled. The constraint on the water level in the borehole H_b ensures that the motor-pump doesn't run dry (the motor-pump water inlet is at -30 m, a 10 m margin is taken to account for the hydrological change with time). The constraint on the total dynamic head TDH ensure that the water head remains lower than the motor-pump maximal pumping height. A similar optimization problem is formulated for the submersible motor-pump.

5.7.2 Inventory analysis

The system elements are shown in Fig. 5.2. Details about the technical and economic parameters can be found in [D3].

Benchmark product system: For the conventional submersible PV motor-pump (see section 5.3), we digitized the characteristic curves of eight SQFlex motor-pumps from Grundfos catalog [216]. We assume a motor-pump lifetime of 10 years [Tab. III.10, D3].

Proposed product system: For SAUREA's PV motor-pump, we digitized the characteristic curves of six PV motor-pumps from SAUREA catalog. Note that projections have been made to estimate the technical and economic parameters of the system, when it will be mass produced. According to SAUREA's pledge "0% électronique, 100% mécanique, 20 ans sans maintenance, garanti 10 ans"; SAUREA's PV motor-pump lifetime is assumed equal to 20 years.

5.7.3 Calculation of indicators

We use the technical and economic models presented in section 5.5.1 [D3]. The optimization is performed by using the multi-objective Particle Swarm Optimization (MOPSO) algorithm [217] with 60 particles and 30 iterations. With a laptop equipped with Intel(R) Core(TM) i7-8665U CPU @ 1.90GHz and 32 GB of RAM, the optimization takes ∼5 minutes.

Table 5.4: Case study optimal results

	Conventional PV motor-pump	SAUREA's PV motor-pump
PV array peak power $P_{pv,p}$ [Wp]	1290	-
Motor-pump reference MP [-]	SQFlex 2.5-2	SMP200sSP
Water tank volume V_t [m^3]	1.0	2.5
$LCOW$ [\$/m^3]	2.38	2.58

The results of the optimization are summarized in Table 5.4. The optimal $LCOW$ for SAUREA's PV motor-pump system is 2.58 \$/m^3, to be compared to a $LCOW$ of 2.38 \$/m^3 for the conventional PV motor-pump system. This indicates that SAUREA's system is slightly less advantageous (8%) for this case study.

5.7.4 Interpretation

We would like to draw here the attention of the reader on a specific point of the optimization problem. The first optimization constraint ($H_t(t) > 0, \forall t$) guarantees that there is always water in the tank to meet the water demand. It means that during operation and maintenance, the motor-pump cannot stop for too long (the tank plays the role of a buffer).

SAUREA's motor-pump has a lifetime of 20 years, so it doesn't need to be replaced during the PVWPS lifetime. But the conventional motor-pump lifetime being 10 years, it needs to be replaced at least once

during the PVWPS lifetime. In practice, in rural communities, a PVWPS piece is replaced only after it breaks (there is no preventive maintenance). The reparation process takes time: someone needs to call a qualified technician who will come from afar to assess the damage, a piece will be ordered, after delivery the technician will come to repair the installation and restart the system. The reparation process can take several months! During this time, the PVWPS doesn't pump.

If the water demand constraint is strong (an interruption of the water access cannot be tolerated):

Although it deserves to be studied, for the conventional PV motor-pump, it is unlikely that a reasonable sizing will make it possible to respect the water demand constraint taking a long repair into account.

In that case, a preventive maintenance plan must be put in place. This comes at a price, on top of the *LCOW* estimated above. In addition, there is always the possibility that the preventive maintenance is not carried out as planned initially, thus adding risk to the system sustainability. For this kind of system, the maintenance need is a key point in the choice of the technology, making SAUREA's system a strong competitor.

If the water demand constraint is not so strong (an interruption of the water access can be tolerated for a short period):

The interruption of the pumping during the repairs impacts the *LCOW* (the denominator of the *LCOW* depends on the amount of water pumped). Since above *LCOW* estimations did not account for the repair duration, we expand here our analysis to account for it.

The submersible motor-pump lifetime was assumed equal to 10 years [Tab. III.10, D3]. It means that it needs to be replaced at least once during the PVWPS lifetime. We underline that there is intense debate about this figure in the pumping community. High quality pump manufacturers can claim such a lifetime, but there is usually no guarantee. Experience reports much shorter practical lifetime in certain environments. Low quality pumps have definitely a shorter lifetime but are less expensive.

To study this point, we calculated the *LCOW* of the optimal conventional system for several motor-pump lifetime L_{mp} and repair duration R_{mp}. The results are shown in Fig. 5.15. It indicates that the *LCOW* of the conventional system is the lowest for a 10 years lifetime. But if its lifetime is reduced to 5 years or if the repair time considerably increases, SAUREA's system becomes the most competitive.

Beyond the *LCOW*, interruptions of the PVWPS and therefore of the water access have a significant negative socio-economic impact. It could be quantified, but this definitely a difficult question!

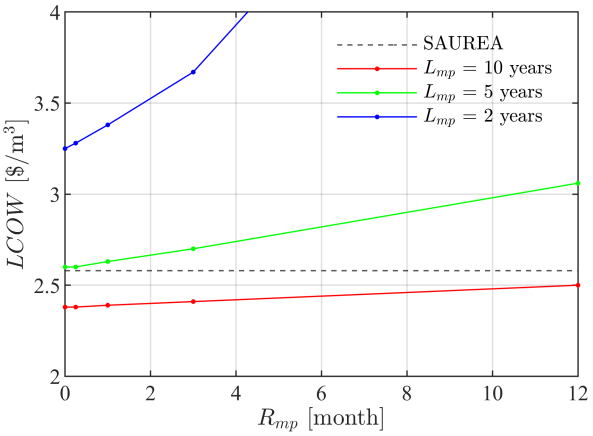

Figure 5.15: Levelized cost of water (*LCOW*) as a function of the motor-pump lifetime L_{mp} and the motor-pump repair duration R_{mp}, for a conventional PV motor-pump system and for SAUREA PV motor-pump system (SAUREA).

5.8 Summary and perspectives

In this chapter, we described the work that has been carried out on the techno-economic assessment of photovoltaic water pumping systems using either conventional submersible or SAUREA's innovative

photovoltaic motor-pump.

The installation of a conventional PVWPS in the rural off-grid village of Gogma in Burkina Faso has been carried out in 2017 and monitored since then. To this date, more than 45 months of technical data have been collected by our data logger (>60e6 data points). They complement a large set of technical and socio-economoic data covering several disciplines, which forms a unique database for the study of such systems.

The data from Gogma have been used to develop and validate improved models and innovative methods. We are committed in keeping on monitoring this system, with the objective of studying the long term impact of the installation on the village. In parallel to further developments, we now need to communicate better around those tools so that they start to be used. Our online "Solar Pumping Workshop" that we organize every other year since 2018 [o1, o2] in collaboration with the association Eau Fil du Soleil could open up to wider audiences: field practitioners, NGOs, economists, politicians, etc. This event could even be complemented by other communication supports: online course, books?

The goal of performing Gogma's installation was to obtain a case of reference. A long term objective would be to install and monitor a PVWPS using SAUREA's motor-pump, and to compare both installations in terms of life-cycle socio-economic impact.

Chapter 6

Perspectives

The following sections are intended to explain the direction I wish to take my research in the coming years. I have arbitrarily divided this chapter into two sections. The first one deals mainly with the development of methods for the techno-economic assessment of technological innovations. The second deals with the study of innovative technologies for power system applications. In practice, methods and applications are almost always developed together.

6.1 Methods

6.1.1 Techno-economic assessment framework

Techno-economic assessments can, as we have seen, quickly become complex. One difficulty comes from the fact that a fair comparison can only be made, from my point of view, for two systems optimized for the same set of specifications and for the same scenario. The optimization of a system is a complex subject, even more so when it comes to estimating the life cycle cost, taking into account the uses (e.g. load factor), the constraints (e.g. weather) and the uncertainties... Some ideas have been proposed in the present document, which should be improved and extended.

The objective would be to obtain a taxonomy and a step-by-step framework for the systematic techno-economic assessment of any system. The output of the method should be easy-to-understand performance indicators (PI). An example of such indicator is the *LCpu* introduced in chapter 1. Eventually, this framework could become a standard, such as the one used to conduct a Life Cycle Assessment (LCA).

6.1.2 Techno-economic comparison of energy systems

A clear methodology should be proposed to unequivocally answer the question: "How do we compare two energy systems over their life cycle?" This methodology would build on the techno-economic assessment framework discussed above. The aim would be to answer the following questions:

- Among different solutions, which ones are technically feasible today? Which ones are economically competitive?
- Among different solutions, which solution is the best one? From an economic point of view? From an environmental point of view? From a social point of view?
- If a solution is not competitive, what needs to be done to make it competitive?
- Which solution has potentially the largest impact (in terms of reduction of greenhouse gases, for example [218, chap 3])?

We will work on this problematic as part of the PhD thesis of Lauro FERREIRA DA SILVA NETO (full PhD scholarship, SuperRail project, start 1/12/2022). Lauro's project focuses on the techno-economic comparison of a conventional solution and several technological innovations for the reinforcement of a railway electrical grid in an urban area. See section 6.2.2 for more information about the SuperRail project.

6.1.3 Socio-economic and environmental impacts

Beyond technological considerations, the interaction of environmental, social and economic dimensions adds to the complexity of any system. This should be taken into account, as the performances of

the system are often dictated by these constraints. This would require coupling the techno-economic assessment with other assessments that could quantify the socio-economic and environmental impacts.

Socio-economic indicator

As part of the Turning Sun into Water project (see section 5.5.1), we proposed a socio-economic indicator that quantifies how a new water source impacts the socio-economic situation of the village (water quality, extraction easiness, water cost, distance household-source and WASH diseases). This indicator was used as an objective function of the optimization to find the optimal position of the system within the villge. The socio-economic indicator and the associated methodology should be further developed, in collaboration with experts in social sciences.

It could then be applied to other types of systems. Systems for which the demand for the service provided depends on the position of the system and which have a significant socio-economic impact constitute excellent case studies. In the context of distribution and transmission grids, one application may be the positioning of public charging stations for electric vehicles. Indeed, the demand at the charging station depends on its position and socio-economic impacts may include time loss to reach the charging station and easier access for people with reduced mobility.

The work on visual decision making tool, started in collaboration with Judith CHERNI during the gap year project of Sebastien FERREIRA [p39], should be continued. Such tool allows for the visualization of performance indicators on a map, allowing decision makers to make more informed decisions.

Environmental indicator

The techno-economic assessment framework discussed in section 1.1.2 is derived from the life cycle assessment (LCA) framework. The LCA evaluates the environmental impacts associated with all stages of the life cycle of a product, process or service (ISO 14040 and ISO 140144, [M12]). The similarity between the two frameworks paves the way for an assessment method, that would include both technical, economic and an environmental considerations [14].

Note that the costs of environmental externalities such as water use, land use, local air pollution, greenhouse gases as well as costs of integrating renewables into the grid (longer transmission distances, variability, and intermittency), can already be accounted for in the "cost" of a technology. But a clear methodology is still lacking.

Sustainability

When considering components with a life span of several decades, it is important to take into account the evolution of their technical performance, of their environment and of their use.

We will address this issue as part of the PhD thesis of Ange SAHUQUET (full PhD scholarship from Université Paris Saclay, start 1/10/2022, supervision Loïc QUEVAL and Simon MEUNIER). Ange's project focuses on the sustainability of photovoltaic pumping systems for rural communities, with the goal of ensuring sustainable access to clean water for residents and thus promoting long-term socio-economic development of the community. The objective of the thesis is to identify the elements that threaten the sustainability of PV pumping systems and determine how to design, operate, and use these systems to mitigate these risks. In particular, we will try to answer the following questions:

- At the design stage of a photovoltaic water pumping system, how can we take into account its evolution (aging of the components, modification of the consumption habits, etc.)?
- Can we improve the availability of the installation by developing fault detection algorithms in order to perform preventive maintenance?
- How to design a water management scheme or an energy control strategy that is socially acceptable and sustainable with regard to water resources and their evolution?
- How to consider the socio-economic aspects to guarantee the sustainability of the installation over its life cycle?

6.1.4 Uncertainty

Uncertainty is associated with unknowns related to data quality, model complexity and modeling choices, or potential future conditions.

Data quality

A serious techno-economic assessment requires up-to-date economic and technical parameters, or it may not be relevant. As a researcher, the access to such data is sometimes difficult. For mature systems, collaboration with industry is essential, as it provides feedback in sometimes very dynamic sectors. For innovative systems, there is necessarily a lack of data. To some extent, this can be filled by breaking down the product system into smaller system elements and referring to reports and databases. The creation of a database for electrical engineering applications, similar to what has already been done in the chemical engineering field [219], may be particularly relevant.

Model complexity and modeling choices

There are three different types of models: element-specific, average, and generic. Element-specific models are obtained from measurement of an existing system element. They are then known with reasonable certainty for this given element. Average models reflect the trend within a set of similar system elements. They are usually obtained by performing fitting of element-specific parameters. Generic models are not based on measurements, but rather are estimated using expert knowledge. Using more element-specific models increases the certainty of the results, but there may have to be significant use of average and generic models for innovative technologies or if one cannot acquire the proper data. This encourages us to keep a strong experimental component in our work. Beyond proof of concept, prototyping is sometimes the only way to quantify a parameter or validate a model.

The computing time of a model is a key factor when performing optimization and life-cycle analysis. Fine models such as finite element models are generally not suitable. This is the motivation behind the development of rapid models for the sizing of modular multi-level converters (see section 4.5.1), semi-analytical models for the optimization of synchronous machines (see section 2.5.2) and planar transformers [D5]. Work is underway in this area.

Potential future conditions

Socio-economic scenarios are plausible representations of the future. They are based on assumptions about the evolution of key social and economic drivers. For example, the evolution of energy consumption, the availability of raw materials, the demography or the economic growth. To identify relevant scenarios for our case studies, new collaborations can be envisaged. This is especially important for system products with long lifetime, such as distribution and transmission grid components.

What can be done about uncertainties?

Uncertainties creates limitations in the usability and the conclusions of techno-economic assessments. This is even more true when considering technological innovations. With this in mind, a few points are worth noting.

In the absence of precise estimates of performance indicators, the trends themselves may nevertheless be interesting. For example, we showed in section 2.7 that for a given wind turbine generator technology, there appears to be a unit power rating that minimizes the $LCOE$.

And in the end, it is often the relative value of an indicator that is interesting, and not its absolute value. When considering relative values, costs that are similar in the two options become irrelevant. For example, we showed in section 4.7 that the $LCOCE$ reduces by 3% when the operating temperature varies from 75 K to 65 K.

To account for cost uncertainty, we have pointed out in section 3.7 a bottom-up approach that consists in using cost intervals for each system element. In this particular case, we have shown that the $LCOTE$ intervals of the two systems overlap: they should both be selected as potential candidates for more detailed studies. The Association for the Advancement of Cost Engineering (AACE) proposes a top-down approach [220]. Rather than modifying some parameters and studying how this affects the cost, this method entails directly applying accuracy range factors to the final indicators based on the system product technology readiness level (TRL). For low TRL technologies, the range of accuracy is -50% to +100%, meaning that if the technology were deployed, the prospective cost is likely be 50% lower or 100% higher than the calculated one. At high TRL, the range of accuracy drops between -10% and +15%.

To go further, sensitivity analyses such as Tornado Diagrams and Monte Carlo analyses should be used to quantify the uncertainty of the results. They can also be used to identify the parameters that are the source of the greatest uncertainty. One should then return to the inventory analysis phase to obtain better data or consider modifying the focus of the study if it cannot be obtained.

6.2 Applications

The challenge for distribution and transmission electric grids is not so much to meet growing energy needs but to develop innovative low-carbon technologies. Among other solutions, high-temperature superconductivity makes it plausible, in my view, to achieve ambitious goals. But the future role to be played by this option is not yet clear... I will therefore continue to work on *superconducting components for the electric grid*. In the meantime, I will keep advancing the development of *power electronic converters for the electric grid*, including cryo-converters and resilient converters for LVDC and MVDC grids.

6.2.1 Superconducting components for the electric grid

SuperRail

The SuperRail project (2022-2025) is financed by Bpifrance (French Public Investment Bank) under the "Investissements d'Avenir" (Investments for the Future) initiative (AMI CORIFER) and coordinated by SNCF Réseau. It regroups 5 partners: Absolut System, CentraleSupélec, Nexans, SNCF Réseau and Université de Lorraine.

As part of this project, we will follow the installation of a superconducting DC cable system in Montparnasse station in Paris. This is the first time that HTS cables will be integrated into a railway electric grid, and it will be the first permanent installation in any electric grid in France.

Paris Montparnasse station, built in 1840, is France's 4th largest train station, with more than 50 million passengers per year. SNCF Réseau expects more than 90 million passengers per year by 2030, and therefore needs to strengthen its electric grid to handle the growing number of trains. The SuperRail HTS cables will help meet this demand, while demonstrating the potential of this technology at a time when rail traffic in megacities is constantly increasing.

The HTS cables will be installed in existing cable ducts to connect the Vouillé substation to the overhead lines of the tracks serving Montparnasse station. Thanks to its small diameter and high power density, a single superconducting cable can replace several copper cables to provide the performance required by SNCF Réseau: 5.3 MW per conduit (3500 A, 1500 VDC). By enabling high capacity connections at 1500 V, HTS cable technology saves significant implementation costs related to infrastructure modifications, avoids potential disruptions to rail and road traffic, and limits risks in terms of time and date of commissioning.

The main stages of this project will be (i) the design and manufacture of the HTS cable system (cable, junction, terminations, line cyrostat, cooling system) by Nexans and Absolut sytem, (ii) the installation of a prototype loop in SNCF Réseau's laboratory in Vitry-sur-Seine, and (iii) the manufacture of the cables and their installation near Montparnasse-Vouillé substation.

In parallel, feasibility studies will be conducted on several alternatives that have been proposed to reduce the termination losses. Indeed, the losses budget (which directly impacts the operating costs) shows that terminations represent a large part of the losses. We will study three options (Figure),

- Proposed product system #1 is the use of a cryo-converter which would benefit from the cold power to improve the global efficiency of the installation.
- Proposed product system #2 is the use of a transformer with a resistive primary winding and a superconducting secondary winding, and a cryo-converter. This option would allow us to get rid of the terminations.
- Proposed product system #3 is the use of a flux pump, which would allow us to inject the current in a superconducting circuit without termination, through the cryostat.

These 3 options will be validated by laboratory prototypes. They will be compared from a technical and economical point of view with the system product benchmark, in order to estimate their potential for future projects.

HTS cables

As part of the SuperRail project, a section of the SuperRail HTS cable will be characterized using our HTS power cable DC test station (section). And our HTS cable design framework (see section) will be improved and extended to DC cables. Data collected during the design, test, installation and operation phases of the SuperRail cable system will be used for validation.

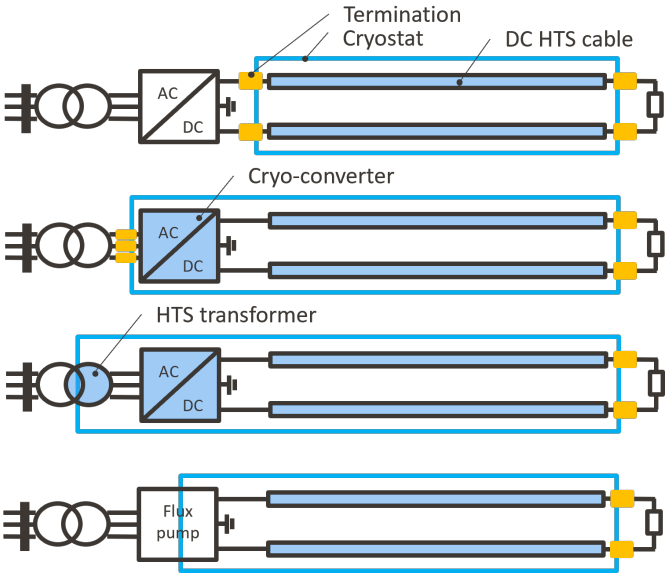

Figure 6.1: SuperRail project. a) System product benchmark b) Proposed product system #1: cryo-converter c) Proposed product system #2: HTS transformer and cryo-converter d) Proposed product system #3: Flux pump.

HTS transformer

As part of the SuperRail project, an HTS transformer having a primary resitive winding and a secondary HTS winding will be designed and tested at GeePs.

HTS flux pump

As part of the SuperRail project, we will study the feasibility of using a flux pump (see section) for the interconnection of an HTS direct current (DC) cable to the alternating current (AC) railway network (Figure 6.1). The overall objective is to determine if an HTS flux pump is suitable for powering an HTS cable for railway applications. The specific objectives are to develop a realistic numerical model of such a flux pump and to study how to use this flux pump to feed an HTS cable. An experimental proof of concept is planned.

6.2.2 Power electronics converter for the electric grid

Cryo-converters

As part of the SuperRail project, Yasmine BAAZIZI (full PhD scholarship, SuperRail project, start 1/12/2022) will study an AC/DC power electronic converter adapted to the supply of a DC railway electrical grid with HTS cables. This converter could work at cryogenic temperature, taking advantage of the available cold power to improve the global efficiency of the installation. The proposal is to size, build and test such "cryo-converter". While most of the previous studies stopped at the characterization of components at cryogenic temperature, we propose here a system approach with an experimental proof of concept. The originality of the approach is to choose an operating temperature adapted to the commercial components currently available (between 77 K and room temperature). Cryogenic tests will allow to validate the proposed technical solutions, the realization processes, as well as the developed numerical models.

The work on the cryo-converter is a direct continuation of the work realized on the cryo-MMC (see chapter 4). We intend to invest significant efforts in this area, taking advantage of our HTS power cable DC test station (section) and of the expertise of the GeePs ENpu group in the design and realization of innovative power electronic converters.

Resilient converters for LVDC and MVDC grids

"Presently, only 30% of all power generated uses power electronics somewhere between the point of generation and end use. By 2030, 80% of all electric power will flow through power electronics." - USDOE Office of Electric Delivery and Energy Reliability

In that context, power electronic converters are gradually penetrating the low voltage (LV) and medium voltage (MV) electric grids. But the technical constraints imposed by the grid operators are strict. Indeed, a grid-connected converter is required to have the same level of availability as conventional components, i.e. 40 years without maintenance, with sometimes harsh operating conditions: heat wave, flooding, plant and animal colonization, etc. This is the reason why the optimal AC/DC converter topology for MV and LV power grids is still an active debate.

On the one hand, two-level voltage source converters (2L-VSC) are attractive due to their low structure complexity. But they are limited to (relatively) low power applications, often requiring paralleling several converters. In addition, they are particularly vulnerable to DC-side short circuits. Without protection, this can lead to their destruction. High-speed fuses and electromechanical circuit breakers are viable alternatives to electronic circuit breakers [ic52], but the current sizing methods result in an oversizing and a lack of selectivity. Frederic REYMOND-LARUINA (funding Cifre EDF/Enedis, started 11/2020, supervision by Marc PETIT and Loïc QUEVAL [D6]) is working on this problem. He is studying an original converter topology, consisting of parallel-connected 2L-VSC, that could be resilient to DC-side faults. A suitable sizing strategy is being developped to take into account the operating requirements of the distribution grid. And a prototype is being built.

One the other hand, multilevel voltage source converters are more complex but deliver a better quality of the energy. Among the various multilevel topologies, the modular multi-level converter (MMC) has already been widely adopted for high voltage (HV) power grid applications, including long distance power transmission and offshore wind power. This is because its modular design makes it inherently reliable, and well suited to operate under fault conditions. In this context, we plan to evaluate the potential of a MMC topology specifically adapted for medium voltage (MV) and low voltage (LV) power grids. The goal is to obtain an experimental proof-of-concept and to demonstrate the continuous operation of the converter even after semiconductor failures.

6.3 Conclusions

In this thesis, I have summarized some contributions to the techno-economic assessment of technological innovations in electrical engineering. The purpose of the Chapter 1 was to summarize some of the key concepts of techno-economic assessment, as well as to discuss how to assess innovative systems. In the following 4 chapters, I have voluntarily concentrated on 4 systems. The chapter 2 covered our work on fully superconducting wind generators, the chapter 3 one on superconducting power cables, the chapter 4 one on a cryo-MMC and the chapter 5 one on SAUREA's photovoltaic motor-pump. Finally, in the chapter 6, I have tried to formulate some perspectives.

This is a good time to recall that this document is the synthesis of the work done by many people, over the years. Many students and young researchers have spent countless hours on sometimes small aspects of certain systems. Many colleagues have devoted considerable time to sharing their expertise. Industrial collaborators brought us the elements of realism that are essential to any applied research. Administrative and legal support made all this possible. It was and always is a great pleasure to work with you. Thank you.

Part II

Curriculum Vitae

Chapter 7

Detailed Curriculum Vitae

7.1 Basic information

Personal background

Family name: Quéval
Given name: Loïc

Contact

CentraleSupélec, University of Paris-Saclay
Plateau de Moulon, 3 rue Joliot Curie
91192 Gif-sur-Yvette cedex, France
www.lqueval.com

7.2 Education

The University of Tokyo, Tokyo, Japan **2010-2013**

Graduate School of Frontier Sciences, Department of Advanced Energy, Ohsaki Laboratory.
Degree: PhD degree in Science, March 2013.
Thesis: "Modeling and simulation of grid-connected superconducting wind turbine generators" under the supervision of H. Ohsaki (link). Jury: H. Fujimoto, Y. Ogawa, A. Yokoyama, J. Baba, T. Koseki, M. Sekino.

UFSC, Federal University of Santa Catarina, Florianópolis, Brazil **March-July 2009**

ENSEEIHT, Toulouse, France **2006-2009**

National Polytechnic Institute of Engineering in Electrotechnology, Electronics, Computer Science, Hydraulics and Telecommunications.
Degree: Electronics Engineering degree, option automatism, September 2009.
Education: Analogical and numerical electronics, Power electronics, Optoelectronics, Electrical machines, Microprocessor, DSP, FPGA, Hyperfrequencies, Signal processing, Automatism, Programming.

7.3 Professional experience

CentraleSupélec, Université Paris-Saclay, Gif-sur-Yvette, France **(50%), since October 2015**

GeePs Laboratory, Université Paris-Saclay, Gif-sur-Yvette, France **(50%), since October 2015**

"Enseignant-chercheur contractuel" at CentraleSupélec. Teaching in the Department of Power & Energy Systems (˜350 hr/year). Carrying research at GeePs in the group Energy/electric grids.

SATIE Laboratory, University of Cergy-Pontoise, France **2014-2015**

Lab for Electrical Machines, Hochschule Düsseldorf, Germany **2013-2014**

SATIE Laboratory, Ecole Normale Supérieure de Cachan, France **June-July 2013**

Developed a photovoltaic motor. Developed advanced models for synchronous machines.

Ohsaki Laboratory, The University of Tokyo, Japan Japan **2010-2013**
Developed superconducting systems for energy, transport and biomedical applications.

GRUCAD Laboratory, UFSC, Florianópolis, Brazil Japan **March-July 2009**
Developed a non-destructive evaluation method by permeance testing.

blueEnergy, Bluefields, Nicaragua **July-December 2008**
Designed and installed small-scale wind turbines. Conceived a testbench. Analyzed wind data.

7.4 Teaching activities

7.4.1 Overview

Since 2015, my teaching activities are mainly at CentraleSupélec, for the engineering curriculum, for the PIE master's program and for CentraleSupelec continuing education center (formation continue). It can be divided into lectures (courses), exercises (TD) and laboratory lectures (TP), and projects. Moreover, I have some tutoring activities: for example, I have been coach for the CentraleSupelec start-up week since its launch. Finally, I have done some vacations at ICAM-EPMI (Cergy-Pontoise) and now at CentraleSupelec EXED. The table below provides an overview of the amount of time spent on each activity over the years (in "heure equivalent TD"). In the following sections, I give the details.

	2015-2016	2016-2017	2017-2018	2018-2019	2019-2020	2020-2021	2021-2022
Lecture (cours)	0	6	6	27.875	3	64.25	82.5
Exercice (TD)	9.55	16.5	32	71.2	113	93.5	66.5
Lab lecture (TP)	129	108.5	117	86.5	20	48	6.5
Projects	42.345	57.375	81.375	96.375	154	184.98	171
Tutoring, others	3.2	10.4	23.92	20.72	27.44	24	31
Total service	184.095	198.775	260.295	302.67	317.44	414.73	357.5
Extra (vacations)	0	45	45	45	45	13.5	39.75
Total	184.095	243.775	305.295	347.67	362.44	428.23	397.25

* in "heure equivalent TD"

7.4.2 Supelec engineering program curriculum

From 2015 to 2019, I taught for the Supelec engineering program curriculum.

- 2016-2017 - TD 1A "Principe et composants electrotechnique"
- 2016-2018 - TD 1A "Initiation à la recherche documentaire"
- 2015-2018 - TP 1A Triphasé, Transfo 1ph, MCC, Inductance

- 2016-2018 - TD 2A "TCEE"
- 2015-2018 - TD 2A "Systeme d energie electrique" at Centrale Paris
- 2016-2018 - TD 2A "Commande des entraînements à vitesse variable"
- ? - TD 2A no1-4 "Teckauto"
- 2015-2018 - TP 2A Pont de Graetz, Machine synchronous, Machine asynchrone 1, Machine asynchrone 2, Tekauto.

- 2016-2019 - BE 3A "Réseaux électriques" load flow réglage tension (M. Petit)
- 2017-2019 - TD 3A "Commande machine électriques" (JC. Vannier)

7.4.3 CentraleSupelec engineering program curriculum

From 2018, I taught for the CentraleSupelec engineering program curriculum that was progressive introduced following the merger of Centrale Paris and Supelec. The sequences I helped create are marked with a double asterisk (**).

- 2018-present - (**) cours 1A ST4 1SC4610 "Climat et transition énergétique" énergies marines renouvelables, photovoltaïque (L. Quéval): 2x3h = 9 HequTD
- 2018-present - (**) TD 1A ST2 1SC2410 "Système de conversion électromagnétique" (M. Bensetti): 4x1.5h = 6 HequTD
- 2018-2019 - TD 1A SG3 1EL2000 "Energie électrique Electif 1.4" (R. Langfried): 3x3h = 9 HequTD
- 2018-present - (**) EI 1A ST4 1SC4693 "Estimation de la production d'un parc éolien offshore" (L. Quéval): 27 HequTD
- 2018-present - Startup week (A. Levey): 21 HequTD
- 2018-present - TP 1A Transfo 1ph, Triphasé, MCC (M. Hennebel)

- 2019-present - (**) cours 2A ST7 2SC7710 "Optimisation des systèmes d'énergies embarqués" Parameter identification in practice (M. Hage Hassan): 1.5h = 2.25 HequTD
- 2019-2020 - TD 2A SG6 2EL1320 "Conversion d'énergie FR" (B. Lorcet): 3x3h = 9 HequTD
- 2019-2020 - TD 2A SG8 2EL1320 "Conversion d'énergie EN" (M. Petit): 7.5x1h30 = 11.25HequTD
- 2019-2020 - (**) TD 2A ST5 2SC5610 "Introduction production d'énergie" (M. Hage Hassan): 2x3h= 6 HequTD
- 2019-present - (**) TD 2A ST7 2SC7710 "Méthode numérique et résolution des problèmes d'optimisation des systèmes d'énergies embarqués" (M. Hage Hassan): 2x3h = 6 HequTD
- 2019-present - (**) EI ST5 2SC5691 "Regulation et commande de systèmes de production et de conversion d'énergie" (G. Sandou): 21 HequTD
- 2020 - EI ST2 1SC2491 "Modélisation d'un coupleur pour la recharge sans contact" (M. Bensetti): 6 HequTD

- 2020-present - (**) cours 3A 3CV3010 "Système d'énergie embarqués" Introduction aux systèmes embarquées, Introduction to applied superconductivity, Magelv technologies (L. Quéval) : 6h = 9 HequTD
- 2020-present - (**) cours 3A 3CV3210 "Système électrique de conversion" (L. Quéval) : 6x3h= 27 HequTD
- 2020-present - (**) cours 3A 3EN3130 "Commande des REZO d'énergie" (E. Godoy) : 1x3h = 4.5 HequTD
- 2020-present - (**) cours 3A 3EN3110 "Supergrids" (M. Petit) : 2x3h = 9 HequTD
- 2020 - (**) TD 3A 3EN3130 "Commande des REZO d'énergie" (E. Godoy) : 1x3h = 3 HequTD
- 2020-present - (**) TD 3A 3CV3220 "Commande des systèmes pour la motorisation et applications" (B. Lorcet) : 1x3h = 3 HequTD

- 2018-present - Coordinateur cours 1A ST4 1SC4610 "Climat et transition energetique", coordinateur d'une équipe de 8 intervenants (incluant 4 vacataires), pour ∼120 élèves.
- 2018-present - Coordinateur EI 1A ST4 1SC4693 "Estimation de la production d'un parc éolien offshore", coordinateur d'une équipe de 5 intervenants (incluants 2 vacataires), pour ∼36 élèves.
- 2020-present - Coordinateur cours 3A 3CV3010 "Systèmes d'énergie embarquée", coordinateur d'une équipe de 4 intervenants (incluant 3 vacataires), pour ∼30 élèves.
- 2020-present - Coordinateur cours 3A 3CV3210 "Système électrique de conversion", pour ∼30 élèves.

7.4.4 M2 PIE curriculum

From 2020, the new M2 Physique et ingénierie de l'énergie (PIE) curriculum was introduced. The sequences I helped create are marked with a double asterisk (**).

- 2020-present - (**) cours M2 PIE NX3900 "Modelisation et commande des actionneurs (MRV)" (G. Krebs): 6h vacation
- 2020-present - (**) cours M2 PIE EN2245 "Actionneurs non-conventionnels" Introduction to applied superconductivity, Magelv technologies (M. Gabsi): 3h vacation

- 2021-present - cours M2 PIE EN2255 "Reseau d'Energie Electrique" Intro système electrique et/ou load flow (M. Petit): 6h = 9 HequTD
- 2020-present - (**) TD M2 PIE EN2254 "Méthode d'optimisation" (M. Hage-Hassan): 2x3h= 6 HequTD

7.4.5 CentraleSupelec continuing education center (formation continue) and CentraleSupelec EXED

- 2017-present - cours "Machine asynchrone"
- 2019 - cours "Convertisseur DC/DC"
- 2015-present - TP "Machine asynchrone"
- 2016-present - (**) TP "Mise en parallèle de 2 transformateurs triphasés"
- 2019-present – TD "Load flow"

7.4.6 ECAM-EPMI

- 2016-2019 – (**) cours "Réseaux électriques de transport et de distribution": 30h

7.5 Research activities

7.5.1 Research results

List of publications

See Appendix 9 or www.lqueval.com

Awards

- EPE Young Author Best Paper Award, 22nd European Conf. on Power Electronics and Applications (EPE'20 ECCE Europe), 2020.
- IOP trusted reviewer, Institute of Physics Publishing, 2020.
- Award of the best paper in renewable energies, 14th Intl Conf. on Ecological Vehicles and Renewable Energy (EVER2019), 2019.
- Superconductor Science and Technology Highlights of 2016.
- The University of Cergy-Pontoise Postdoc Fellowship (1 year), 2014.
- The University of Tokyo International Student Special Fellowship (full PhD scholarship), The University of Tokyo, 2010-2013.
- Excellence Graduate Research Grant , Japanese Government (Monbukagakusho: Ministry of Education, Culture, Sports, Science and Technology), 2013.
- Secure-Life Electronics Global COE Research Scholarship, Japanese Government (Monbukagakusho: Ministry of Education, Culture, Sports, Science and Technology), 2010-2012.

Startup

Cofunder of Saurea (April 2016): Saurea develops and commercializes solar autonomous and reliable applications, including a solar motor for water pumping in off-grid locations.

7.5.2 Collaborations

	Visits out/in	Journal	Conf intl/nat
Prof. G.-T. Ma, Southwest Jiaotong Univ. SWJTU, China	3/0	11	7/1
Dr. J. Cherni, Imperial College London, UK	0/1	6	4/4
Prof. F. Trillaud, Univ. autonome Mexico UNAM, Mexico	1/3	4	11/4
Dr. M. Ainslie, Univ. Cambridge, UK	0/0	3	5/0
Prof. F. Grilli, Karlsruhe Institute of Technol. KIT, Germany	1/0	2	4/0
Prof. B. Douine, Univ. de Lorraine, GREEN, Nancy, France	6/3	3	9/5

7.5.3 Research projects

Academic

- 2022-2025, "SuperRail" {co-coordinator, funding AMI CORIFER - BPI}.
- 2019-2020, "Superconducting power filter" {coordinator, funding Appel à projets internes GDR SEEDS 2019}.
- 2016-present, "Turning Sun into Water" {coordinator, funding IDI-IDEX + 3× crowdfundings}.
- 2016-present, "EolSupra20" {coordinator, funding CEA + LaSIPS + scholarship CSC China}.

Industrial

- 2022-2023, Industrial research contract "Cryo-filter" {coordinator, funding Airbus Next}.
- 2019-2020, Industrial research contract "Superconducting power filter" {coordinator, funding RTE}.
- 2019-2020, "Power system's transmission network joint optimization with large share of renewable energy" {coordinator, funding FMJH program PGMO and EDF}.
- 2019-2020, Contrat d'étude industrielle (CEI Supélec), "Utilisation des matériaux à changement de phase pour le refroidissement d'enroulements de machines électriques" {coordinator, funding SafranTech}.
- 2017-2018, Contrat d'étude industrielle (CEI Supélec), "Dimensionnement et réalisation d'une sonde de courant BF pour mesure foudre" {co-coordinator, funding SafranTech}.

7.5.4 Community involvement

Professional society memberships

- Member of the international standardization committee IEC/TC90 (Superconductivity).
- Cigre working group B4.A3.86 (Fault Current Limiting Technologies for DC Grids).

Reviewing

A partial list of my contributions as a peer reviewer is available on Publons.

- Technical editor and reviewer for IEEE Transactions on Applied Superconductivity.
- Occasional reviewer for Superconductor Science and Technology, Cryogenics, IEEE Transactions on Energy Conversion, and IEEE Industrial Electronics magazine.
- Occasional reviewer for international conferences, including EUCAS, MT, ASC.
- Reviewer for national conferences, including SGE and JCGE.

PhD thesis defense committee

- 10/2019, PhD thesis defense of J. Avronsart (CEA), invited.
- 01/2020, PhD thesis defense of A. Colle (GREEN, SafranTech), invited.

Committee member for international conferences

- Member of the organization and technical committee of the Solar Pumping Workshop, Gif-sur-Yvette, France, Sept. 2018 & [online], Dec. 2020.

- Member of the organization committee of the conference on Evolution of Functional Performance and Expected Lifetime of Electrical Equipments (ELTEE2018), Grenoble, France, Oct. 2018.
- Member of the technical committee of the International Conference on COmponents and SYStems for DC Grids (COSYS-DC), Grenoble, France, 2017.

Chapter 8

Advising and mentorship

I have been supervising students and young researchers, both as a researcher at GeePs (postdoc, PhD thesis, master thesis, bachelor thesis, others) and as a teacher at CentraleSupelec (project 1A, 2A, 3A, others). The exhaustive list is given bellow with the following notation (link){% of supervision, funding}[publications].

8.1 Postdocs

[P4] Gustavo HENN, "Cryogenic power filter for a superconducting conversion chain," 1-year postdoc project, Jun. 2022-Jun. 2023. (){100%, funding Airbus Next}

[P3] Hong CAI, "Power system's transmission network joint-optimization with large share of renewables," 1-year postdoc project, Dec. 2019-Dec. 2020. (){25%, funding FMJH program PGMO and EDF}[o3]

[P2] Jilin GUO, "Eolsupra20: étude conceptuelle d'une éolienne supraconductrice de 20 MW," 1-year postdoc project, Nov. 2017-Nov. 2018. (){100%, funding China Scholarship Council NO. 201707005056 2017 and SWJTU}[p24, ic33]

[P1] Trung-Kien HOANG, "Etude conceptuelle d'une éolienne supraconductrice de 20 MW," 1-year postdoc project, Dec. 2016-Dec. 2017. (){33%, funding Labex LASIPS 2015}[p40, p11, ic21, ic17]

8.2 PhD theses

[D6] Frédéric REYMOND-LARUINA, "Architecture d'un poste de distribution HTA/BT hybride AC/DC," ongoing PhD thesis (2A) under the supervision of M. Petit. (){50%, funding Cifre EDF/Enedis}[ic52]

[D5] Lucas PNIAK, "Convertisseur modulaire GaN DC-DC isolé à faible impact électromagnétique," ongoing PhD thesis (3A) under the supervision of O. Bethoux. (){30%, funding Cifre Safran-Tech}[p41,i57,nc28]

[D4] Rafael COELHO MEDEIROS, "A modular multilevel converter with superconducting coupled arm coils," PhD thesis defended in 2022, under the supervision of J.-C. Vannier. (){30%, funding Cifre EDF R&D}[thesis, p38, ic54, ic51, ic48, ic39, nc30, nc20]. He is now research engineer at Schneider Electric, France.

[D3] Simon MEUNIER, "Optimal design of photovoltaic water pumping systems for rural communities – a technical, economic and social approach," PhD thesis defended in 2019, under the supervision of C. Marchand. (thesis){33%, funding IDI-IDEX}[p33, p30, p26, p25, p18, p17, ic40, ic32, ic31, ic28, nc26, nc25, nc24, nc23, nc19, nc18, nc17, nc16, nc15, nc14]. He is now assistant professor at CentraleSupelec.

[D2] Bogdan DZONLAGA, "Contribution to the sizing of the modular multilevel converter," PhD thesis defended in 2019, under the supervision of J.-C. Vannier. (thesis){70%, funding MESR}[p15,ic39, ic37, ic24, ic15, nc30, nc21, nc13]. He is now research engineer at EDF R&D, La Renardière, France.

[D1] Davi Rabelo JOCA, "An AC-DC topology based on an interleaved modular multilevel converter feasible to solid-state transformer applications," PhD thesis defended in 2019, under the supervision of L.H.S.C. Barreto (Universidade federal do Ceará) and J.-C. Vannier. (thesis){70%, funding Erasmus Mundus SMART2}[p15, ic24, ic15, nc13]. He is now assistant professor at Univ. de Fortaleza, Brazil.

8.3 Master theses

[M12] Fatima HERMOSIN, "A life cycle analysis of storage batteries for photovoltaic water pumping systems (PVWPS) in Sub-Saharan remote areas," Master thesis, Imperial College London, UK, Aug. 2021. (thesis){25%}[]

[M11] Alexander SHERRED, "Assessment of the potential for photovoltaic water pumping systems to improve water access in sub-Saharan Africa", Master thesis, Imperial College London, UK, Sept. 2021. (){50%}[]

[M10] Batoul ZBIB, "Modeling and simulation of HVDC power converters," rapport de stage recherche M2, GeePs, CentraleSupélec, France, Sept. 2021. (){50%}[]

[M9] Mohammed Lamine ZINET, "Modélisation et conception d'une inductance de puissance haute fréquence," rapport de stage recherche M2, GeePs, CentraleSupélec, France, Sept. 2021. (){50%}[]

[M8] Feilian XIE, "Modeling of the AC loss in superconducting tapes of the second generation with the PEEC method," rapport de stage de fin d'étude, INSA Lyon, France, 2020. ()33%[]

[M7] Camille SOENEN, "An analysis of adapted storage approaches for photovoltaic water pumping systems in developing countries", Master thesis, Imperial College London, UK, Aug. 2020. (thesis){33%}[p33]

[M6] Anne CHARPENTIER, "Influence of photovoltaic water pumping systems operation on groundwater sustainability", Master thesis, Imperial College London, UK, Aug. 2020. (thesis){33%}[]

[M5] Ignacio SALSAS, "Impact assessment of photovoltaic pumping systems for water access in developing countries – The case of burkina faso", Master thesis, Imperial College London, UK, Aug. 2019. (){33%}[]

[M4] Elvire A. DE LA FRESNAYE, "A financial and technical assessment of solar versus hand water pumping for off-grid area", Master thesis, Imperial College London, UK, Aug. 2018. (thesis){33%}[p30, ic32, ic31]

[M3] Vitali CAPLAIN, "Water demand and organization and payment schemes for solar pumping systems in emerging countries: a case study in Burkina Faso", Master thesis, Imperial College London, UK, Aug. 2018. (thesis){33%}[]

[M2] Mamour DIOP, "Modélisation dynamique d'un câbles HVDC souterrain", rapport de stage recherche M2, University Paris-Saclay, GeePs, Gif-sur-Yvette, France, 2016. (){100%}[]

[M1] Bogdan DZONLAGA, "Simulation d'un réseau multi-terminaux HVDC," rapport de stage recherche M2, University Paris-Saclay, GeePs, Gif-sur-Yvette, France, 2016. (){100%}[]

8.4 Bachelor theses

[B7] Lourdes PLATERO DE HEREDIA, "Techno-economic optimization of superconducting cables," Trabajo fin de grado, Comillas Pontifical University, ICAI, Spain, 2022. (){LQ 1}[]

[B6] Celia GOMEZ LIMIA, "Characterization of HTS coils," Trabajo fin de grado, Comillas Pontifical University, ICAI, Spain, Jun. 2022. (){LQ 1}[]

[B5] Carmen MARTIN-SANZ GARRIDO, "Efforts towards the standardization of superconducting cables," Trabajo fin de grado, Comillas Pontifical University, ICAI, Spain, 2021. (){LQ 1}[]

[B4] Tomás REILLY ROCKETT, "Techno-economic optimal cable layouts for offshore wind farms," Bachelor thesis, Universitat Politècnica de València, Oct. 2021. (){LQ 0.5}[]

[B3] Elisa RAZZERA GAJARDO, "Optimization of the layout of an offshore wind farm using binary particle swarm optimization," Bachelor thesis, Universidade Federeal do Rio Grande do Sul, 2021. (){LQ 1}[]

[B2] Yassin KHARMIZ, "Optimierung einer supraleitenden Magnetschwebebahn," (German) Bachelor thesis, University of Applied Sciences Düsseldorf, Germany, Apr. 2015. (){LQ 1}[p6, ic12]

[B1] Elhoucin MOKHLIS, "Validierung einer Berechnungsformel für ein neuartiges Design Supraleitender Spulen mit Hilfe einer numerischen Lösung des Gesetzes von Biot-Savart," (German) Bachelor thesis, University of Applied Sciences Düsseldorf, Germany, Apr. 2015. (){LQ 1}[]

8.5 Research projects

Since October 2015, I supervised >80 research projects (TIPE, projet ou stage L2/L3, projet 1A/2A CS, contrat d'étude industrielle 3A CS, projet M2 PIE, césure, visiting researcher, etc.) involving >175 students.

8.5.1 Gap year project

- Sebastien FERREIRA, "Turning Sun Into Water: water demand," projet de césure M1, 9/2020-6/2021. (){LQ 0.3, AD 0.3, SM 0.4, crowdfunding}[p39]
- Thomas VEZIN, "Etude de l'impact du pompage photovoltaïque sur les ressources en eaux souterraintes," projet de césure 3/2019-08/2019. (){LQ 0.3, AD 0.3, SM 0.4, crowdfunding}[p25, ic40, nc25]
- Matthias HEINRICH, "Fiabilité technique et impact socio-économique des systèmes photovoltaïques de pompage d'eau," projet de césure, 01/2018-06/2018. (){LQ 0.3, AD 0.3, SM 0.4, crowdfunding}[p39, p30, p26, p17, ic40, ic32, ic31, ic28, nc26, nc25, nc24, nc23, nc19, nc18, nc17, nc16, nc15, nc14]

8.5.2 Projet 3A

- Maximilien MARC, Abdelaziz OUDGHIRI, "Dimensionnement d'un élément d'une chaîne de propulsion aéronautique électrique supraconductrice," Projet 3A CEI acad CentraleSupélec, 2021-2022. (){LQ 1}[]
- Matthieu DECOATPONT, Marion GAUTEUR, Camille HENRIQUES, "Analyse technico-economique du raccordement d'une ferme éolienne," Projet 3A CEI acad CentraleSupélec, 2021-2022. (){LQ 1}[]
- Théau FERROUILLAT, William ROPERT, "Estimation de volatilités sur les marchés de l'énergie," projet 3A CEI indus CentraleSupélec, 2020-2021. (){MH 0.5, LQ 0.5}[]
- Martin ALADJIDI, "Superconducting power filter for HVDC grids," projet 3A CEI acad CentraleSupélec, 2020-2021. (){LQ 1}[]
- Lucie EMPRIN, Leïla MOKHTARI, "Monitoring des pompes solaires pour améliorer l'accès à l'eau dans les communautés rurales projet 3A CEI acad CentraleSupélec, 2020-2021. (){SM 0.66, LQ 0.33}[]

- Hajar GUECHCHATI, Paul CAPPUCCIO, "Technico-economic analysis of power transmission systems for offshore wind farms,' projet 3A CEI acad CentraleSupélec, 2020-2021. (){TDL 0.5, LQ 0.5}[]
- Odelin BAUDOUIN, Raphaëlle PLUVINAGE, Augustin CUIGNET, "Ressource en eau," projet 3A CEI acad CentraleSupélec, 2020-2021. (){SM 0.66, LQ 0.33}[]
- Axel HWANG, Baptiste KLEIN, Oussama GHAZOUANI GHARBI, "Réalisation d'un filtre supraconducteur," projet 3A filière métiers de la recherche CentraleSupélec, 2020-2021. (){LQ 1}[]
- Vincent ROY, Adnan ZEDDOUN, "Prédiction de la consommation en eau d'un village Burkinabé isolé," projet 3A Supélec d'initiation à la recherche, option math appliqué, 2019-2020. (){LQ 1}[]
- Laetitia GERBIER, Vincent BRETON, "Etude sur les stratégies de protection des réseaux HVDC," projet 3A CEI Supélec, 2019-2020. (){TDL 0.5, LQ 0.5}[]
- Antoine ROUSSET, Paul-Adrien MARTEL, "Étude technico-économique d'une liaison courte distance forte puissance supraconductrice," projet 3A CEI Supélec, 2019-2020. (){LQ 1}[]
- Virgile NAUDE, Thibault BENRAMDANE, "Etude de faisabilité d'un filtre supraconducteur pour les réseaux à courant continu haute tension," projet 3A CEI Supélec, 2019-2020. (){LQ 1}[]
- Clement BERGEGERE, Arnaud DROULERS, Antoine MAITRE, "Utilisation de matériaux à changement de phase pour le refroidissement d'enroulements de machines électriques," projet 3A CEI Supélec, 2019-2020. (){LQ 1}[]
- Abdelouahab LAKBIR, Souhail BELGHITI, "Plateforme Test de système de protection pour les réseaux électriques," projet 3A CEI Supélec, 2019-2020. (){TDL 0.9, LQ 0.1}[]
- Mateus RIBEIRO PEREIRA, Caio VASCONCELOS PEREIRA, Krishynan Shanty FERNANDES MEIRELLES ARAUJO, "Etude technico eco liaison DC supra," projet 3A CEI Supélec, 2018-2019. (){LQ 1}[]
- Clément LE MARECHAL, Henry DE PIMODAN, Pierre MASSE, "Liaison forte puissance courte distance supraconductrice," projet 3A CEI Supélec, 2018-2019. (){LQ 1}[]
- Issam HASSANI, Izarab CHAHDI-ELOUAZANI, "Disjoncteur DC," projet 3A CEI Supélec, 2018-2019. (){AA, LQ 0.5}[]
- Jeanne BONNEL, Clémentine LAURE, "Disjoncteur DC," projet 3A CEI Supélec, 2017-2018. (){AA, LQ 0.5}[]
- Vincent ANDRAUD, Rémi LAUVERGNE, "Sonde de courant de foudre," projet 3A CEI Supélec, 2017-2018. (){MB 0.5, LQ 0.5}[]
- Omayma MALEK, Romain GUICHARD, "Liaison souterraines," projet 3A CEI Supélec, 2017-2018. (){AA, LQ 0.5}[]
- 3 students, "DC circuit breaker," projet 3A CEI Supélec, 2016-2017. (){AA, LQ 0.1}[]
- 3 students, "Coupleur magnétique," projet 3A CEI Supélec, 2016-2017. (){BL 0.5, LQ 0.5}[]
- 3 students, "Impacts de liaisons souterraines," projet 3A CEI Supélec, 2015-2016. (){AA, LQ 0.1}[]
- 3 students, "Impacts de liaisons souterraines," projet 3A CEI Supélec, 2015-2016. (){AA, LQ 0.1}[]
- 3 students, "Commande d'un onduleur multi-niveau MMC," projet 3A CEI Supélec, 2015-2016. (){AA, LQ 0.1, PEL}[]
- 3 students, "Interactions entre les marchés de l'électricité et les capacités de transits des lignes électriques," projet 3A CEI Supélec, 2015-2016. (){MH, LQ 0.1}[]
- 3 students, "Interactions entre les marchés de l'électricité et les capacités de transits des lignes électriques," projet 3A CEI Supélec, 2015-2016. (){MH, LQ 0.1}[]
- 3 students, "Simulation et commande des alternateurs lors des creux de tension sur le réseau," projet 3A CEI Supélec, 2015-2016. (){BL, JCV, LQ 0.2}[]
- 3 students, "Conception d'un disjoncteur DC," projet 3A CEI Supélec, 2015-2016. (){AA, LQ 0.1}[]
- 3 students, "Conception d'un disjoncteur DC," projet 3A CEI Supélec, 2015-2016. (){AA, LQ 0.1}[]

8.5.3 Projet 2A

- Matias BUSTOS, "Station de test câble supra," Projet 2A CentraleSupélec parcours recherche S7, 2021-2022. (){LQ 1}[]
- Celia GOMEZ, Marine HEYRAUD, "Station de test câble supra," Projet 2A CentraleSupélec pole projet P17 NCE S7 2SL8000, 2021-2022. (){LQ 1}[]
- Celia GOMEZ, "Station de test câble supra," Projet 2A CentraleSupélec pole projet P17 NCE S8 2SL8100, 2021-2022. (){LQ 1}[]
- Xavier CUNIN, Alban CASSIER, Pierre-Elie BEAUDOUIN, Lourdes PLATERO, "Composants supraconducteurs pour les réseaux électriques," Projet 2A CentraleSupélec pole projet P13 MSE

S7 2SL8000, 2021-2022. (){LQ 1}[]

- Xavier CUNIN, Pierre-Elie BEAUDOUIN, Lourdes PLATERO, "Composants supraconducteurs pour les réseaux électriques," Projet 2A CentraleSupélec pole projet P13 MSE S8 2SL8100, 2021-2022. (){LQ 1}[]
- Mateus LEMOS, Dunan SIMONIS, Rania ELKASMI, Josefina HENRIQUEZ, "Eolienne supraconductrice," Projet 2A CentraleSupélec pole projet P13 MSE S7 2SL8000, 2021-2022. (){LQ 1}[]
- Mateus LEMOS, Clemente GON, Rania ELKASMI, Yann WALTER, Josefina HENRIQUEZ, Thomas SALTON, Louis CROIX, "Eolienne supraconductrice," Projet 2A CentraleSupélec pole projet P13 MSE S8 2SL8100, 2021-2022. (){LQ 1}[]
- Justin RIGAL, Amine SLIMANI-HOUTI, Corentin FLOCHLAY, Arthur WALKER, Hugues CHARDIN, "Propulsion aéronautique 1," Projet 2A CentraleSupélec ST7 2SC7792, 2021-2022. (){LQ 1}[]
- Lola ESCANDE, Maxime ROBIN, Antoine CROUET, Alejandro ROAQUINTERO, Baptiste FREMY, "Propulsion aéronautique 2," Projet 2A CentraleSupélec ST7 2SC7792, 2021-2022. (){LQ 1}[]
- Malo DELAPORTE, Robin TRUFFINET, Jim WOUDA, Timothee GRANDCHAMP, Ludovic LAGAY, "Propulsion navale," Projet 2A CentraleSupélec ST7 2SC7792, 2021-2022. (){LQ 1}[]
- Antoine DUPONT, Carmen MARTIN-SANZ GARRIDO, "Station de test câble supra," projet 2A CentraleSupélec pole projet P17 NCE S7, 2020-2021. (){LQ 1}[]
- Antoine DUPONT, Carmen MARTIN-SANZ GARRIDO, Antoine FASQUEL, Timothé MENARD, "Station de test câble supra," Projet 2A CentraleSupélec pole projet P17 NCE S8, 2020-2021. (){LQ 1}[]
- Elisa GAJARDO, Francois PHILIPPE, Tomas REILLY, Mehdi BAROUD, Violette ISORE, "Eolienne supraconductrice," Projet 2A CentraleSupélec pole projet P13 MSE S8, 2020-2021. (){LQ 1}[]
- Pierre BOUJARD, Carmen MARTIN SANZ, Clara RIEFFEL, Madeleine DIDELOT, Pierre CROZIER, "Propulsion aéronautique," Projet 2A CentraleSupélec ST7 2SC7792, 2020-2021. (){LQ 1}[]
- Audrey GRANGEON, Hugo BORSONI, Clement DEGEYERDORTH, Joseph VERNIER, Thomas BRUNET, "Propulsion navale," Projet 2A CentraleSupélec ST7 2SC7792, 2020-2021. (){LQ 1}[]
- Abdelhak KALLEL, Abdelhaq HADRI, Amalio CORON, Jeremy BESSON, Joao Victor Evangelista MATOSO, "Propulsion aéronautique," Projet 2A CentraleSupélec ST7 2SC7792, 2019-2020. (){LQ 1}[]
- Etienne TROCELLIER, Guodong ZHENG, Irenee FROISSART, Lisa BOUGLE, Valentin ANTOINE, John-Evan KARCENTY, "Propulsion navale," Projet 2A CentraleSupélec ST7 2SC7792, 2019-2020. (){LQ 1}[]
- Jean RAMAMONJISOA, "Résolution formelle équation de poisson," projet 2A CentraleSupélec, 2019-2020. (){LQ 1}[]
- Yahya CHAHLI, "Validation fonction calcul inductance mutuelle pour BSmag," projet 2A CentraleSupélec, 2019-2020. (){LQ 1}[]
- Cesar Henrique PEINADO MORAES, "Plateforme MMC," projet long 2A Supélec, 2018-2019. (){LQ 1}[]
- Vincent ROY, "Instrumentation d'une pompe solaire," projet long 2A Supélec, 2018-2019. (){PhD 0.5, LQ 0.5}[]
- Cyrille BÉTOUS, Marie BILLES GARABEDIAN, "Protection réseau HVDC," projet long 2A Supélec, 2018-2019. (){TL 0.5, LQ 0.5}[]
- Claire DUAN, Amandine DEBUS, "Etude PVT," projet long 2A Supélec, 2018-2019. (){TP 0.5, LQ 0.5}[]
- Aurélie DESHONS, Océane GREMBERT, "Capteur d'irradiance no. 1," projet 2A Supélec, 2018-2019. (){LQ 1}[]
- Gabriel CHAVES D'OLIVEIRA, Benoît PHILBERT, Vladimie BERAUD-PEIGNE, "Capteur d'irradiance no. 2," projet 2A Supélec, 2018-2019. (){LQ 1}[]
- 2 students, "BSmag materiel non-linéaire," projet long 2A Supélec, 2017-2018. (){PhD 0.5, LQ 0.5}[]
- 2 students, "HVDC fault," projet long 2A Supélec, 2017-2018. {TL 0.5, LQ 0.5}
- Paul LORANG, Joséphine DEMAY, "Instrumentation d'une pompe solaire," projet long 2A Supélec, 2017-2018. (){PhD 0.5, LQ 0.5}[]
- Laetitia GERBIER, Paul-Adrien MARIE, Pierre MICHELET, "Etude d'un moteur de véhicule électrique no.1," projet 2A Supélec, 2017-2018. (){LQ 1}[]
- Candice GUEVEL, Noemie PERROT, Manon TSCHUPP, "Etude d'un moteur de véhicule électrique no.2," projet 2A Supélec, 2017-2018. (){LQ 1}[]

- Mohammed Amine MOUK, Rayane SEBBAN, William VANHUFFEL, "Simulation of a photovoltaic installation," projet 2A Supélec, 2017-2018. (){LQ 1}[]
- BADIANE Issa, CHEN Yang, "BSmagV," projet long 2A Supélec, 2016-2017. (){PhD 0.5, LQ 0.5}[]
- Tianyang LIU, Agathe VAUQUIER, "HVDC fault," projet long 2A Supélec, 2016-2017. (){TL 0.85, LQ 0.5}[]
- Carolina MONTEIRO FERREIRA, Jonathan FERREIRA PASSONI, Maria Jose BASCUNANASECHI, Santi CORTEZON , "WT upscaling," projet long 2A Supélec, 2016-2017. (){LQ 1}[]
- Pierre LE GOFF, Celia GARCIA OLIVER, "Simulation d'une installation PV," projet 2A Supélec, 2016-2017. (){LQ 1}[]
- Pierre BORFIGA, Amine BEN AMOR, "Calcul B nouille galactique," projet 2A Supélec, 2016-2017. (){LQ 1}[]
- Zhinan CHEN, Charlie GINHOUX, Pauline LOTTIER , "RaspPI + IGBT," projet 2A Supélec, 2016-2017. (){LQ 1}[]
- Mehdi BENCHEQROUN, Valentin LETOURNEUX DE LA PERRAUDIERE, "Rentabilité d'une installation photovoltaique," projet 2A Supélec, 2015-2016. (){LQ 1}[]
- Gabrielle POULLIN, Adrien CHAO, "Protection d'un réseau HVDC," projet 2A Supélec, 2015-2016. (){LQ 1}[]
- Étienne LORANG, Julien MERLE, Loïc MARIEZ, "Limiteur de courant supraconducteur," projet 2A Supélec, 2015-2016. (){LQ 1}[]
- Pierre DELAUNAY, Julien NAU, "Intégration source volumique BSmag," projet 2A Supélec, 2015-2016. (){LQ 1}[]

8.5.4 Projet 1A

- Enrique Leon PAILLO STATQUEVIOS, Saad AAFFOUTE, Maxime LIMOUSIN, "Station de test câble supra," Projet 1A CentraleSupélec pole projet P17 NCE 1SL8000, 2021-2022. (){LQ 1}[]
- Thomas CORBIN, Marc-Cesar GARCIA-GRENET, Louis DUPONT, Sarah MAGNA VIEIRA-RODRIGUES, Amparo Isidora CORVALAN SCHINDLER, "Eolienne supraconductrice," Projet 1A CentraleSupélec pole projet P13 MSE 1SL8000, 2021-2022. (){LQ 1}[]
- Louis CONREUX, Enzo MICHEL-NIL, Mohamed NDIAYE, Guerric LOUËT, "Station de test câble supra," Projet 1A CentraleSupélec pole projet P17 NCE, 2020-2021. (){LQ 1}[]
- Xavier CUNIN, Remi RIGAL, Martin DOUYSSET, Baptiste BAUD, Remi FOURAULT, "Composants supraconducteurs pour les réseaux électriques," Projet 1A CentraleSupélec pole projet P13 MSE, 2020-2021. (){LQ 1}[]
- Dunan SIMONIS, Mathieu LAPEZE, Melen LE CORRE, Sarah MAGNA VIEIRA RODRIGUEZ, "Eolienne supraconductrice," Projet 1A CentraleSupélec pole projet P13 MSE, 2020-2021. (){LQ 1}[]
- Matias BUSTOS, "Station de test câble supra," Projet 1A CentraleSupélec parcours recherche, 2020-2021. (){LQ 1}[]
- Alexandre BELOT, Elisa PARGA, "Composants supraconducteurs pour les réseaux électriques: filtre," projet 1A CentraleSupélec, 2019-2020. (){LQ 1}[]
- Adrien MULLER, Mattéo BRAURE, "Composants supraconducteurs pour les réseaux électriques: cable," projet 1A CentraleSupélec, 2019-2020. (){LQ 1}[]
- Damien TASSO, Lou BERNABEU, "Cable Supraconducteur," projet 1A CentraleSupélec, 2019-2020. (){LQ 1}[]
- Alban FALCK , "Composants supraconducteurs pour les réseaux électriques," projet 1A CentraleSupélec, 2019-2020. (){LQ 1}[]
- Yasmine BENNANI, Romain BIGNOTTI, "Identification des paramètres d'une cellule photovoltaïque à l'aide d'un algorithme génétique," projet 1A Supélec, 2017-2018. (){LQ 1}[]
- Yanis EL BAROUDI, Alexandre GAENG, "Contrôle d'une MCC avec Arduino et Raspberry Pi sous Matlab/Simulink," projet 1A Supélec, 2017-2018. (){LQ 1}[]
- Guilhem POIRIER COUTANSAIS, Guillaume VAGNER, "Validation of an open source code for the calculation of the magnetic field in 3D BSmag," projet 1A Supélec, 2017-2018. (){LQ 1}[]
- GEORGIN, GERARD, MICHELET, "Banc de test cellules PVT," projet 1A Supélec, 2016-2017. (){LQ 1}[]
- LIU, PARAIN, "Calculation force BSmag," projet 1A Supélec, 2016-2017. {LQ 1}[]
- Theophile DANJOU, Alexandre DE MESMAY, "Simulation metro," projet 1A Supélec, 2015-2016.

(){LQ 1}[]
- Alejandra GONZALEZ MOLINA, Timothee TOUDIC, "Installation photovoltaïque," projet 1A Supélec, 2015-2016. (){LQ 1}[]

8.5.5 Projet M2

- Ayoub HARCHADI, Lokmane HAOUCHINE, El Mehdi KARMANI, "Datalogger," Projet M2 PIE initiation à la recherche NX150299, 2021-2022. (){LQ 0.5, SM 0.5}[]
- Sébastien FERREIRA, Walid MEBARKI, Yasmine BAAZIZI, "Optimisation production centrale PV," Projet M2 PIE initiation à la recherche NX15029, 2021-2022. (){LQ 0.5, SM 0.5}[]
- Abdelaaziz BENOUDINA, Athanasios KORRES, Saad BELBARD, "Développement d'une plateforme de contrôle de convertisseur," Projet M2 PIE, 2020-2021. (){LQ 1}[]
- Oussama MALAOUI, Zenatou SORE, Kheir-eedine TAREB, "Optimisation production centrale PV," Projet M2 PIE, 2020-2021. (){LQ 1}[]
- Pamela ZOGHBY, Elsy ELSAYEGH, "Validation d'un Code Open-Source pour le Calcul du Champ Magnétique 3D," Projet M2 PIE, 2019-2020. (){LQ 1}[]
- James WANG, "Permanent magnet guideway topologies," Projet M2 PIE, 2019-2020. (){LQ 1}[]
- Raicha IKBAL, "Realisation d'un support de bobine par impression 3D," stage M2, 2019-2020. (){LQ 1}[]
- Hussam HALLAK, Mike MARTIAL, "Stabilisation d'un réseau DC en utilisant une bobine supraconductrice," projet M2 PIE-PDE projet, 2017-2018. (){LQ 1}[]
- Jura ARKHANGELSKI, Wafae CHOUIB, "Simulation of PV installation," projet M2 PIE anglais, 2016-2017. (){LQ 1}[]
- Cedric COLONNA, Jorel FLAMBAR, "Validation of an open source code for the calcul of the magnetic field in 3D," projet M2 PIE anglais, 2016-2017. (){LQ 1}[]
- Kanta MOUSSA, "Calculation of the force on a filament with an open source code for the calcul of the magnetic field in 3D," projet M2 PIE anglais, 2016-2017. (){LQ 1}[]
- Mokrane BALA, "Simulation line 18," projet M2 PIE anglais, 2016-2017. (){LQ 1}[]
- Sonia BARRIOS, "Modélisation de convertisseurs HVDC," projet M2 PIE temps partiel, 2015-2016. (){LQ 1}[]
- Ralph HALLAK, "Modélisation d'un câbles HVDC," projet M2 PIE temps partiel, 2015-2016. (){LQ 1}[]

8.5.6 Projet M1

- Amaury CORDIER, "Cartographie du potentiel de l'énergie photovoltaïque," stage M1, 2020-2021. (){SM 0.9, LQ 0.1}[]
- Yasmine BENZAAMA, "Réalisation et caractérisation d'un capteur d'irradiance," stage M1, 2019-2020. (){LQ 1}[]
- Rajalakshmi DORERADJOU, "Montage d'une vidéo d'une expérience de lévitation supraconductrice," stage M1, 2019-2020. (){LQ 1}[]
- Robin GUYON, "Exploration des performances du RaspberryPi et de l'Arduino," Stage M1, 2017-2018. (){LQ 1}[]

8.5.7 Projet L3

- Baptiste HAMARD, "Filtre supraconducteur," Stage L3, 2017-2018. (){LQ 1}[]
- Marie Thérèse DIOUF, "Convertisseur DC/DC," Stage L3, 2018-2019. (){LQ 1}[]
- Badr SBANE, "Convertisseur DC/DC," Stage L3, 2018-2019. (){LQ 1}[]

8.5.8 Projet L2

- Arthur DALLEMAGNE, Jean MARTINI, "Réalisation et caractérisation d'un capteur d'irradiance," Stage L2 immersion recherche, 2020-2021. (){LQ 1}[]
- Myriam YEROU, Douchka DIMITRIJEVIC, "Réalisation et caractérisation d'un capteur d'irradiance," Stage L2 immersion recherche, 2020-2021. (){LQ 1}[]
- Jakub HAJDAS, Sébastien BILLÈS, "Réalisation et caractérisation d'un capteur d'irradiance," stage L2 immersion recherche, 2019-2020. (){LQ 1}[]

- Jugurta ALOUACHE, Hardiata DIAGNE, "Réalisation et caractérisation d'un capteur d'irradiance," stage L2 immersion recherche, 2019-2020. (){LQ 1}[]
- Noémie DAMERVAL, Aymane ROUABAH, "Réalisation et caractérisation d'un capteur d'irradiance," stage L2 immersion recherche, 2019-2020. (){LQ 1}[]
- Yves SCHMIT, Dounia MOHAMADI, "Conception d'un capteur d'irradiance," Stage L2, 2018-2019. (){LQ 1}[]
- Martial GUIDEZ, Clemence MARI, "Conception d'un capteur d'irradiance," Stage L2, 2018-2019. (){LQ 1}[]
- Nejma HASSINI, Francois LI, "Contrôle d'un convertisseur buck à l'aide d'une carte Arduino," TIPE (L2), 2018-2019. (){LQ 1}[]

Chapter 9

Publications

9.1 Peer-reviewed journals

[p41] L. Pniak, L. Quéval, B. Revol, J.-S. Ngoua Teu, C. Gautier, O. Béthoux, "AC resistance and leakage inductance estimation for planar transformers with parallel connected windings," accepted for publication in *IEEE Transactions on Power Electronics*, Aug. 2022.

[p40] T.-K. Hoang, L. Quéval, L. Vido, D.-Q. Nguyen, "Levelized cost of energy comparison between permanent magnet and superconducting wind generators for various nominal power," *IEEE Transactions on Applied Superconductivity*, vol. 32, no. 7, id. 5202606, Oct. 2022. (DOI, link)

[p39] S. Ferreira, S. Meunier, M. Heinrich, J.A. Cherni, A. Darga, L. Quéval, "A decision support tool to place drinking water sources in rural communities," *Science of The Total Environment*, vol. 833, no. 155069, Aug. 2022. (DOI, link)

[p38] R. Coelho-Medeiros, L. Quéval*, J. Dai, J.-C. Vannier, P. Egrot, "Integration of HTS coils in a lab-scale modular multilevel converter," *IEEE Transactions on Applied Superconductivity*, vol. 32, no. 4, id. 5400904, Jun. 2022. (DOI, link)

[p37] W.-J. Yang, L. Quéval, G.-T. Ma*, "Numerical studies of dynamic characteristics of a stack-type HTS maglev system based on H-formulation," *IEEE Transactions on Applied Superconductivity*, vol. 32, no. 6, id. 3602704, Sep. 2022. (DOI, link)

[p36] B. Douine*, L. Quéval, F. Trillaud, S. Fawaz, H. Menana, I. Schwenker, O. Despouys, N. Ivanov, "Characterization of a superconducting power filter for embedded electrical grid application," *IEEE Transactions on Applied Superconductivity*, vol. 32, no. 4, Jun. 2022. (DOI, link)

[p35] S. Fawaz*, H. Menana, B. Douine, L. Quéval, "DC modeling & characterization of HTS coils with non uniform current density distribution," *Superconductor Science and Technology*, vol. 34, no. 12, pp. 124001, Nov. 2021. (DOI, link)

[p34] A. Ghabeli*, M. Ainslie, E. Pardo, L. Quéval, R. Mataira, "Modeling the charging process of a coil by an HTS dynamo-type flux pump," *Superconductor Science and Technology*, vol. 34, no. 8, pp. 4002, Jul. 2021. (DOI, link, preprint, data)

[p33] C. Soenen*, V. Reinbold, S. Meunier, J.A. Cherni, A. Darga, P. Dessante, L. Quéval, "Comparison of tank and battery storages for photovoltaic water pumping," *MDPI Energies*, vol. 14, no. 9, id. 2483, Apr. 2021. (DOI, link)

[p32] F. Trillaud, B. Douine, L. Quéval*, "Superconducting power filter for aircraft electric DC grids" *IEEE Transactions on Applied Superconductivity*, vol. 31, no. 5, pp. 1-5, Aug. 2021. (DOI, link, postprint)

[p31] M.D. Ainslie*, L. Quéval, R.C. Mataira, C.W. Bumby, "Modelling the frequency dependence of

the open-circuit voltage of a high-Tc superconducting dynamo," *IEEE Transactions on Applied Superconductivity*, vol. 31, no. 5, pp. 1-7, Aug. 2021. (DOI, link)

[p30] S. Meunier*, L. Quéval, A. Darga, P. Dessante, C. Marchand, M. Heinrich, J.A. Cherni, E.A. de la Fresnaye, L.Vido, B. Multon, P.K. Kitanidis, "Sensitivity analysis of photovoltaic pumping systems for domestic water supply," *IEEE Transactions on Industry Applications,* vol. 56, no. 6, pp. 6734-6743, Nov. 2020. (DOI, link, HAL)

[p29] M.D. Ainslie*, F. Grilli, L. Quéval, E. Pardo, F. Perez-Mendez, R. Mataira, A. Morandi, A. Ghabeli, C. Bumby, R. Brambilla, "A new benchmark for electromagnetic modelling of superconductors: the high-Tc superconducting dynamo," *Superconductor Science and Technology*, vol. 33, no. 10, pp. 105009, Aug. 2020. (DOI, link, preprint, data)

[p28] W.-J. Yang, L. Quéval, G.-T. Ma*, C.-Q. Ye, G. Li, T.-Y. Gong, "A 3-D strong-coupled electromagnetic thermal model for HTS bulk and its uses to study the dynamic characteristics of a linear HTS maglev bearing," *IEEE Transactions on Applied Superconductivity*, vol. 30, no. 6, id. 3602814, Sep. 2020. (DOI, link, postprint)

[p27] W.-J. Yang, L. Quéval, G. Li, C.-X. Yao, G.-T. Ma*, "Comparison of linear superconducting magnetic bearings using isotropic and anisotropic materials," *IEEE Transactions on Applied Superconductivity*, vol. 30, no. 4, id. 4901205, Jun. 2020. (DOI, link, postprint)

[p26] M.Heinrich*, S. Meunier, A. Samé, L. Quéval, A. Darga, L. Oukhellou, B. Multon, "Detection of cleaning interventions on photovoltaic modules with machine learning," *Applied Energy*, vol. 263, id. 114642, Apr. 2020. (DOI, link) – Featured in pv magazine

[p25] T. Vezin*, S. Meunier, L. Quéval, J. A. Cherni, L. Vido, A. Darga, P. Dessante, P. K. Kitanidis, C. Marchand, "Borehole water level model for photovoltaic water pumping systems," *Applied Energy*, vol. 258, id. 114080, Jan. 2020. (DOI, link)

[p24] J.-L. Guo, L. Quéval*, B. Roucaries, L. Vido, L. Liu, F. Trillaud, C. Berriaud, "Nonlinear current sheet model of electrical machines," *IEEE Transactions on Magnetics*, vol. 56, no. 1, id. 7502904, Jan. 2020. (DOI, link, postprint, code)

[p23] W.-J. Yang, G.-T. Ma*, L. Quéval, G. Li, C.-Q. Ye, Y.-K. Deng, "Vibration characteristics research on HTS magnetic levitation system based on a strong-coupled multi-physics model," (in Chinese), *Chinese Science Bulletin*, vol. 64, no. 31, pp. 3255-3266, Oct. 2019. (DOI, link)

[p22] J.J. Perez-Chavez, F. Trillaud, L.M. Castro, L. Quéval*, A. Polasek, R. de Andrade Jr, "Generic model of three-phase (RE)BCO resistive superconducting fault current limiters for transient analysis of power systems," *IEEE Transactions on Applied Superconductivity*, vol. 29, no. 6, id. 5601811, Sep. 2019. (DOI, link)

[p21] P.-B. Zhou, C. Wang, H.-Y. Qian, L. Quéval, Z. Luo, Y. Deng, J. Li, Y.-J. Li, G.-T. Ma* "Frequency-dependent transport AC losses of coated superconductors up to tens of kilohertz," *IEEE Transactions on Applied Superconductivity*, vol. 29, no. 5, id. 8201705, Aug. 2019. (DOI, link)

[p20] Z.-Y. Yan, W.-J. Yang, C.-Q. Ye, R.-C. Wang, L. Quéval, G. Li, K. Liu, G.-T. Ma*, "Numerical prediction of levitation properties of HTS bulk in high magnetic fields," *IEEE Transactions on Applied Superconductivity*, vol. 29, no. 5, id. 3602805, Aug. 2019. (DOI, link)

[p19] P.-B. Zhou, G.-T. Ma*, L. Quéval, "Transition frequency of transport AC losses in high temperature superconducting coated conductors," *Journal of Applied Physics*, vol. 126, id. 063901, Jul. 2019. (DOI, link)

[p18] S. Meunier*, D.T. Manning, L. Quéval, J.A. Cherni, P. Dessante, D. Zimmerle, "Determinants of the marginal willingness to pay for improved domestic water and irrigation in partially electrified Rwandan villages," *International Journal of Sustainable Development & World Ecology*, vol. 26,

no. 6, pp. 547-559, Jun. 2019. (DOI, link)

[p17] S. Meunier*, M. Heinrich, L. Quéval, J.A. Cherni, L. Vido, A. Darga, P. Dessante, B. Multon, P.K. Kitanidis, C. Marchand, "A validated model of a photovoltaic water pumping system for off-grid rural communities," *Applied Energy*, vol. 241, pp. 580-591, May 2019. (DOI, link, data)

[p16] P.-B. Zhou, L. Quéval, G.-T. Ma*, "Magnetic coupling enhancement using a flux transformer," *Journal of Physics D: Applied Physics*, vol. 52, no. 7, pp. 5001, Dec. 2018. (DOI, link)

[p15] D.R. Joca, L.H.S.C. Barreto, D.S. Oliveira Jr., J.-C. Vannier, B. Dzonlaga, L. Quéval*, "Estudo e validação experimental de um conversor multinível modular entrelaçado ca-cc monofásico para aplicações de transformadores de estado sólido," *Revista Eletrônica de Potência*, pp. 1-10, Oct. 2018. (DOI, link)

[p14] L.F.N. Lourenço*, M.B.C. Salles, R.M. Monaro, J.R. Cardoso, L. Quéval, "Evaluation of the reactive power support and associated technical cost of photovoltaic farms operation," *MDPI Energies*, vol. 11, no. 6, pp. 1567, Jun. 2018. (DOI, link)

[p13] L. Quéval, K. Liu, W. Yang, V.M.R. Zermeño, G.-T. Ma*, "Superconducting magnetic bearings simulation using an H-formulation finite element model," *Superconductor Science and Technology*, vol. 31, no. 8, pp. 084001, Mar. 2018. (DOI, link, preprint) – China top cited paper award 2021

[p12] L.F.N. Lourenço*, M.B.C. Salles, R.M. Monaro, L. Quéval, "Technical cost of operating a photovoltaic installation as a STATCOM at nighttime," *IEEE Transactions on Sustainable Energy*, vol. 10, no. 1, pp. 75-81, Apr. 2018. (DOI, link)

[p11] T.-K. Hoang, L. Quéval*, C. Berriaud, L. Vido, "Design of a 20 MW fully superconducting wind turbine generator to minimize the levelized cost of energy," *IEEE Transactions on Applied Superconductivity*, vol. 28, no. 4, pp. 1-4, Jun. 2018. (DOI, link, postrpint) – Featured in IEEE Spectrum (Chinese)

[p10] L. Makong*, A. Kameni, L. Quéval, F. Bouillault, P. Masson, "H-formulation using the discontinuous Galerkin method for the 3D modeling of superconductors," *IEEE Transactions on Magnetics*, vol. 54, no. 3, pp. 1-4, Mar. 2018. (link)

[p9] K. Liu, W. Yang, G.-T. Ma*, L. Quéval, T. Gong, C. Ye, X. Li, Z. Luo, "Experiment and simulation of superconducting magnetic levitation with REBCO coated conductor stacks," *Superconductor Science and Technology*, vol. 31, no. 1, pp. 015013, Dec. 2017. (link)

[p8] L. Quéval*, A. Coty, L. Vido, R. Gottkehaskamp, B. Multon, "A switched reluctance motor drive using photovoltaic transistors: principle, prototype, experimental and numerical results," *IEEE Transactions on Industry Applications*, vol. 53, no. 5, pp. 4886-4893, Sept.-Oct. 2017. (link, postprint)

[p7] P.-B. Zhou, G.-T. Ma*, C. Yang, L. Quéval, K. Liu, H.-Y. Qian, K. Liu, "Magnetic field transfer of superconductor-ferromagnet heterostructures up to 10 kHz," *IEEE Transactions on Applied Superconductivity*, vol. 27, no. 4, pp. 0601105, Jun. 2017. (link)

[p6] L. Quéval*, G.G. Sotelo, Y. Kharmiz, D.H.N. Dias, F. Sass, V.M.R. Zermeño, R. Gottkehaskamp, "Optimization of the superconducting linear magnetic bearing of a maglev vehicle," *IEEE Transactions on Applied Superconductivity*, vol. 26, no. 3, pp. 3601905, Apr. 2016. (link, preprint)

[p5] L. Quéval*, V.M.R. Zermeño, F. Grilli, "Numerical models for AC loss calculation in large-scale applications of HTS coated conductors," *Superconductor Science and Technology*, vol. 29, no. 2, pp. 074007, Jan. 2016. (link, preprint, see [ic8, ic9]) – SuST 2016 highlights

[p4] L. Quéval*, R. Gottkehaskamp, "Analytical field calculation of modulated double helical coils," *IEEE Transactions on Applied Superconductivity*, vol. 25, no. 6, pp. 4901307, Dec. 2015. (link, code)

[p3] L. Quéval*, H. Ohsaki, "Nonlinear abc-model for electrical machines using N-D lookup tables," *IEEE Transactions on Energy Conversion*, vol. 30, no. 1, pp. 316-322, Mar. 2015. (link)

[p2] L. Quéval*, H. Ohsaki, "AC losses of a grid-connected superconducting wind turbine generator," *IEEE Transactions on Applied Superconductivity*, vol. 23, no. 3, pp. 5201905, Jun. 2013. (link)

[p1] L. Quéval*, M. Sekino, H. Ohsaki, "A coupled FE phase-domain model for superconducting synchronous machine," *IEEE Transactions on Applied Superconductivity*, vol. 22, no. 3, pp. 5200804, Jun. 2012. (link)

9.2 International conferences

[ic57] L. Pniak, B. Revol, L. Quéval, J.-S. Ngoua Teu Magambo, O. Béthoux, "Pre-sizing of a modular high power density DC/DC converter with GaN components," *14th International Conference of the International Association for Mathematics and Computer in Simulation (Electrimacs 2022)*, Nancy, May 2022. ()

[ic56] A. Kameni, H. Matar, L. Quéval, "Linearization of E(J) power law used for HTS superconductors modeling," *23rd International Conference on the Computation of Electromagnetic Fields (Compumag2021)*, id. 488, [online], Jan. 2022. ()

[ic55] S. Fawaz, H. Menana, B. Douine, L. Quéval, "DC characterization of HTS coils with non-uniform current density distribution using E(J) and Jc(B) dependency," *7th International Conference on Superconductivity and Magnetism (ICSM2021)*, Bodrum, Turkey, Oct. 2021. (HAL, see [p35])

[ic54] R. Coelho-Medeiros, L. Quéval, J. Dai, J.-C. Vannier, P. Egrot, "Integration of HTS Coils in a lab-scale modular multilevel converter," *15th European Applied Superconductivity Conference (EUCAS)*, Moscow, Russia, Sep. 2021. ()

[ic53] B. Douine*, L. Quéval, F. Trillaud, S. Fawaz, H. Menana, I. Schwenker, O. Despouys, N. Ivanov, "Characterization of superconducting power filter for embedded electrical grid application," *15th European Applied Superconductivity Conference (EUCAS)*, Moscow, Russia, Sep. 2021. (HAL, see [p36])

[ic52] F. Reymond-Laruina, M. Petit, L. Quéval, D. Hadbi, P. Egrot, "Assessment of the AC/DC converters resilience to DC grid fault by electro-thermal modelling," *23rd European Conference on Power Electronics and Applications (EPE'21 ECCE Europe)*, [online], Sep. 2021. (link)

[ic51] R. Coelho-Medeiros, L. Quéval, J. Dai, J. -C. Vannier, P. Egrot, "Cryo-MMC: a modular multilevel converter with superconducting arm coils," *23rd European Conference on Power Electronics and Applications (EPE'21 ECCE Europe)*, [online], Sep. 2021. (link)

[ic50] H. Ben Ahmed, O. Bethoux, A. Cizeron, E. Hoang, A. Juton, E. Labouré, A. Mercier, E. Monmasson, J. Ojeda, L. Quéval, G. Remy (alphabetical order), "Electric Traction Chain with Segmented Power Supply," *23rd European Conference on Power Electronics and Applications (EPE'21 ECCE Europe)*, [online], Sep. 2021. (link, HAL, video)

[ic49] L. Quéval, W.-J. Yang, K. Liu, G.-T. Ma, "Modeling of the non-uniform Jc distribution along the c-axis of seeded melt growth (RE)BCO bulks," *7th International Workshop on Numerical Modelling of High Temperature Superconductors*, [online], Jun. 2021. (link, HAL)

[ic48] R. Coelho-Medeiros, L. Quéval, J. Dai , J.-C. Vannier, P. Egrot, "Modeling of high-temperature superconducting pancake coils using the axisymmetric partial element equivalent circuit method," *7th International Workshop on Numerical Modelling of High Temperature Superconductors*, [online], Jun. 2021. (link, HAL)

[ic47] M.D. Ainslie, F. Grilli, L. Quéval, E. Pardo, F. Perez-Mendez, R. Mataira, A. Morandi, A. Ghabeli, C. Bumby, R. Brambilla, "A new benchmark numerical model: the high-Tc superconducting dy-

namo," *7th International Workshop on Numerical Modelling of High Temperature Superconductors*, [online], Jun. 2021. (link, HAL)

[ic46] A. Ghabeli, E. Pardo, M. Ainslie, L. Quéval, "Modeling HTS dynamo-type flux pumps: open-circuit mode and charge of an HTS coil," *7th International Workshop on Numerical Modelling of High Temperature Superconductors*, [online], Jun. 2021. (link, HAL)

[ic45] S. Fawaz, H. Menana, B. Douine, L. Quéval, "DC modeling and characterization of HTS coils with non uniform current density distribution," *7th International Workshop on Numerical Modelling of High Temperature Superconductors*, [online], Jun. 2021. (link, HAL, see [p35])

[ic44] L. Quéval*, B. Douine, I. Schwenker, D. Huchet, F. Trillaud, O. Despouys, "Superconducting power filter HVDC and onboard DC grids," *COST ACTION 19108 Hi-Scale first joint WG3/4 industry-academia workshop on applications for HTS technologies in the electrical energy chain*, [online], Apr. 2021. (ppt) – Invited

[ic43] F. Trillaud, B. Douine, L. Quéval*, "Superconducting power filter for aircraft electric DC grids" *Applied Superconductivity Conference (ASC 2020), id. Wk2LPo1I-03*, [online], Nov. 2020. (see [p32], poster)

[ic42] M.D. Ainslie, L. Quéval, R. Mataira, C. Bumby, R. Badcock, "Frequency dependence of the open-circuit voltage of a high-Tc superconducting dynamo," *Applied Superconductivity Conference (ASC 2020)*, [online], Nov. 2020. (see [p31])

[ic41] M.D. Ainslie, F. Grilli, L. Quéval, E. Pardo, F. Perez Mendez, R. Mataira, A. Morandi, A. Ghabeli, C. Bumby, R. Brambilla, "A new benchmark numerical model: the high-Tc superconducting dynamo," *Applied Superconductivity Conference (ASC 2020)*, [online], Nov. 2020. (see [p29]) – Invited

[ic40] J. Cherni, A. Darga, Ph. Dessante, M. Heinrich, P. Kitanidis, C. Marchand, D.T. Manning, S. Meunier, B. Multon, L. Quéval, T. Vezin, L. Vido (in alphabetical order), "Turning Sun into Water – Current status & perspectives," *Wind Empowerment Online Conference (WEOnline2020)*, [online], Nov. 2020. (ppt)

[ic39] R. Coelho-Medeiros*, B. Džonlaga, J.-C. Vannier, J. Dai, L. Quéval, P. Egrot, "A comparison between different models of the modular multilevel converter," *22nd European Conference on Power Electronics and Applications (EPE'20 ECCE Europe)*, Lyon, France, Sep. 2020. (DOI, link)

[ic38] L. Quéval*, O. Despouys, F. Trillaud, B. Douine, "Feasibility study of a superconducting power filter for HVDC grids," *22nd European Conference on Power Electronics and Applications (EPE'20 ECCE Europe)*, Lyon, France, Sep. 2020. (DOI, link, video) – EPE Young Author Best Paper Award

[ic37] B. Dzonlaga, L. Quéval, J.-C. Vannier, "Impact of the arm resistance and inductance on the PQ diagram of a modular multilevel converter," *20th International Symposium on Power Electronics (Ee2019)*, Novi Sad, Serbia, Oct. 2019. ()

[ic36] W.-J. Yang, L. Quéval, G.-T. Ma, "Comparison of linear superconducting magnetic bearings using isotropic and anisotropic materials," *26th International Conference on Magnet Technology (MT26)*, id. Thu-Mo-Po4.13-01, Vancouver, Canada, Oct. 2019. ()

[ic35] L. Quéval, F. Trillaud, B. Douine, "Progress towards the realization of a DC superconducting power filter," *14th European Conference on Applied Superconductivity (EUCAS2019)*, id. 3-LO-TG-05S, Glasgow, UK, Sep. 2019. ()

[ic34] M.D. Ainslie, L. Quéval, R.C. Mataira, R.A. Badcock, C.W. Bumby, "Modelling an HTS dynamo using a segregated finite-element model," *14th European Conference on Applied Superconductivity (EUCAS2019)*, id. 2-LP-SMA-S07, Glasgow, UK, Sep. 2019. (poster)

[ic33] J.-L. Guo, L. Quéval, B. Roucaries, L. Vido, L. Liu, C. Berriaud, F. Trillaud, "Semi-analytical nonlinear model of slotless electrical machines," *22nd International Conference on the Computation of Electromagnetic Fields (Compumag2019)*, id. 114, Paris, France, Jul. 2019. (see [p24])

[ic32] S. Meunier, L. Quéval, M. Heinrich, E. A. de la Fresnaye, J. A. Cherni, L. Vido, A. Darga, P. Dessante, B. Multon, P. K. Kitanidis, and C. Marchand, "Effect of irradiance data on the optimal sizing of photovoltaic water pumping systems," *IEEE Photovoltaic Specialists Conference* (PVSC), Chicago, USA, Jun. 2019. () – Invited, Nominated for the best student paper award

[ic31] S. Meunier, L. Quéval, A. Darga, P. Dessante, C. Marchand, M. Heinrich, J.A. Cherni, E.A. Fresnaye, L. Vido, B. Multon, P.K. Kitanidis, "Modelling and optimal sizing of photovoltaic water pumping systems – Sensitivity analysis," *14th International Conference on Ecological Vehicles and Renewable Energies (EVER2019)*, id. 19-73, Monaco, May 2019. (DOI, link, HAL) – Award of the best paper on renewable energies

[ic30] P.-B. Zhou, C. Wang, H.-Y. Qian, L. Quéval, Z. Luo, Y. Deng, J. Li, Y.-J. Li, G.-T. Ma "Frequency-dependent transport AC losses of coated superconductors up to tens of kilohertz," *Applied Superconductivity Conference 2018 (ASC 2018)*, id. 1MPo2C-07, Seattle, USA, Nov. 2018. () – Best student paper 3rd prize winner (Materials)

[ic29] Z.-Y. Yan, W.-J. Yang, C.-Q. Ye, R.-C. Wang, L. Quéval, G. Li, K. Liu, G.-T. Ma, "Numerical prediction of levitation properties of HTS bulk in high magnetic fields," *Applied Superconductivity Conference 2018 (ASC 2018)*, id. 3LPo1K-01, Seattle, USA, Nov. 2018. ()

[ic28] S. Meunier, L. Quéval, M. Heinrich, J.A. Cherni, L. Vido, A. Darga, P. Dessante, B. Multon, C. Marchand, "Influence of the temporal resolution of the water consumption profile on photovoltaic water pumping systems modelling and sizing," *7th International Conference on Renewable Energy Research and Applications (ICRERA 2018)*, Paris, France, Oct. 2018. (DOI, link, postprint)

[ic27] L. Quéval, K. Liu, W.-J. Yang, V.M.R. Zermeño, G.-T. Ma, "Simulation of stack-type superconducting magnetic bearings," *6th International Workshop on Numerical Modelling of High Temperature Superconductors*, Caparica, Portugal, Jun. 2018. ()

[ic26] W.-J. Yang, C.-Q Ye, K. Liu, L. Quéval, G. Li, T.-Y. Gong, G.-T. Ma, "Numerical modeling for the dynamic characteristics of HTS magnetic levitation system," *6th International Workshop on Numerical Modelling of High Temperature Superconductors*, Caparica, Portugal, Jun. 2018. ()

[ic25] K. Berger, L. Quéval, F. Trillaud, G. Escamez, B. Ramdane, G. Dilasser, H. Menana, J. Lévêque, "Hybrid analytical and integral methods for simulating HTS materials," *6th International Workshop on Numerical Modelling of High Temperature Superconductors*, Caparica, Portugal, Jun. 2018. (ppt)

[ic24] B. Džonlaga, D.R. Joca, L. Quéval, J.-C. Vannier, "Transient analysis of a modular multilevel converter with coupled arm inductors," *2018 IEEE Applied Power Electronics Conference and Exposition (APEC 2018)*, San Antonio, USA, Mar. 2018. (DOI, link)

[ic23] L.F.N. Lourenço, M.B.C. Salles, R.M. Monaro, L. Quéval, "Technical cost of PV-STATCOM applications," *6th International Conference on Renewable Energy Research and Applications (ICRERA 2017)*, id. 188, San Diego, USA, Nov. 2017. (link)

[ic22] L. Quéval, F. Trillaud, J.J. Pérez-Chavez, B. Douine, "Superconducting power filter for DC electrical grids," *13th European Conference on Applied Superconductivity (EUCAS2017)*, id. 1LP6-19, Geneva, Switzerland, Sep. 2017. ()

[ic21] T.-K. Hoang, L. Quéval, C. Berriaud, L. Vido, "Design of a 20 MW fully superconducting wind turbine generator to minimize the levelized cost of energy," *13th European Conference on Applied Superconductivity (EUCAS2017)*, id. 4LP6-14, Geneva, Switzerland, Sep. 2017. ()

[ic20] J.J. Pérez-Chavez, F. Trillaud, L.M. Castro, L. Quéval, A. Polasek, R. de Andrade Jr., "Modelling of (Re)BCO resistive superconducting fault current limiter with application to an AC electric power circuit," *13th European Conference on Applied Superconductivity (EUCAS2017)*, id. 4LP7-17, Geneva, Switzerland, Sep. 2017. ()

[ic19] K. Berger, G. Escamez, L. Quéval, A. Kameni, L. Alloui, B. Ramdane, F. Trillaud, L Makong, G. Meunier, P. Masson, J. Lévêque, "Benchmark on the 3D numerical modeling of a superconducting bulk," *21st International Conference on the Computation of Electromagnetic Fields (Compumag2017)*, id. 110, Daejeon, Korea, Jun. 2017. (link, poster)

[ic18] L. Makong, A. Kameni, L. Quéval, F. Bouillault, P. Masson, "H-formulation using the discontinuous Galerkin method for the 3D modeling of superconductors," *21st International Conference on the Computation of Electromagnetic Fields (Compumag2017)*, Daejeon, Korea, Jun. 2017. ()

[ic17] T.-K. Hoang, L. Quéval, L. Vido, C. Berriaud, "Impact of the rotor blade technology on the levelized cost of energy of an offshore wind turbine," *Joint International Conference OPTIM-ACEMP*, Brasov, Romania, May 2017. (link)

[ic16] L. Quéval, F. Trillaud, B. Douine, "DC grid stabilization using a resistive superconducting fault current limiter," *International Conference on Components and Systems for DC grids (COSYS-DC 2017)*, Grenoble, France, Mar. 2017. (link, ppt)

[ic15] D.R. Joca, B. Dzonlaga, L.H.S.C. Barreto, D.S. Oliveira, J.C. Vannier, L. Quéval, "AC-DC interleaved modular multilevel converter with medium-frequency isolation transformer for DC microgrids," *International Conference on Components and Systems for DC grids (COSYS-DC 2017)*, Grenoble, France, Mar. 2017. (link)

[ic14] P.-B. Zhou, G.-T. Ma, C. Yang, L. Quéval, K. Liu, H.-Y. Qian, K. Liu, "Magnetic field transfer of superconductor-ferromagnet heterostructures up to 10 kHz," *2016 Applied Superconductivity Conference (ASC 2016)*, id. 2LPo2L-07, Denver, USA, Sep. 2016. (link)

[ic13] L. Quéval, A. Coty, L. Vido, R. Gottkehaskamp, B. Multon, "A switched reluctance motor drive using photovoltaic transistors: principle, prototype, experimental and numerical results," *4th International Conference on Renewable Energy Research and Applications (ICRERA 2015)*, id. 112, Palermo, Italy, Nov. 2015. (link, see [p8])

[ic12] L. Quéval, G.G. Sotelo, Y. Kharmiz, D.H.N. Dias, F. Sass, V.M.R. Zermeño, R. Gottkehaskamp, "Optimization of the superconducting linear magnetic bearing of a maglev vehicle," *12th European Conference on Applied Superconductivity (EUCAS2015)*, id. 3A-LS-P-04.03, Lyon, France, Sep. 2015. (preprint, poster)

[ic11] L. Quéval, A. Coty, L. Vido, R. Gottkehaskamp, B. Multon, "Photovoltaic switched reluctance motor modeling and simulation," *15th IEEE International Conference on Environment and Electrical Engineering (EEEIC2015)*, id. 587, Rome, Italy, Jun. 2015. (link)

[ic10] L. Quéval, A. Coty, L. Vido, B. Multon, "Photovoltaic motors review, comparison and switched reluctance motor prototype," *10th International Conference on Ecological Vehicles and Renewable Energies (EVER2015)*, id. 87, Monaco, Apr. 2015. (link)

[ic9] F. Grilli, V.M.R. Zermeño, L. Quéval, "Numerical models of HTS coated conductors are now ready for realistic applications," *Coated Conductors for Applications 2014 (CCA2014)*, Jeju, South Korea , Nov. 2014. (ppt)

[ic8] V.M.R. Zermeño, F. Grilli, L. Quéval, "A multiscale model for calculating hysteretic losses in superconducting stacks and coils for large scale applications," *2014 Applied Superconductivity Conference (ASC 2014)*, id. 2LOr3D-03, Charlotte, USA, Aug. 2014. ()

[ic7] L. Quéval, C. Joulain, C.E. Casillas, "Measuring the power curve of a small-scale wind turbine: a

practical example," *1st International e-Conference on Energies (ece1)*, Sciforum Electronic Conference Series, vol. 1, id. c011, Mar. 2014. (link, code)

[ic6] H. Ohsaki, L. Quéval, Y. Terao, "Design and characteristic analysis of 10 MW class superconducting wind turbine generators with different types of stator and rotor configurations," *4th International Conference on Clean Electrical Power (ICCEP 2013)*, Alghero, Italy, Jun. 2013. (link)

[ic5] L. Quéval, H. Ohsaki, "Back-to-back converter design and control for synchronous generator-based wind turbines," *International Conference on Renewable Energy Research and Applications (ICRERA 2012)*, Nagasaki, Japan, Nov. 2012. (link)

[ic4] L. Quéval, H. Ohsaki, "Study on the implementation of the phase-domain model for rotating electrical machines," *15th International Conference on Electrical Machines and Systems (ICEMS2012)*, Sapporo, Japan, Oct. 2012. (link)

[ic3] L. Quéval, H. Ohsaki, "AC losses of a grid-connected superconducting wind turbine generator," *2012 Applied Superconductivity Conference (ASC 2012)*, id. 4LPE-02, Portland, USA, Oct. 2012. (link)

[ic2] L. Quéval, H. Ohsaki, "Grid integration of offshore superconducting wind turbine generators," *15th International Power Electronics and Motion Control Conference (EPE-PEMC 2012)*, id. 207, Novi Sad, Serbia, Sep. 2012. (link)

[ic1] L. Quéval, M. Sekino, H. Ohsaki, "A coupled FE phase-domain model for superconducting synchronous machine," *22nd International Conference on Magnet Technology (MT22)*, id. 2EP5-5, Marseille, France, Sep. 2011. (link)

9.3 National conferences

[nc33] S. Fawaz, H. Menana, B. Douine, L. Quéval, "Modélisation et caractérisation en courant continu des bobines SHTC avec une distribution non uniforme de la densité de courant," *13es Journées de Cryogénie et de Supraconductivité*, Oct. 2021, Aussois, France. (HAL, see [p35])

[nc32] H. Ben Ahmed, O. Bethoux, A. Cizeron, E. Hoang, A. Juton, E. Labouré, A. Mercier, E. Monmasson, J. Ojeda, L. Quéval, G. Remy (alphabetical order), "Chaîne de traction à alimentation fractionnée," *Journée mobilité électrique Ampère 200 ans*, Paris, France, Oct. 2021. ()

[nc31] H. Ben Ahmed, O. Bethoux, A. Cizeron, E. Hoang, A. Juton, E. Labouré, A. Mercier, E. Monmasson, J. Ojeda, L. Quéval, G. Remy (alphabetical order), "Les enjeux du concept CTAF : chaîne de traction à alimentation fractionnée," *Symposium de Génie Electrique (SGE 2021)*, Nantes, France, Jul. 2021. (link, HAL)

[nc30] R. Coelho-Medeiros, B. Džonlaga, J.-C. Vannier, J. Dai, L. Quéval, P. Egrot, "Comparaison entre différents modèles du convertisseur modulaire multiniveau," *Symposium de Génie Electrique (SGE 2021)*, Nantes, France, Jul. 2021. ()

[nc29] L. Quéval, B. Douine, I. Schwenker, D. Huchet, F. Trillaud, O. Despouys, "Evaluation de la faisabilité d'un filtre de puissance supraconducteur pour les réseaux à courant continu haute tension, " *Symposium de Génie Electrique (SGE 2021)*, Nantes, France, Jul. 2021. (HAL)

[nc28] L. Pniak, J.-S. Ngoua Teu Magambo, C. Rizet, B. Revol, L. Quéval, O. Bethoux, "Convertisseur DC-DC modulaire composants GaN: pertinence du DAB en configuration ISOP, " *Symposium de Génie Electrique (SGE 2021)*, Nantes, France, Jul. 2021. ()

[nc27] L. Quéval, B. Douine, I. Schwenker, D. Huchet, F. Trillaud, O. Despouys, "Superconducting power filter for DC electrical grids," *4a Escuela de superconductividad*, [online], Nov. 2020. () – Invited

[nc26] S. Meunier, A. Darga, M. Heinrich, L. Quéval, "Qualité et fiabilité des équipements solaires photo-

voltaïques vendus sur le marché informel ouagalais," *2ème Conférence Ouest Africaine – Energies renouvelables*, Saint-Louis, Sénégal, Feb. 2020. ()

[nc25] J. Cherni, A. Darga, Ph. Dessante, M. Heinrich, P. Kitanidis, C. Marchand, D.T. Manning, S. Meunier, B. Multon, L. Quéval, T. Vezin, L. Vido (in alphabetical order), "Turning Sun into Water – Etat actuel & perspectives," *Journées Nationales du Photovoltaïque 2019 (JNPV 2019)*, Dourdan, France, Dec. 2019. (video)

[nc24] M. Heinrich, S. Meunier, A Samé, L. Quéval, L. Oukhellou, A. Darga, "Détection des interventions de nettoyage des modules photovoltaïques d'une installation isolée par arbres décisionnels," *Journées Nationales du Photovoltaïque 2019 (JNPV 2019)*, Dourdan, France, Dec. 2019. (see [p26])

[nc23] A. Darga, S. Meunier, M. Heinrich, L. Quéval, "Reliability of solar photovoltaic modules : case study of defective and fake modules from high demand market," *4ème Colloque de la Fédération d'électronique*, Sorbonne Université – ISEP, Paris, France, Nov. 2019. ()

[nc22] L. Quéval, "Superconducting Magnetic Bearings," *EASISchool 2 on Cryogenics*, CEA Saclay, France, Oct. 2019. (link) – Invited

[nc21] B. Džonlaga, L. Quéval, J.-C. Vannier, "Impact of the arm resistance and inductance on the PQ diagram of a modular multilevel converter," *Conférence des Jeunes Chercheurs en Génie Electrique (JCGE2019)*, Oléron, France, Jun. 2019. ()

[nc20] R. Medeiros, J.-C. Vannier, J. Dai, L. Quéval, P. Egrot, "Harmoniques de courant du convertisseur modulaire multi-niveau pour la modulation NLC," *Conférence des Jeunes Chercheurs en Génie Electrique (JCGE2019)*, Oléron, France, Jun. 2019. ()

[nc19] S. Meunier, M. Heinrich, L. Quéval, J.A. Cherni, L. Vido, A. Darga, P. Dessante, B. Multon, P.K. Kitanidis, C. Marchand, "Conception optimale des systèmes photovoltaïques de pompage d'eau en sites isolés avec prise en compte des aspects socio-économiques," *Conférence des Jeunes Chercheurs en Génie Electrique (JCGE2019)*, Oléron, France, Jun. 2019. (link)

[nc18] A. Darga, A. Jaffre, S. Meunier, M. Heinrich, L. Quéval, "Identification de cellules solaires photovoltaïques contrefaites par photoluminescence et Raman," *Journée technique IDIL : Spectroscopie électromagnétique et vibrationnelle*, AgriParistech Paris, France, May 2019. ()

[nc17] A. Darga, M. Heinrich, S. Meunier, L. Quéval, "Projet Turning Sun Into Water : récit d'une aventure collective humaine et scientifique," *Journées Nationales du Photovoltaïque 2018 (JNPV 2018)*, Dourdan, France, Dec. 2018. () – Invited

[nc16] A. N'Dour, S. Meunier, A. Kaboré, M. Heinrich, L. Quéval, A. Darga, "Modules photovoltaïques contrefaits en vente sur le marché Africain : détection et caractérisation électrique d'échantillons issus du marché Burkinabé," *Journées Nationales du Photovoltaïque 2018 (JNPV 2018)*, Dourdan, France, Dec. 2018. (link)

[nc15] S. Meunier, M. Heinrich, L. Quéval, A. Darga, J.A. Cherni, L. Vido, P. Dessante, B. Multon, C. Marchand, "Étude multidisciplinaire d'un système de pompage photovoltaïque dans une communauté rurale du Burkina Faso," *Journées Nationales du Photovoltaïque 2018 (JNPV 2018),* Dourdan, France, Dec. 2018. (link)

[nc14] S. Meunier, M. Heinrich, J. A. Cherni, L. Quéval, P. Dessante, L. Vido, A. Darga, B. Multon, C. Marchand, "Modélisation et validation expérimentale d'un système de pompage photovoltaïque dans une communauté rurale isolée du Burkina Faso," *Symposium de Génie Electrique (SGE 2018)*, Nancy, France, Jul. 2018. ()

[nc13] B. Džonlaga, D.R. Joca, L. Quéval, D. Huchet, A. Arzandé, J.C. Vannier, "Etude expérimentale d'un convertisseur modulaire multiniveau monophasé aux bras couplés," *Symposium de Génie Electrique (SGE 2018)*, Nancy, France, Jul. 2018. ()

[nc12] L. Quéval, F. Trillaud, J.J. Pérez-Chavez, B. Douine, "Filtre de puissance supraconducteur pour les réseaux à courant continu," *12es Journées de Cryogénie et de Supraconductivité*, Aussois, France, Jun. 2018. ()

[nc11] L. Quéval, "Superconducting magnetic levitation," *Fundamentos de electromagnetismo y aplicaciones*, Mexico city, Mexico, Mar. 2018. (see [p6, s1])

[nc10] K. Berger, G. Escamez, L. Quéval, A. Kameni, L. Alloui, B. Ramdane, "Modélisations 3-D d'un cube supraconducteur, influence du maillage," *9ème Conf. Européenne sur les Méthodes Numériques en Electromagnétisme (NUMELEC 2017)*, id. 153677-O3-5, Paris, France. Nov. 2017. (link)

[nc9] L. Quéval, F. Trillaud, J.J. Pérez-Chavez, B. Douine, "Superconducting power filter for DC electrical grids," *Scientific workshop – Micro and Smart grid*, Champs-sur-Marne, France, Oct. 2017. ()

[nc8] L. Quéval, A. Coty, B. Hebert, L. Vido, B. Multon, "Moteur photovoltaïque, " *Matlab Expo 2017*, Paris, France, May 2017. (poster)

[nc7] P.-B. Zhou, G.-T. Ma, C. Yang, L. Quéval, G.-M. Mei, K. Liu, H.-Y. Qian, K. Liu, "Enhancement of the magnetic coupling using a superconductor-ferromagnet heterostructure from 1 to 10 kHz," *Colloque national métamatériaux (cnm2017)*, Orsay, France, 27-28 Mar. 2017. (poster, see [p7])

[nc6] L. Quéval, "Superconducting Maglev," *journées thématique du club EEA section électrotechnique*, Nancy, France, Mar. 2016. (see [p6])

[nc5] L. Quéval, A. Coty, L. Vido, R. Gottkehaskamp, B. Multon, "Moteur solaire : Système innovant pour le pompage d'eau en site isolé," *24ème colloque A. Bouyssy*, Orsay, France, Feb. 2016. (see [ic10, ic11, ic13])

[nc4] L. Quéval, H. Ohsaki, "abc-modeling of permanent magnet machines using N-D lookup tables: a finite element validation," *Symposium de génie électrique (SGE'2014)*, Cachan, France, Jul. 2014. (link)

[nc3] L. Quéval, H. Ohsaki, "LVRT capability of superconducting wind turbine generator," *2012 Annual Conference of I.E.E. of Japan, Industry Applications Society (JIASC2012)*, id. R3-1-3-2, Chiba, Japan, Aug. 2012.

[nc2] L. Quéval, M. Sekino, H. Ohsaki, "Modeling of grid-connected superconducting synchronous machines," *85th Conference of the Cryogenics and Superconductivity Society of Japan (CSJ85)*, id. 2P-p09, p. 126, Kanazawa, Japan, Nov. 2011.

[nc1] L. Quéval, M. Sekino, H. Ohsaki, "A phase-domain model for superconducting synchronous machines," *84th Conference of the Cryogenics and Superconductivity Society of Japan (CSJ84)*, id. 2A-a03, p. 91, Tsukuba, Japan, May 2011.

9.4 Software

[s1] L. Quéval, "BSmag toolbox user manual," Tech. report, Dept. Elect. Eng., University of Applied Sciences Düsseldorf, Germany, Apr. 2015. (code)

9.5 Others

[o4] L. Quéval, L. Vido, C. Berriaud, "EolSupra20, current status and perspectives," *Technical report*, GeePs, Université Paris-Saclay, Jul. 2021. (link)

[o3] H. Cai, L. Quéval, M. Hennebel, C. Gisbert, M. Petitet, "Long-term unit commitment problem with optimal zone configuration: a case study in Martinique," *Technical report*, GeePs, Université

Paris-Saclay, Nov. 2020. (link, data)

[o2] "Solar pumping workshop 2020 – Program," *Solar pumping workshop*, Gif-sur-Yvette, France, Dec. 2020. (link)

[o1] "Solar pumping workshop 2018 – Programme," *Solar pumping workshop*, Gif-sur-Yvette, France, Sep. 2018. (link)

Bibliography

[1] IPCC, 2022: Climate Change 2022: Impacts, Adaptation, and Vulnerability. Contribution of Working Group II to the Sixth Assessment Report of the Intergovernmental Panel on Climate Change [H.-O. Pörtner, D.C. Roberts, M. Tignor, E.S. Poloczanska, K. Mintenbeck, A. Alegría, M. Craig, S. Langsdorf, S. Löschke, V. Möller, A. Okem, B. Rama (eds.)]. Cambridge University Press. In Press.

[2] European Commission, "2030 climate & energy framework". Available at: https://ec.europa.eu/clima/eu-action/climate-strategies-targets/2030-climate-energy-framework_en (Accessed 2022/08).

[3] R. Belu, *Energy Storage, grid Integration, energy Economics, and the environment*, CRC PRess, 2020.

[4] M. Ertz, S. Leblanc-Proulx, E. Sarigollu, V. Morin, "Made to break? A taxonomy of business models on product lifetime extension" *Journal of Cleaner Production*, vol. 234, pp. 867–880, Oct. 2019.

[5] J. Foster, L. Wager, A.Bratanova, "LCOE models: a comparison of the theoretical frameworks and key assumptions," technical report, 2014. Available at: www.researchgate.net/publication/264311516_LCOE_models_A_comparison_of_the_theoretical_frameworks_and_key_assumptions (Accessed 2020/05).

[6] J. Aldersey-Williams, T. Rubert, "Levelised cost of energy – A theoretical justification and critical assessment," *Energy Policy*, vol. 124, pp. 169-179, 2019.

[7] S. Blumsack, "Project decision metrics: levelized cost of energy (LCOE)," lecture notes, EME 801: Energy Markets, Policy, and Regulation, PennState University. Available at: www.e-education.psu.edu/eme801/node/560 (Accessed 2020/05).

[8] W. Kenton, "Understanding Revenue," Investopedia, Jul. 2019. Available at: www.investopedia.com/terms/r/revenue.asp (Accessed 2020/05).

[9] . IEA, "Are renewable heating options cost-competitive with fossil fuels in the residential sector?," 2021. Available at: https://www.iea.org/articles/are-renewable-heating-options-cost-competitive-with-fossil-fuels-in-the-residential-sector (Accessed 2022/09).

[10] Life Cycle Initiative, "Glossary of Life Cycle Terms". Available at: https://www.lifecycleinitiative.org/resources/life-cycle-terminology-2/ (Accessed 2022/09).

[11] I. Arzoumanidis, *et al.*, "Functional unit definition criteria in life cycle assessment and social life cycle assessment: a discussion," *Perspectives on social LCA*, Springer, Cham, pp. 1-10, 2020.

[12] L. Giacomella, "Techno-Economic Assessment (TEA) and Life Cycle Costing Analysis (LCCA): discussing methodological steps and integrability," *Insights into Regional Development*, Entrepreneurship and Sustainability Center, vol. 3, no. 2, pp.176 - 197, 2021.

[13] T. Langhorst, *et al.* "Techno-Economic Assessment & Life Cycle Assessment Guidelines for CO2 Utilization (Version 2.0)," Global CO2 Initiative, 2022.

[14] G. Thomassen, *et al.* "How to assess the potential of emerging green technologies? Towards a prospective environmental and techno-economic assessment framework," *Green Chemistry*, vol. 21, no. 18, pp. 4868-4886, 2019.

[15] AssessCCUS - Techno-Economic and Life Cycle Assessment for Carbon Capture, Utilization, and Storage, "Glossaries". Available at: https://assessccus.globalco2initiative.org/glossaries/ (Accessed 2022/09).

[16] O. Schmidt, *et al.*, "Projecting the future levelized cost of electricity storage technologies." *Joule*, vol. 3, no. 1, pp. 81-100, 2019.

[17] V. Jülch, "Comparison of electricity storage options using levelized cost of storage (LCOS) method." *Applied energy*, vol. 183, pp. 1594-1606, 2016.

[18] Fuel Cells and Hydrogen Observatory, "Levelised Cost of Hydrogen". Available at: https://www.fchobservatory.eu/observatory/technology-and-market/levelised-cost-of-hydrogen-grid-connected-electrolysis (Accessed 2022/09).

[19] G. Allan, M. Gilmartin, P. McGregor, K. Swales, "Levelised costs of wave and tidal energy in the UK. Cost competitiveness and the importance of 'banded' Renewables Obligation Certificates," *Energy Policy*, vol. 39, no. 1, pp. 23–39, 2011.

[20] P.L. Joskow, "Comparing the costs of intermittent and dispatchable electricity generating technologies," EUI Working Paper RSCAS 45, 2011.

[21] C S. Lai, M.D. McCulloch, "Levelized cost of energy for PV and grid scale energy storage systems," Computing Research Repository, 2016. Accessible Online at http://arxiv.org/abs/1609.06000.

[22] Z. Liu, W. Zhang, C. Zhao, J. Yuan, "The economics of wind power in china and policy implications," *Energies*, vol. 8, no. 2, pp. 1529–1546, 2015.

[23] A. Orioli, A. Di Gangi, "The recent change in the Italian policies for photovoltaics. Effects on the pay-back period and levelized cost of electricity of grid-connected photovoltaic systems installed in urban contexts," *Energy*, vol. 93, pp. 1989–2005, 2015.

[24] G. Díaz, J. Gómez-Aleixandre, J. Coto, "Dynamic evaluation of the levelized cost of wind power generation," *Energy Conversion and Management*, vol. 101, pp. 721–729, 2015.

[25] R. Tidball, J. Bluestein, N. Rodriguez, S. Knoke, "Cost and performance assumptions for modeling electricity generation technologies," National Renewable Energy Laboratory, 2010. Accessible Online at https://www.nrel.gov/docs/fy11osti/48595.pdf, checked last on 26.09.2017.

[26] A. Myhr, C. Bjerkseter, A. Ågotnes, T.A. Nygaard, "Levelised cost of energy for offshore floating wind turbines in a life cycle perspective," *Renewable Energy*, vol. 66, pp. 714–728, 2014.

[27] K. Branker, M.J.M. Pathak, J.M. Pearce, "A review of solar photovoltaic levelized cost of electricity," *Renewable and Sustainable Energy Reviews*, vol. 15, no. 9, pp. 4470–4482, 2011.

[28] X. Ouyang, B. Lin, "Levelized cost of electricity (LCOE) of renewable energies and required subsidies in China," *Energy Policy*, vol. 70, pp. 64–73, 2014.

[29] International Renewable Energy Agency, "Floating foundations: A game changer for offshore wind power," technical report, 2016.

[30] K. Surana, S.M. Jordaan, "The climate mitigation opportunity behind global power transmission and distribution," *Nature Climate Change*, vol. 9, pp. 660–665, 2019.

[31] CIGRE B4, "Guide for the Development of Models for HVDC Converters in a HVDC Grid," Technical brochure, no. 604, 2014.

[32] D. Westermann, A. Kuester, D. van Hertem, D. Soerangr, G. Real, G. Asplund, M. Meisingset, M. Takasaki, T. Rauhala, B. Kloeckl, M. Kurra, B. Deppe, M. Bennett, R. Atmuri, K. Friedrich, "Voltage source converter (VSC) HVDC for power transmission - Economic aspects and comparison with other AC and DC technologies," Cigre Workgroup B4.46, no. 492, 2012.

[33] P. Wheeler, A. Watson, J. Clare, E. Amankwah, R. Feldman, "Power electronic converters for HVDC renewable energy applications," *2015 CHILEAN Conference on Electrical, Electronics Engineering, Information and Communication Technologies (CHILECON)*, pp. 425-428, Santiago, Chile, 2015.

[34] H.S. Mohamed Ramadan, "Non-linear control and stabilization of VSC-HVDC transmission systems," PhD thesis, University Paris Sud - Paris XI, France, 2012.

[35] M. Petit, S. Bacha, X. Guillaud, H. Morel, D. Planson, B. Raison, "Les réseaux HVDC multi-terminaux : des défis multiples en génie électrique," *Symposium de Génie Electrique 2014 (SGE2014)*, Cachan, France, Jul 2014.

[36] E. Koldby, M. Hyttinen, "Challenges on the road to an offshore HVDC grid," *Nordic Wind Power Conf. 2009 (NWPC2009)*, Bornholm, Denmark, Sept. 2009.

[37] G. Asplund, K. Lindén, C. Barker, A. Marzin, U. Baur, N. Pahalawaththa, J. Beerten, M. Rashwan, P. Christensen, J. Rittiger, S. Cole, K. Sogaard, D. van Hertem, D. Westermann, W. Jialiang, E.-D. Wilkening, D. Jovcic, C. Yue, P. Labra, "HVDC grid feasibility study," Cigre Workgroup B4.52, no. 533, Apr. 2013.

[38] J.L. Thomas, M. Boyra, G. Bergna, "Les technologies de liaisons à courant continu pour l'interconnexion des réseaux électriques du pourtour méditerranéen: Le rêve de Thomas Edison se réalise...," *Revue de l'électricité et de l'électronique*, no. 5, pp. 38-57, 2011.

[39] P. Kundur, *Power System Stability and Control*, 6 ed., McGraw-Hill, 1994.

[40] H. Saad, J. Peralta, S. Dennetiere, J. Mahseredjian, J. Jatskevich, J.A. Martinez, A. Davoudi, M. Saeedifard, V. Sood, X. Wang, J. Cano, A. Mehrizi-Sani, "Dynamic averaged and simplified models for MMC-based HVDC transmission systems," *IEEE Trans. on Power Delivery*, vol. 28, no. 3, pp. 1723-1730, 2013.

[41] C.E. Spallarossa, T.C. Green, C. Lin, X. Wu, "A DC voltage control strategy for MMC MTDC grids incorporating multiple master stations," *2014 IEEE PES T&D Conf. and Exp.*, pp. 1-5, Chicago, IL, USA, 2014.

[42] N.M. Kirby, M.J. Luckett, L. Xu, W. Siepmann, "HVDC transmission for large offshore windfarms," *7th Intl. Conf. on AC-DC Power Transmission*, pp. 162-168, London, UK, 2001.

[43] N. Stankovic, G. Bergna, A. Arzandé, E. Berne, P. Egret, J.C. Vannier, "An optimization-based control strategy for modular multilevel converters: Design and implementation," *IEEE 11th Intl. Conf. on Power Electronics and Drive Systems (PEDS2015)*, pp. 12-17, Sydney, Australia, 2015.

[44] S. Akkari, J. Dai, M. Petit, X. Guillaud, "Coupling between the frequency droop and the voltage droop of an AC/DC converter in an MTDC system," *IEEE PowerTech*, pp. 1-6, Eindhoven, Netherlands, 2015.

[45] P. Rault, "Modélisation dynamique et commande des réseaux à courant continu multi-terminaux haute tension," PhD thesis, Ecole Centrale de Lille, France, 2014.

[46] P. Rault, X. Guillaud, F. Colas, S. Nguefeu, "Investigation on interactions between AC and DC grids," *IEEE PowerTech*, Grenoble, France, pp. 1-6, 2013.

[47] H.A. Saad, "Modélisation et simulation d'une liaison HVDC de type VSC-MMC," PhD thesis, University of Montreal, Canada, 2015.

[48] M.S. Baazzim, M.S. Al-Saud, M.A. El-Kady, "Comparison of finite-element and IEC methods for cable thermal analysis under various operating environments," *International Journal of Electrical Computer, Energetic, Electronic and Communication Engineering*, vol 8, no 3, 2014.

[49] IEC, "Electric cables - Calculations for current ratings - Finite element method," Standard TR 62095:2003.

[50] G. Chen, M. Hao, Z.-Q. Xu, A. Vaughan, J.-Z. Cao, H.-T. Wang, "Review of high voltage direct current cables," *CSEE Journal of power and energy systems*, vol. 1, no. 2, Jun. 2015.

[51] CIGRE, "Guide for electromagnetic transient studies involving VSC converters," 2021. Available at: https://e-cigre.org/publication/832-guide-for-electromagnetic-transient-studies-involving-vsc-converters (Accessed 2021/12).

[52] Siemens, "HVDC PLUS Brochure," p.8. Available at: https://assets.siemens-energy.com/siemens/assets/api/uuid:9555eb71-7b92-40d3-99a1-20be282abc87/2021-09-23-hvdc-plus.pdf (Accessed 2021/09).

[53] N. Evans, P. Dworakowski, M. Al-Kharaz, S. Hegde, E. Perez, F. Morel, "Cost-performance framework for the assessment of modular multilevel converter in HVDC transmission applications," *45th Annual Conference of the IEEE Industrial Electronics Society (IECON 2019)*, pp. 4793-4798, Lisbon, Portugal, Oct. 2019.

[54] W.R.L. Garcia, A. Bertinato, P. Tixador, B. Raison, B. Luscan, "Full-selective protection strategy for MTDC grids based on R-type superconducting FCLs and mechanical DC circuit breakers," *5th IET International Conference on Renewable Power Generation (RPG 2016)*, pp. 1-7, Sep. 2016.

[55] P. Egrot, R. Coelho-Medeiros, "Convertisseur alternatif-continu de type MMC," patent FR 3110304, May 2020.

[56] P. Egrot, R. Coelho-Medeiros, "Convertisseur alternatif-continu de type MMC," patent FR 2004974, May 2020.

[57] K. Sharifabadi, L. Harnefors, H.-P. Nee, S. Norrga, R. Teodorescu, *Design, control, and application of modular multilevel converters for HVDC transmission systems*, John Wiley & Sons, pp. 60-132, 2016.

[58] D. Caverly, K. Pointner, R. Presta, P. Griebler, H. Reisinger, O. Haslehner, "Air core reactors: magnetic clearances, electrical connection and grounding of their supports," *Minnesota Power Systems Conference (MIPSYCON)*, Nov. 2017.

[59] W.R.L. Garcia, P. Tixador, B. Raison, A. Bertinato, B. Luscan, C. Creusot, "Technical and economic analysis of the R-type SFCL for HVDC grids protection," *IEEE Transactions on Applied Superconductivity*, vol. 27, no. 7, pp. 1-9, Oct. 2017.

[60] M. W. Rupich, "4 - Second-Generation (2G) Coated High-Temperature Superconducting Cables and Wires for Power Grid Applications," In: Superconductors in the Power Grid. Ed. by C. Rey. Woodhead Publishing Series in Energy. Woodhead Publishing, pp. 97–1, 2015.

[61] J. Kozak, M. Majka, T. Janowski, S. Kozak, G. Wojtasiewicz, B. Kondratowicz-Kucewicz. "Tests and performance analysis of coreless inductive HTS fault current limiters," *IEEE Transactions on Applied Superconductivity*, vol. 21, no. 3, pp. 1303–1306, Jun. 2011.

[62] Y.-H. Kim *et al.*, "The application of the cryogenic system on the HTS power cable circuit in actual grid," *Cryogenics*, vol. 52, no. 12, pp. 661–666, Dec. 2012.

[63] G.B. Diaz, "Modular multilevel converter control for HVDC operation: Optimal shaping of the circulating current signal for internal energy regulation," PhD thesis, CentraleSupélec & Norwegian University of Science and Technology (Trondheim, Norvège), July 2015.

[64] N. Stanković, M.J. Jiménez Carrizosa, A. Arzandé, P. Egrot, J.-C. Vannier, "An HVDC experimental platform with MMC and two-level VSC in the back-to-back configuration," *2016 IEEE 25th International Symposium on Industrial Electronics (ISIE)*, pp. 436–441, Jun. 2016.

[65] McGraw-Hill Dictionary of Scientific & Technical Terms, 6E, 2003 by The McGraw-Hill Companies, Inc.

[66] P. Tixador, "Development of superconducting power devices in Europe." *Physica C: Superconductivity and its applications*, vol. 470, no. 20, pp. 971-979, 2010.

[67] A. Hobl, *et al.*, "Superconducting fault current limiters: A new tool for the 'grid of the future'," *CIRED 2012 Workshop: Integration of Renewables into the Distribution Grid*, p. 296, Lisbon, Portugal, May 2012.

[68] H.-P. Kraemer, *et al.*, "Superconducting fault current limiter for transmission voltage." *Physics Procedia*, vol. 36, pp. 921-926, 2012.

[69] M. Moyzykh, *et al.*, "First Russian 220 kV superconducting fault current limiter (SFCL) for application in city grid," *IEEE Transactions on Applied Superconductivity*, vol. 31, no. 5, pp. 1-7, 2021.

[70] J. Rebled Lluch, "Power transmission systems for offshore wind farms: Technical-economic analysis," Bachelor thesis, Universitat Politecnica de Catalunya - BarcelonaTech (UPC), Spain, Jul. 2015.

[71] D. Kottonau *et al.*, *Bewertung des einsatzes supraleitender 380-kV-Kabel*, vol. 26. KIT Scientific Publishing, 2019.

[72] F. Noack, "Zur Bewertung der 380 kV -Steiermark- Leitung aus energietechnischer Sicht," Tech. report, Technische Universität Ilmenau, Germany, 2005. (in German)

[73] HVAC single core copper conductor, XLPE insulated, copper wire screen and HDPE sheath cable, (Elsewedy Electric, Egypt, Cat. # CX8-TX01-K85). Available at: https://www.elsewedyelectric.com/media/1067/power-cables-catalogue.pdf (Accessed 2022/07).

[74] Kassø-Tjele high-voltage transmission line, (Wikipedia). Available at: https://en.wikipedia.org/wiki/Kass%C3%B8-Tjele_high-voltage_transmission_line (Accessed 2022/07).

[75] J. Cho, J.-H. Bae, H.-J. Kim, K.-D. Sim, S. Kim, H.-M. Jang, C.-Y. Lee, D.-W. Kim, "Development of a single-phase 30m HTS power cable," *Cryogenics*, vol. 46, no. 5, pp. 333-337, 2006.

[76] G. Venkataramanan, B. K. Johnson, "A superconducting DC transmission system based on VSC transmission technologies," *IEEE Trans. on Applied Superconductivity*, vol. 13, no. 2, pp. 1922–1925, Jun. 2003.

[77] L. Graber, J.G. Kim, C.H. Kim, S.V. Pamidi, "Thermal network model for HTS cable systems and components cooled by helium gas," *IEEE Trans. on Applied Superconductivity*, vol. 26, no. 4, id. 4803805, Jun. 2016.

[78] D.I. Doukas, Z.D. Blatsi, A.N. Milioudis, D.P. Labridis, L. Harnefors, G. Velotto, "Damping of electromagnetic transients in a superconducting VSC transmission system," *IEEE Eindhoven Power Tech*, pp. 1–6, Jun. 2015.

[79] B. Yang, J. Kang, S. Lee, C. Choi, Y. Moon, "Qualification test of a 80 kV 500 MW HTS DC cable for applying into real grid," *IEEE Trans. on Applied Superconductivity*, vol. 25, no. 3, id. 5402705, Jun. 2015.

[80] M. Hamabe, H. Watanabe, J. Sun, N. Yamamoto, T. Kawahara, S. Yamaguchi, "Status of a 200-meter DC superconducting power transmission cable after cooling cycles," *IEEE Trans. on Applied Superconductivity*, vol. 23, no. 3, id. 5400204, Jun. 2013.

[81] D. Zhang *et al.*, "Testing results for the cable core of a 360 m/10 kA HTS DC power cable used in the electrolytic aluminum industry," *IEEE Trans. on Applied Superconductivity*, vol. 23, no. 3, id. 5400504, Jun. 2013.

[82] J.H. Lim *et al.*, "Cryogenic system for 80-kV DC HTS cable in the KEPCO power grid," *IEEE Trans. on Applied Superconductivity*, vol. 25, no. 3, id. 5402804, Jun. 2015.

[83] V.E. Sytnikov *et al.*, "HTS DC cable line project: On-going activities in Russia," *IEEE Trans. on Applied Superconductivity*, vol. 23, no. 3, id. 5401904, Jun. 2013.

[84] M. Stemmle, K. Allweins, F. Merschel, T. Kugel, F. Herzog, T. Kutz, J.M. Saugrain, "Three years operation experience of the ampacity system installation in essen Germany," *13th European Conference on Applied Superconductivity (EUCAS2017)*, id. 3LO4-05, Geneva, Switzerland, Sep. 2017.

[85] CIGRE B1, "Recommendations for testing of superconducting cables," Technical brochure, no. 538, June 2013.

[86] IEC "HTS-AC power cables and their accessories - Test methods and requirements," Standard IEC 63075:2019.

[87] T. Matsushita *et al.*, "Japanese project of standardization of DC critical current test method of superconducting cables," *14th European Conference on Applied Superconductivity (EUCAS2019)*, id. 1-LP-PC-I05, Glasgow, UK, Sept. 2019.

[88] A. Marian, C.-E. Bruzek, "Advancing superconducting links for very high power transmission," White paper Best Paths Project, 2018.

[89] M. Noe, "EUCAS short course on power applications: superconducting cables", *13th European Conference on Applied Superconductivity (EUCAS2017)*, Geneva, Switzerland, Sep. 2017.

[90] T.Jacob, A. Buchholz, M. Noe, M. Weil, "Comparative life cycle assessment of different cooling systems for high-temperature superconducting power cables," *IEEE Transactions on Applied Superconductivity*, vol. 32, no. 4, pp. 1-5, 2022.

[91] J.P. Stovall, J.A. Demko, "Installation and operation of the southwire 30-meter HTS power cable," *IEEE Transactions on Applied Superconductivity*, vol 1, no.1, pp. 2467-2472, 2011.

[92] D. Willen, F. Hansen, "First operation experiences from a 30 kV, 104 MVA HTS power cable in a utility substation," *Physica C: Superconductivity*, vol. 372 pp. 1571-1579, 2002.

[93] M. Tonnensen, "Operation experiences with a 30 kV/100 MVA HTS cable system," *Superconductor Science and Technology*, 2004.

[94] Y. Xin, B. Hou, "China's 30 m 35 kV/2 kA AC HTS power cable project," *Superconductor Science and Technology*, vol 17. pp 332-335.

[95] J.A. Demko, R.C. Duckworth, "Testing of a liquid nitrogen-cooled 5-meter, 3000 A tri-axial HTS cable system," *AIP Conference*, 2006.

[96] D. Linsday, M. Roden, "Operating experience of 13.2 kV superconducting cable system at AEP bixby station," CIGRE, 2008.

[97] H. Yumura, Y. Ashibe, "Phase II of the Albany HTS cable project," *IEEE Transactions on Applied Superconductivity*, pp. 1698-1701, 2009.

[98] F. Schmidt, J. Maguire, "Operation, experience and further development of an HTS power cable in the Long Island Power Authority grid," *J. Physics Procedia, Superconductivity Centennial Conference*, vol 36, pp. 1137-1144, 2012.

[99] S. Sohn, H. Yang, "Installation and power grid demonstration of a 22.9 kV, 50 MVA HTS cable for KEPCO," *IEEE Transactions on Applied Superconductivity*, 2012.

[100] R. Cheolhwi, J. Hyunman, "Current status of demonstration and commercialization of HTS cable system grid in Korea," *IEEE International Conference on Applied Superconductivity and Electromagnetic Devices*, id. 3231, Beijing, 2013.

[101] J.F. Maguire, J. Yuan, "Progress and status of a 2G HTS power cable to be installed in the Long Island Power Authority (LIPA)", *IEEE Transactions on Applied Superconductivity*, vol. 21, no. 3, pp 961-966. 2011.

[102] H. Hiroyasu, Y. Ashibe, "Update of Yokohama HTS cable project," *IEEE Transactions on Applied Superconductivity*, 2013.

[103] "AmpaCity – Installation of advanced Superconducting 10 kV system in city center replaces conventional 110 kV cables," *IEEE International Conference on Applied Superconductivity and Electromagnetic Devices*, Beijing, 2013.

[104] L. Geon, B. Su, "Condition monitoring of 154 kV cable systems via temporal sliding LSTM networks," *IEEE Transactions on Applied Superconductivity*, 2020.

[105] M. Cupelli, F. Ponci, G. Sulligoi, A. Vicenzutti, CS. Edrington, T. El-Mezyani, A. Monti, "Power flow control and network stability in an all-electric ship," *Proceedings of the IEEE*, vol. 103, no. 12, pp. 2355-2380, Dec. 2015.

[106] R.W. Erickson, "Optimal single resistor damping of input filters," *Applied Power Electronics Conf. (APEC)*, pp. 1073-1079, Dallas, Texas, USA, March 1999.

[107] WindEurope, "Offshore Wind in Europe, Key trends and statistics 2019," Feb. 2020. Available at: https://windeurope.org/about-wind/statistics/offshore/european-offshore-wind-industry-key-trends-statistics-2019/ (Accessed 2022/09).

[108] WindEurope, "Offshore Wind in Europe, Key trends and statistics 2020," Feb. 2021. Available at: https://windeurope.org/intelligence-platform/product/offshore-wind-in-europe-key-trends-and-statistics-2020/ (Accessed 2022/09).

[109] IEA, "Renewables 2021," 2021. Available at: https://www.iea.org/reports/renewables-2021 (Accessed 2022/09).

[110] European commission, "2050 long-term strategy". Available at: https://ec.europa.eu/clima/eu-action/climate-strategies-targets/2050-long-term-strategy_en (Accessed 2022/03).

[111] UpWind, "Design limits and solutions for very large wind turbines," 2011.

[112] INNWIND.EU, "LCOE reduction for the next generation offshore wind turbines," *technical report*, 2017.

[113] J. Puigcorbe, A. De-Beaumont, "Wind turbine gearbox reliability: the impact of rotor support," *Renewable Energy World Magazine*, 2010.

[114] M. Liserre, R. Cardenas, M. Molinas, J. Rodriguez, "Overview of multi-MW wind turbines and wind parks," *IEEE Trans. on Industrial Electronics*, vol. 58, no. 4, pp. 1081-1095, 2011.

[115] M. Popescu, M.V. Cistelecan, L. Melcescu, M. Covrig, "Low speed directly driven permanent magnet synchronous generators for wind energy applications," *2007 International Conference on Clean Electrical Power*, pp. 784–788, May 2007.

[116] H. Chen, R. Qu, J. Li, B. Zhao, "Comparison of interior and surface permanent magnet machines with fractional slot concentrated windings for direct-drive wind generators," *2014 17th International Conference on Electrical Machines and Systems (ICEMS)*, pp. 2612–2617, Oct 2014.

[117] A. McDonald, N.A. Bhuiyan, "On the optimization of generators for offshore direct drive wind turbines," *IEEE Transactions on Energy Conversion*, vol. 32, no. 1, pp. 348–358, March 2017.

[118] L. Frosini, M. Pastura, "Analysis and design of innovative magnetic wedges for high efficienc ypermanen tmagne tsynchronou smachines," *Energies*, vol. 13, no. 1, 2020.

[119] N. Maki, T. Takao, S. Fuchino, H. Hiwasa, M. Hirakawa, K. Okumura, M. Asada, R. Takahashi, "Study of practical applications of HTS synchronous machines," *IEEE Trans. on Applied Superconductivity*, vol. 15, no. 2, pp. 2166-2169, 2005.

[120] C. Lewis, J. Muller, "A direct drive wind turbine HTS generator," *IEEE Power Engineering Society General Meeting*, pp. 1-8, Jun. 2007.

[121] A.B. Abrahamsen, N. Mijatovic, E. Seiler, T. Zirngibl, C. Traeholt, P.B. Norgard, N.F. Pederson, N.H.Andersen, J. Ostergard, "Superconducting wind turbine generators," *Superconductor Science and Technology*, vol. 23, no. 3, pp. 1–8, 2010.

[122] S.S. Kalsi, K. Weeber, H. Takesue, C. Lewis, H.W. Neumueller, R.D. Blaugher, "Development status of rotating machines employing superconducting field windings," *Proc. IEEE*, vol. 92, p. 1688, 2004.

[123] Y. Terao, M. Sekino, H. Ohsaki, "Comparison of conventional and superconducting generator concepts for offshore wind turbines," *IEEE Trans. on Applied Superconductivity*, vol. 23, no. 3, pp. 52009+4, 2013.

[124] L. Quéval, "Modeling and simulation of grid-connected superconducting wind turbine generators," PhD thesis, The University of Tokyo, Tokyo, Japan, 2013. Online: www.lqueval.com

[125] S. Bendali, P. Letellier, J. Lévêque, G. Male, S. Mezani, D. Netter, "État de l'art des moteurs et générateurs supraconducteurs," *Journée des Jeunes Chercheurs en Génie électrique (JCGE 2013)*, Saint-Nazaire, France, Jun. 2013.

[126] M. Biasion, F.P. João Fernandes, P.J.d.C. Branco, S. Vaschetto, A. Cavagnino, A. Tenconi, "A comparison of cryogenic-cooled and superconducting electrical machines," *IEEE Energy Conversion Congress and Exposition (ECCE)*, pp. 4045-4052, 2021.

[127] A.B. Abrahamsen, N. Magnusson, D. Liu, E. Stehouwer, HB Hendriks, H. Polinder, "Design study of a 10 MW MgB2 superconductor direct drive wind turbine generator," *Proceedings of the EWEA Conference*, Barcelona, 2014.

[128] G. Sarmiento, S. Sanz, A. Pujana, J. María Merino, I. Marino, M. Tropeano, D. Nardelli, G. Grasso, "Design and testing of real scale MgB2 coils for Suprapower 10 MW wind generators," *12th European Conf. on Applied Superconductivity (EUCAS2015)*, Lyon, France, Sept. 2015.

[129] M. Shafiee, F. Brennan, I.A. Espinosa, "A parametric whole life cost model for offshore wind farms," *The International Journal of Life Cycle Assessment*, vol 21, pp. 961–975, 2016.

[130] Y. Terao, M. Sekino, H. Ohsaki, "Electromagnetic design of 10 MW class fully superconducting wind turbine generators," *IEEE Transactions on Applied Superconductivity*, vol. 22, no. 3, id. 5201904, June 2012.

[131] S. S. Kalsi, "Superconducting wind turbine generator employing MgB2 windings both on rotor and stator," *IEEE Transactions on Applied Superconductivity*, vol. 24, no. 1, pp. 47–53, Feb 2014.

[132] D. Liu, H. Polinder, A. B. Abrahamsen, J. A. Ferreira, "Topology comparison of superconducting generators for 10-MW direct-drive wind turbines: Cost of energy based," *IEEE Transactions on Applied Superconductivity*, vol. 27, no. 4, pp. 1–7, June 2017.

[133] Y. Guan, Z.Q. Zhu, G.J. Li, Z. Azar, A.S. Thomas, F. Vedreno-Santos, M. Odavic, "Influence of pole number and stator outer diameter on volume, weight, and cost of superconducting generators with iron-cored rotor topology for wind turbines," *IEEE Transactions on Applied Superconductivity*, vol. 27, no. 6, pp. 1–9, Sept 2017.

[134] C. Zhou, X. Huang, L. Wu, Y. Fang, "Comparison of electromagnetic performance of superconducting permanent magnet wind power generator with different topologies," *2018 IEEE International Conference on Applied Superconductivity and Electromagnetic Devices (ASEMD)*, pp. 1–2, 2018.

[135] X. Zhu, M. Cheng, "Design and analysis of 10 MW class HTS exciting double stator direct-drive wind generator with stationary seal," *IEEE Access*, vol. 7, pp. 51129–51139, 2019.

[136] M. Bauer, "Superconducting generators for wind power, EcoSwing generator and outlook," *COST ACTION 19108 Hi-Scale first joint WG3/4 industry-academia workshop on applications for HTS technologies in the electrical energy chain*, [online], Apr. 2021.

[137] S. Sung, W. Jung, "Economic competitiveness evaluation of the energy sources: comparison between a financial model and levelized cost of electricity analysis", *Energies*, vol. 12, no. 21, p. 4101, 2019.

[138] International Renewable Energy Agency (IRENA), "Renewable power generation costs in 2021," Technical report, 2021. Available at: www.irena.org/publications (Accessed 2021/09).

[139] Enercon, "WEC components - Constant innovation". Available at: www.enercon.de/en/technology/wec-components/ (Accessed 2020/07).

[140] R. Flüukiger, *MgB2 Superconducting Wires: Basics and Applications*, World Scientific, Singapore, 2016.

[141] L. Kopera *et al.*, "Critical currents of Rutherford MgB2 cables compacted by two-axial rolling," *Supercond. Sci. Technol.*, vol. 30, no. 1, pp. 5002, 2017.

[142] B.L.J. Gysen, K.J. Meessen, J.J.H. Paulides, E.A. Lomonova, "General formulation of the electromagnetic field distribution in machines and devices using fourier analysis," *IEEE Trans. on Magnetics*, vol. 46, no. 1, pp. 39-52, 2010.

[143] E. Devillers, J. Le Besnerais, T. Lubin, M. Hecquet, J.-P. Lecointe, "A review of subdomain modeling techniques in electrical machines: performances and applications," *22th Intl. Conf. Elec. Machines ICEM2016*, pp. 86-92, Lausanne, Switzerland, 2016.

[144] A. Hughes, T.J.E. Miller, "Analysis of fields and inductances in air-cored and iron-cored synchronous machines," *Proc. Inst. Elect. Eng.*, vol. 124, no. 2, pp. 121-126, 1977.

[145] T.J.E. Miller, A. Hughes, "Comparative design and performance analysis of air-cored and iron-cored synchronous machines," *Proc. Inst. Elect. Eng.*, vol. 124, no. 2, pp. 127–132, 1977.

[146] P. Elhaminia, M. Yazdanian, M.R. Zolghadri, M. Fardmanesh, "An analytical approach for optimal design of rotor iron for superconducting synchronous machine," *37th Annual Conf. IEEE Industrial Electronics Society IECON2011*, Melbourne, Australia, pp. 1741–1745, 2011.

[147] M. Yazdanian, P. Elhaminia, M.R. Zolghadri, M. Fardmanesh, "Analytical modeling of magnetic flux in superconducting synchronous machine," *IEEE Trans. on Applied Superconductivity*, vol. 23, no. 1, id. 5200406, 2013.

[148] W. Zhang, D. Xia, D. Zhang, G. Zhang, "Parameter design by a novel method and optimization of the field coil for a 500 kW air-gap HTS generator," *IEEE Trans. on Applied Superconductivity*, vol. 24, no. 3, id. 5201704, 2014.

[149] J.R. Bumby, *Superconducting Rotating Electrical Machines*. Oxford, U.K.: Clarendon, 1983.

[150] S. Safi, J. Bumby, "Analysis of magnetic fields in the slotted structure of a superconducting AC generator," *Proc. Inst. Elect. Eng.*, vol. 139, no. 5, pp. 411–422, 1992.

[151] Z. Djelloul-Khedda, K. Boughrara, F. Dubas, R. Ibtiouen, "Nonlinear analytical prediction of magnetic field and electromagnetic performances in switched reluctance machines," *IEEE Trans. on Magnetics*, vol. 53, no. 7, pp. 1-11, 2017.

[152] C. Hoffmann, D. Pooke, A.D. Caplin, "Flux Pump for HTS Magnets," *IEEE Trans. on Applied Superconductivity*, vol. 21, no. 3, pp. 1628-1631, Jun. 2011

[153] J. Volger, P.S. Admiraal, "A dynamo for generating a persistent current in a superconducting circuit," *Physics Letters*, vol. 2, no. 5, pp. 257-259, 1962.

[154] H. Van Beelen *et al.* "Flux pumps and superconducting solenoids," *Physica*, vol. 31, no. 4, pp. 413-443, 1965.

[155] Z.-M. Bai, G. Yan, C.-L. Wu, S.-F. Ding, C. Chen, "A novel high temperature superconducting magnetic flux pump for MRI magnets," *Cryogenics*, vol. 50, no. 10, pp. 688-692, 2010.

[156] C.W. Bumby *et al.*, "Development of a brushless HTS exciter for a 10 kW HTS synchronous generator," *Superconductor Science and Technology*, vol. 29, no. 2, pp. 4008, 2016.

[157] Z. Jiang, K. Hamilton, N. Amemiya, R.A. Badcock, C.W. Bumby, "Dynamic resistance of a high-Tc superconducting flux pump," *Applied Physics Letters*, vol. 105, no. 11, p. 112601, 2014.

[158] J. Geng, B. Shen, C. Li, H. Zhang, K. Matsuda, J. Li, X. Zhang, T.A. Coombs, "Voltage-ampere characteristics of YBCO coated conductor under inhomogeneous oscillating magnetic field," *Applied Physics Letters*, vol. 108, no. 26, p. 262601, 2016.

[159] J. Geng, K. Matsuda, L. Fu, J.F. Fagnard, H. Zhang, X. Zhang, B. Shen, Q. Dong, M. Baghdadi, T.A. Coombs, "Origin of dc voltage in type II superconducting flux pumps: field, field rate of change, and current density dependence of resistivity," *Journal of Physics D: Applied Physics*, vol. 49, no. 11, p.11LT01, 2016.

[160] C.W. Bumby, Z. Jiang, J.G. Storey, A.E. Pantoja, R.A. Badcock, "Anomalous open-circuit voltage from a high-Tc superconducting dynamo," *Applied Physics Letters*, vol. 108, no. 12, p.122601, 2016.

[161] A.M. Campbell, "A finite element calculation of flux pumping," *Superconductor Science and Technology*, vol. 30, no. 12, p. 125015, 2017.

[162] W. Wang, T.A. Coombs, "Macroscopic magnetic coupling effect: The physical origination of a high-temperature superconducting flux pump," *Physical Review Applied*, vol. 9, no. 4, p. 044022, 2018

[163] I. Giaever, "A dc transformer," *IEEE spectrum*, vol. 3, no. 9, pp. 117-122, 1966.

[164] V. Kaplunenko, S. Moskvin, V. Schmidt Fiz. Nizk. Temp. 11 846, 1985. Available at: https://fnte.ilt.kharkov.ua/fnt/pdf/11/11-8/f11-0846r.pdf (Accessed 2022/08).

[165] L.J.M. Van de Klundert, H.H. ten Kate, "Fully superconducting rectifiers and fluxpumps Part 1: Realized methods for pumping flux," *Cryogenics*, vol. 21, no. 4, pp. 195-206, 1981.

[166] R.C. Mataira, M.D. Ainslie, R.A. Badcock, C.W. Bumby, "Origin of the DC output voltage from a high-Tc superconducting dynamo," *Applied Physics Letters*, vol. 114, no. 16, p.162601, 2019.

[167] V.S. Vysotsky, V.R. Karasik, E.V. Pechen, P.N. Lebedev, N.V. Markovsky, O.A. Shevchenko, "The possibility of using high-Tc superconducting films as elements of a rectifier," *Superconductor Science and Technology*, vol. 3, no. 5, p.259, 1990.

[168] A. Ghabeli, E. Pardo, "Modeling of airgap influence on DC voltage generation in a dynamo-type flux pump," *Superconductor Science and Technology*, vol. 33, no. 3, p. 035008, 2020.

[169] R. Mataira, M.D. Ainslie, R. Badcock, C.W. Bumby, "Modeling of stator versus magnet width effects in high-T_c superconducting dynamos," *IEEE Trans. on Applied Superconductivity*, vol. 30, no. 4, pp.1-6, 2020.

[170] V.M.R. Zermeno, F. Grilli, F. Sirois, "A full 3D time-dependent electromagnetic model for Roebel cables," *Supercond. Sci. Technol.*, vol. 26, no. 05, pp. 2001, 2013.

[171] BVG associates, "Offshore wind cost reduction pathways - Technology workstream," Technical report, 2012.

[172] I.U. Haq, Q. Khan, I. Khan, R. Akmeliawati, K.S. Nisar, I. Khan, "Maximum power extraction strategy for variable speed wind turbine system via neuro-adaptive generalized global sliding mode controller," *IEEE Access*, vol. 8, pp. 128536–128547, 2020.

[173] T.A.M. Shafiee, "A economic assessment framework for decommissining of offshore wind farms using a cost breakdown structure," *The International Journal of Life Cycle Assessment*, vol. 26, pp. 344–370, Jan. 2021.

[174] H. Li, Z. Chen, H. Polinder, "Optimization of multibrid permanent-magnet wind generator systems," *IEEE Transactions on Energy Conversion*, vol. 24, no. 1, pp. 82–92, Mar. 2009.

[175] H. Polinder, F.F.A. van der Pijl, G.-J. de Vilder, P.J. Tavner, "Comparison of direct-drive and geared generator concepts for wind turbines," *IEEE Transactions on Energy Conversion*, vol. 21, no. 3, pp. 725-733, Sept. 2006.

[176] L. Sethuraman, M. Maness, K. Dykes, "Optimized generator designs for the DTU 10-MW offshore wind turbine using generator SE," National Renewable Energy Laboratory, Tech. Rep., Jan. 2017.

[177] G. Shrestha, H. Polinder, J. A. Ferreira, "Scaling laws for direct drive generators in wind turbines," *2009 IEEE International Electric Machines and Drives Conference*, pp. 797-803, 2009.

[178] R. Gasch, J. Twele, "Scaling wind turbines and rules of similarity," Wind Power Plants, pp. 257-271. Springer, Berlin, Heidelberg, 2012.

[179] A. Penzkofer, K. Atallah, "Scaling of pseudo direct drives for wind turbine application," *IEEE Transactions on Magnetics*, vol. 52, no. 7, pp. 1-5, id. 8700205, July 2016.

[180] J.F. Manwell, J.G. Mcgowan, A.L. Rogers, *Wind energy explained*, John Wiley & Sons, Ltd, 2010.

[181] L. Ziegler, E. Gonzalez, T. Rubert, U. Smolka, J.J. Melero, "Lifetime extension of onshore wind turbines: A review covering Germany, Spain, Denmark, and the UK," *Renewable and Sustainable Energy Reviews*, vol. 82, pp. 1261–1271, 2018.

[182] G. Abeynayake, T. Van Acker, D.V. Hertem, J. Liang, "Analytical model for availability assessment of large-scale offshore wind farms including their collector system," *IEEE Transactions on Sustainable Energy*, vol. 12, no. 4, pp. 1974–1983, 2021.

[183] S.S. Chandel, M.N. Naik, R. Chandel, "Review of performance studies of direct coupled photovoltaic water pumping systems and case study," *Renew. Sustain. Energy Rev.*, vol. 76, pp. 163–175, 2017.

[184] F. Carlevaro, C. Gonzalez, *Costing improved water supply systems for low-income communities: A practical manual*, 1 st ed, IWA Publishing, 2015.

[185] WaterAid, "Handpumps Technical Brief," 2013. Available at: https://washmatters.wateraid.org/sites/g/files/jkxoof256/files/technical-brief-handpumps_1.pdf (Accessed 2018/10).

[186] G.F. White, D.J. Bradley, A.U. White, "Drawers of water: Domestic water use in East Africa," *Bulletin World Health Organization*, vol. 80, no. 1, pp. 63-73, 1972.

[187] J. Ntouda, F. Sikodf, M. Ibrahim, I. Abba, "Access to drinking water and health of populations in Sub-Saharan Africa," *Comptes Rendus Biologies*, vol. 336, no. 5–6, pp. 305–309, 2013.

[188] Agence Française de Développement (AFD) and Programme Solidarité Eau, "Réalisation et gestion des forages équipés d'une pompe à motricité humaine en Afrique subsaharienne", 2011. Available at: https://www.pseau.org/outils/ouvrages/afd_realisation_et_gestion_des_forages_equipes_d_une_pompe_a_motricite_humaine_en_afrique_subsaharienne_2011.pdf (Accessed 2018/10).

[189] J. Bartram, S. Cairncross, "Hygiene, sanitation, and water: forgotten foundations of Health", *PLoS Med*, vol. 7, no. 11, 2010.

[190] World health organization (WHO) and United Nations Children's Fund (UNICEF), "Progress on Sanitation and Drinking Water - Joint Monitoring Programme on Water Supply and Sanitation," 2010, [Online]. Available at: http://www.who.int/water_sanitation_health/monitoring/9789241563956/en/ (Accessed 2018/10).

[191] A.M. MacDonald, H.C. Bonsor, B.E.O. Dochartaigh, R.G. Taylor, "Quantitative maps of groundwater resources in Africa", *Environmental Research Letters*, vol. 7, no. 2, 2012

[192] S. Cairncross, V. Valdmanis, *Disease Control Priorities in Developing Countries*, Chap. 41 Water supply, sanitation and hygiene promotion, 2nd ed, New York: Oxford University Press, 2006.

[193] J. Smet, C. van Wijk, "Small community water supplies," *Technical Paper Series 40 - IRC International Water and Sanitation Centre*, 2002.

[194] H. Ritchie, M. Roser, "Water use and sanitation," 2015. Available at: https://ourworldindata.org/water-use-sanitation (Accessed 2018/10).

[195] World Bank, "Access to electricity, rural (% of rural population)," 2016. Available at: https://data.worldbank.org/indicator/EG.ELC.ACCS.RU.ZS (Accessed 2018/12).

[196] W. Ratterman, J. Cohen, A. Garwood, "Green Empowerment Solar Pumping Systems (SPS) Introductory and Feasibility Guide," 2003. Available at: https://sswm.info/sites/default/files/reference_attachments/RATTERMAN%20et%20al%202003%20Solar%20Pumping%20Systems.pdf (Accessed 2018/12).

[197] S.S. Chandel, M. Nagaraju Naik, R. Chandel, "Review of solar photovoltaic water pumping system technology for irrigation and community drinking water supplies," *Renewable and Sustainable Energy Reviews*, vol. 49, pp. 1084–1099, 2015.

[198] R. Foster, A. Cota, "Solar water pumping advances and comparative economics," *Energy Procedia*, vol. 57, pp. 1431–1436, 2014.

[199] R. Parajuli, G.R. Pokharel, P.A. Ostergaard, "A comparison of diesel, biodiesel and solar PV-based water pumping systems in the context of rural Nepal," *International Journal of Sustainable Energy*, 2013.

[200] B. Singh, A.K. Mishra, R. Kumar, "Solar powered water pumping system employing switched reluctance motor drive", *IEEE Trans. on Industry Applications*, vol. 52, no. 5, pp. 3949-3957, 2016.

[201] M.I. Chergui, M.O. Benaissa, "Strategy photovoltaic pumping system in scattered area," *4th International Conference on Renewable Energy Research and Applications (ICRERA)*, pp. 283–286, Palermo, Italy, 2015.

[202] J.V. Mapurunga Caracas, G. De Carvalho Farias, L.F. Moreira Teixeira, L.A. De Souza Ribeiro, "Implementation of a high-efficiency, high-lifetime, and low-cost converter for an autonomous photovoltaic water pumping system," *IEEE Trans. on Industry Applications*, vol. 50, no. 1, pp. 631–641, 2014.

[203] S.K. Jha, "Application of solar photovoltaic system in Oman – Overview of technology, opportunities and challenges," *International Journal of Renewable Energy Research*, vol. 3, no. 2, pp. 331–340, 2013.

[204] R. Sen, S.C. Bhattacharyya, "Off-grid electricity generation with renewable energy technologies in India: An application of HOMER," *Renewable Energy*, vol. 62, pp. 388–398, 2014.

[205] A.M. Armanuos, A. Negm, A.H.M.H. El Tahan, "Life cycle assessment of diesel fuel and solar pumps in operation stage for rice cultivation in Tanta, Nile delta, Egypt," *Procedia Technology*, vol. 22, pp. 478–485, 2016.

[206] P.R. Mishra, R. Panguloori, N. Udupa, D. Mitra, "Economic evaluation of solar hybrid DC grid for petrol pump stations," *Annual IEEE India Conference (INDICON)*, 2013.

[207] Eau Fil du Soleil, "Gogma - Crowdfunding," 2017. Available at: https://www.kisskissbankbank.com/fr/projects/turning-sun-into-water/tabs/description (Accessed 2019/08).

[208] Eau Fil du Soleil, "Eau fil du soleil - website," 2019. Available at: https://eaufildusoleil.blogspot.com/ (Accessed 2019/08).

[209] DargaTech SARL, "DargaTech," 2019. Available at: https://www.facebook.com/dargatech/ (Accessed 2019/08).

[210] Grundfos, "Grundfos solar water supply systems," Technical brochure, 16 p., n.d. Available at: www.grundfos.com (Accessed 2020/08).

[211] J. Appelbaum, "Starting and steady-state characteristics of DC motors powered by solar cell generators," *IEEE Trans. on Energy Conversion*, vol. EC-1, no. 1, pp. 17-25, 1986.

[212] S.R. Bhat, A. Pittet, B.S. Sonde, "Performance optimization of induction motor-pump system using photovoltaic energy source," *IEEE Trans. on Industry Applications*, vol. IA-23, no. 6, pp. 995-1000, 1987.

[213] A. Coty, "Automatically switched photovoltaic motor," Patent WO2010082007A2, published Jul. 22, 2010.

[214] A. Coty, "Autoswitched photovoltaic motor with augmented power," Patent WO2012069447A1, published May. 31, 2012.

[215] T.J.E. Miller, *Switched Reluctance Motors And Their Control*, Magna Physics Pub., 1993.

[216] Off-Grid Europe, "Off-grid Europe products," 2019. Available at: https://www.off-grid-europe.com/ (Accessed 2019/09).

[217] J. Aubry, "Optimisation du dimensionnement d'une chaîne de conversion électrique directe incluant un système de lissage de production par supercondensateurs : application au houlogénérateur SEAREV," PhD thesis, École normale supérieure de Cachan, Cachan, France, 2011.

[218] B. Gates, *How to avoid a climate disaster: the solutions we have and the breakthroughs we need*, Knopf, 2021.

[219] Y. Cortes-Peña, D. Kumar, V. Singh, J.S. Guest, "BioSTEAM: A fast and flexible platform for the design, simulation, and techno-economic analysis of biorefineries under uncertainty," *ACS Sustainable Chemistry & Engineering*, vol. 8, no. 8, pp. 3302–3310, Mar. 2020.

[220] AACE International "AACE International Recommended Practice 18R-97: Cost Estimate Classification System as Applied in Engineering, Procurement, and Construction for the Process Industries," 2020 revision, Aug. 2020.